DOCTORAL THESIS

Development and application of numerical simulation tools for the prediction of the structural behaviour of paving block pavements

submitted in satisfaction of the requirements for the degree
Doctor of Science in Civil Engineering
of the Vienna University of Technology, Faculty of Civil Engineering

DISSERTATION

Entwicklung und Anwendung von numerischen Simulationstools für die Vorhersage des Strukturverhaltens von Pflasterbefestigungen

ausgeführt zum Zwecke der Erlangung des akademischen Grades eines
Doktors der technischen Wissenschaften
eingereicht an der Technischen Universität Wien, Fakultät für Bauingenieurwesen

von

Dipl.-Ing. **Herwig Leopold Hengl**
Matrikelnr.: 0425310
Burggasse 128/35, 1070 Wien, Österreich

Betreuer:

Dipl.-Ing. Dr. techn. **Josef Füssl**
Institut für Mechanik der Werkstoffe und Strukturen, TU Wien
Karlsplatz 13/202, 1040 Wien, Österreich

Univ. Prof. Dipl.-Ing. Dr. techn. DDr.h.c. **Josef Eberhardsteiner**
Institut für Mechanik der Werkstoffe und Strukturen, TU Wien
Karlsplatz 13/202, 1040 Wien, Österreich

Gutachter:

Univ. Prof. Dipl.-Ing. Dr. techn. **Ronald Blab**
Institut für Verkehrswissenschaften, TU Wien
Gußhausstraße 28/230/3, 1040 Wien, Österreich

Univ. Prof. Dr.-Ing. habil. **Frohmut Wellner**
Institut für Stadtbauwesen und Straßenbau, TU Dresden
Georg-Schumann-Straße 7, 01187 Dresden, Deutschland

Wien, im Juli 2017

....

Abstract

Paving block pavements are an ecological, economical, and space forming valuable type of road surface, and therefore, the demand is continuously increasing. Nevertheless, immature design concepts often lead to unexpected performance, which reduces confidence in these types of constructions. Especially the mechanical performance of the vertical joints between paving blocks as well as the interaction behavior to the underlying base courses is often not depicted realistically enough. This motivated the development of the numerical simulation tools for paving block structures presented within this thesis, which are able to take into account the complex non-linear behavior between structural elements of this type of pavement constructions more reliable. Numerous identification experiments were carried out to determine material and interaction properties of paving block superstructures. Therefrom, material models and parameters were obtained and implemented into numerical models. The resulting simulation tools have been partially validated by means of accelerated pavements tests and full scale experiments.

The first part of this thesis (Publications A to C) is devoted to paving block structures with sand-filled vertical joints. Three different identification experiments to derive material models for the interaction behavior between paving blocks are proposed. The developed structural simulation tool was validated by means of accelerated pavement tests, on two full scale test sections. Furthermore, the influence of superelevated cross-profiles of paving block structures on their load bearing capacity was investigated by means of comprehensive parameter studies. Thereby, two main structural failure mechanisms could be identified, and based on the numerical results a recommendation for an optimum size of superelevation could be given. The structural response due to horizontal loadings, a very often neglected but for the performance of paving block structures essential load condition, was investigated using a further numerical model. Realistic frictional behavior between different types of paving blocks could be assessed from identification experiments and implemented into numerical simulations. The resulting 3D deformation fields of several laying patterns and types of paving block superstructures revealed improved insights into horizontal load transfer mechanisms. A fully automated numerical model generation allowed for a comprehensive performance evaluation with respect to the horizontal shifting resistance of different superstructure.

The second part of this thesis (Publications D and E) focuses on the mechanical behavior of paving block pavements with mortar-filled vertical joints, mainly addressing the prediction of cracking mechanisms under thermal loading. By means of the proposed simulation tool, basic structural failure mechanisms, due to different temperature events, could be identified and relationships between crack widths and different bonding strengths as well as installation temperatures were obtained. Moreover, estimates for necessary bonding strengths between paving blocks and mortar bed to prevent large (visible) cracks due to temperature loads could be given.

Finally, it can be concluded that by taking the interaction behavior between structural elements of such type of pavements appropriately into account, a more reliable description of complex structural response mechanisms becomes possible. Thus, sophisticated numerical simulation tools are able to deliver new insights into the mechanical behavior of paving block pavements and have the potential to significantly enhance performance predictions, especially in combination with appropriate identification and validation experiments.

Kurzfassung

Pflasterbefestigungen sind eine ökologisch und ökonomisch sinnvolle und zudem visuell ansprechende Art von Straßenbefestigung. Aus diesem Grund steigt auch die Nachfrage nach ihnen kontinuierlich an. Dennoch führen unzureichende Bemessungskonzepte oft zu einer unerwartet schlechten Performance, welche das Vertrauen in diese Konstruktionen stark verringert. Speziell das mechanische Verhalten der vertikalen Fugen zwischen Pflastersteinen sowie das Interaktionsverhalten mit den darunterliegenden Tragschichten werden oft nicht realistisch modelliert. Dies motivierte die Entwicklung der in dieser Arbeit vorgestellten numerischen Simulationstools, welche das komplexe nichtlineare Verhalten zwischen Strukturelementen realistisch berücksichtigen können. Zahlreiche Identifikationsexperimente wurden durchgeführt, um die Material- und Interaktionseigenschaften von Pflastersteinaufbauten zu bestimmen. Daraus wurden Materialmodelle und Parameter abgeleitet, die als Input in numerische Modelle dienten. Die entwickelten numerischen Simulationstools wurden durch Großfeldversuche teilweise validiert.

Der erste Teil dieser Arbeit (Publikationen A bis C) widmet sich Pflasterbefestigungen mit sandgefüllten vertikalen Fugen. Es werden drei verschiedene Identifikationsexperimente zur Ableitung von Materialmodellen für das Interaktionsverhalten zwischen Pflastersteinen vorgestellt. Das entwickelte Simulationstool wurde anhand von Großfeldversuchen auf zwei Versuchsaufbauten validiert. Darüber hinaus wurde der Einfluss von überhöhten Querprofilen von Pflasterbefestigungen auf ihre Tragfähigkeit mittels umfangreicher Parameterstudien untersucht. Dabei konnten zwei wesentliche strukturelle Versagensmechanismen identifiziert werden und anhand der numerischen Ergebnisse eine Empfehlung für eine optimale Größe der Bombierung gegeben werden. Das Strukturverhalten zufolge horizontaler Belastungen, welches sehr oft vernachlässigt wird aber für die Performance von Pflasterbefestigungen wesentlich ist, wurde mit einem weiteren numerischen Modell untersucht. Ein realistisches Reibungsverhalten zwischen verschiedenen Arten von Pflastersteinen konnte aus Identifikationsversuchen gewonnen und in numerischen Simulationen umgesetzt werden. Die daraus resultierenden 3D-Verformungsfelder von mehreren Verbandsarten und Typen von Pflastersteinen zeigten interessante Einblicke in horizontale Lastübertragungsmechanismen. Eine vollautomatische numerische Modellgenerierung ermöglichte eine umfassende Performancebewertung in Bezug auf den horizontalen Verschiebewiderstand unterschiedlicher Pflasterverbände.

Der zweite Teil dieser Arbeit (Publikationen D und E) befasst sich mit dem mechanischen Verhalten von Pflasterbefestigungen mit mörtelgefüllten vertikalen Fugen, wobei der Schwerpunkt auf der Vorhersage von Rissmechanismen unter thermischer Beanspruchung liegt. Mit dem vorgestellten Simulationstool konnten grundlegende strukturelle Versagensmechanismen zufolge unterschiedlicher Temperaturereignisse identifiziert und Beziehungen zwischen Rissbreiten und unterschiedlichen Haftverbindungen zwischen Pflastersteinen untereinander sowie zum Mörtelbett ermittelt werden. Darüber hinaus war es möglich, Schätzwerte für notwendige Haftverbindungen zwischen Pflastersteinen und Mörtelbett zur Vermeidung großer (sichtbarer) Risse aufgrund von Temperaturbelastungen anzugeben.

Zusammenfassend kann gesagt werden, dass durch geeignete Berücksichtigung des Interaktionsverhaltens zwischen Strukturelementen dieser Aufbauten eine realistische Beschreibung des komplexen Strukturverhaltens möglich wird. Anspruchsvolle nu-

merische Simulationstools sind also in der Lage neue Einblicke in das mechanische Verhalten von Pflasterbefestigungen zu geben und haben das Potential, Vorhersagen über deren Performance deutlich zu verbessern. Speziell in Kombination mit darauf abgestimmten Identifikationsexperimenten und einer möglichst umfangreichen Validierung.

Acknowledgements

This thesis is based on the work done during my employment as a research assistant at the Institute for Mechanics of Materials and Structures (IMWS) at the Vienna University of Technology (TU Wien). Numerous people contributed to the scientific results and provided essential boundary conditions for this work. I especially thank my advisor Dr. Josef Füssl for giving me this opportunity and for his constant support and guidance throughout the last years. He is a mentor for me not only in scientific matters.

I would like to thank Dr. Wolfgang Kluger-Eigl for his help and significant contributions to this thesis. Prof. Josef Eberhardsteiner, vice-rector of the Technical University of Vienna, as well as the head of the IMWS, Prof. Christian Hellmich are thanked for their support, as well as for creating a positive working environment. Furthermore, I would like to thank Prof. Ronald Blab, dean of the Faculty of Civil Engineering, for his support and contributions. Prof. Frohmut Wellner (TU Dresden, Germany) is thanked for serving as co-examiner of this thesis.

I further want to thank my loving parents, Dr. Brigitte Hengl-Pirker and DI Herbert Hengl who have taken care of me and helped me to get to this point in life. In addition, I want to thank my sisters, Ines Hengl-Pirker and Mag. Alice Vidal-Hengl for their support during all these years. Furthermore, I want to thank my brother Peter Hengl for having my back and being such a good friend.

Special thanks go to my girlfriend Mag. Kerstin Just for patiently managing so many things for me during the last months, but mostly for her care and love. I also want to thank my friend Mag.(FH) Immanuel Neureiter for going with me through so many adventures. Further, I want to thank all of my friends for their friendship and loyalty, especially Mathias Winter and Olaf Prokop for so many good memories. In addition, I want to thank Mag. Hüseyin Keskin and Markus Brenner for their faith in me.

My appreciation goes also to my colleagues Dr. Markus Lukacevic, Dr. Georg Kandler, DI Wolfgang Lederer for their help and advice. Furthermore, I want to thank my roommates DI Hawraa Kariem, DI Luis Zalaya-Lainez and Dr. Giuseppe Balduzzi for their good accompany. Additionally, I would like to thank Mag.(FH) Martina Pöll, Gabriele Ostrowski and Astrid Schuh for their help with administrative issues. Last but not least, I also want to thank DI Thomas Kiefer, DI Maximilian Autengruber, Dr. Christian Schranz, Dr. Leopold Wagner, Dr. Mehran Shahidi, Dr. Krzysztof Luczynski, MSc. Mingjing Li, DI Michael Schweigler, Dr. Vitezlav Stembera, DI Thomas Schlappal, MSc. Hui Wang, Dominic Hassan, Dr. Mehdi Aminbaghai, Dr. Georg Hochreiner and all my other colleagues at the IMWS for the good times we had.

Contents

Introduction

Motivation

Paving block structures, as schematically illustrated in Figure 1, are experiencing an increasing popularity in urban areas due to their ecological, economical, and space forming qualities compared to common asphalt pavements. Especially in communal areas, the large number of design possibilities they deliver, such as shape, colour and texture, are greatly appreciated. Even in areas with high traffic volumes, paving block structures are expected to represent a suitable alternative to common pavement building systems in future.
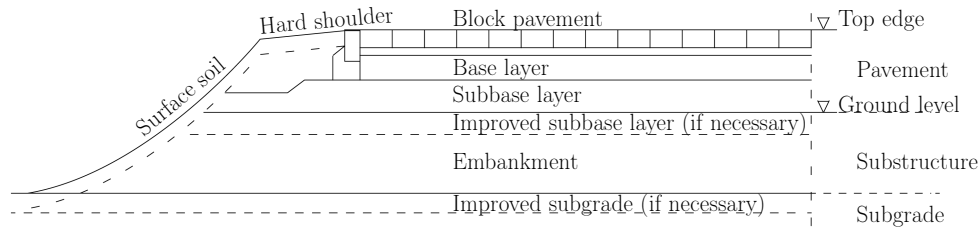
Figure 1: Section of a typical paving block structure, showing the different base layers and a classical border construction.

This trend is, however, continuously weakened by unexpected damage of newly built paving block pavements. The reason for this are immature design concepts and standards, which are heavily based on the concepts for asphalt pavements and do not take the specific characteristics of this block-like structures sufficiently into account. The success of a project is therefore strongly dependent on the quality of planning and construction provided by experienced engineers and executing companies, rather than on reliable scientific knowledge implemented into design concepts and standards. More knowledge about the mechanical mechanisms of these systems and advanced prediction tools are necessary to exploit the potential of this type of construction and to serve as basis for a more extensive use and possible new areas of application.

For this reason, within this thesis, numerous identification experiments are presented to identify the load transmission capability of different joint formations. Mechanical models and corresponding material parameter to describe the joint behaviour have been obtained and implemented into numerical models. The resulting simulation tools were validated by means of data obtained from full-scale accelerated tests and field experiments. The knowledge, gained from these full-scale experiments, together with insights

from identification experiments and the validated numerical simulation tools, should contribute to a better utilization of paving blocks and slabs. Moreover, the improvement of existing design schemes and the development of new design methods and rules may be accomplished.

An overview of the work carried out and proposed in this thesis is given in Figure 2. The four publications (denoted as PA, PB, PC, and PD) and one chapter (denoted as CE) constituting this thesis are assigned to the respective step of this conceptual overview.
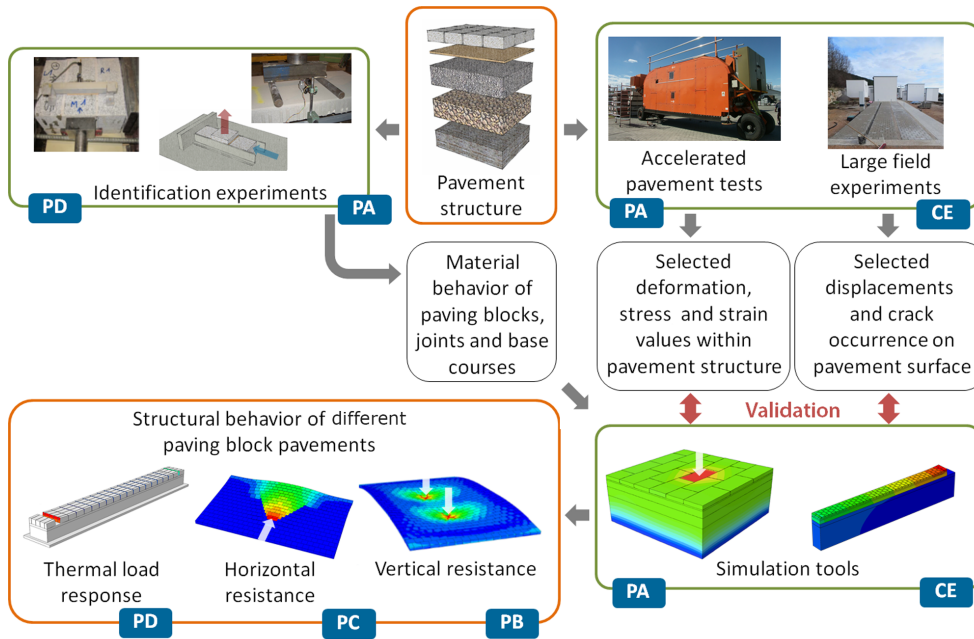
Figure 2:   Conceptual overview of the work carried out and proposed in this thesis. The publications/chapters building up this thesis are denoted as PA to PD and CE, and are assigned to the respective conceptual step of this overview.

The challenges tackled, with respect to performance prediction of paving block structures, can be distinguished into the following points of interest:

1. Structural response of paving block structures due to **vertical loadings** occurring from traffic and the critical stresses and strains in the underlying base layers. For the structural response, the layers and the interactions between the layers play a significant role, which are examined in Publication A (PA) and Chapter E (CE), respectively. Industry experts expect a positive influence from superelevated cross profiles which motivated the work in Publication B (PB).

2. In addition to the vertical resistance, however, the structural resistance to **horizontal loadings** is assumed to represent an equally important performance characteristic for paving block structures. According to experienced engineers, it is often observed in practice that due to braking and steering maneuver of heavily loaded trucks or buses damage is introduced into paving block structures. Such

loadings are commonly not part of design approaches and also rarely addressed in scientific literature. Neglecting these horizontal loadings can cause damage in form of permanent deformations in the superstructure and chipped edges of paving blocks. The identification and assessment of such horizontal deformation mechanisms of paving block superstructures with sand-filled joints, as shown in Figure 3 (left), represents the main objective of Publication C (PC).

3. **Thermal loadings**, which usually affect paving block structures with mortar filled vertical joints, as shown in Figure 3 (right). Such structures can exhibit a significantly higher load capacity as comparable structures with sand-filled joints. For this reason, this pavement construction method is increasingly being used or would be used, respectively, if its performance could be estimated more reliably. Specifically, the exact cause of cracks due to cooling in winter has not been fully understood yet and appropriate prediction tools do not exist. As a result of thermally induced stresses cracks often appear on surfaces. Apart from the mechanical issues caused by such cracks, they also affect the visual appearance of these, not damaged very attractive, pavements. This greatly reduces the confidence in and acceptance of this type of construction and prevents a more frequent use. A major reason for this performance problem can be attributed to the lack of appropriate design codes for the construction of rigidly laid paving block structures. For this reason, numerous investigations proposed in Publication D (PD) and Chapter E (CE) were carried out.
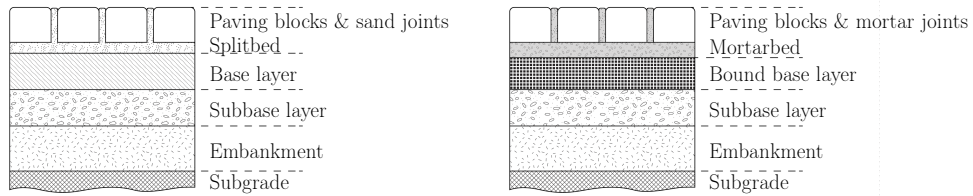
Figure 3: Typical paving block structure with (left) sand-filled joints and (right) mortar-filled joints.

Outline of the thesis

The first part of the thesis (Publications A to C) is devoted to the investigation of the mechanical behaviour of paving block structures with sand-filled joints. Large-scale experiments, identification experiments of mechanical properties, and numerical simulations have been carried out.

In **Publication A**, a finite element method-based numerical simulation tool for paving block pavements, with emphasis on characterisation of the interaction behaviour between paving blocks is presented. Identification experiments were carried out for the mechanical behaviour of the vertical joints, the unbound base courses and the concrete blocks. An orthotropic elasto-plastic material law in tangential direction and a non-linear elastic relationship in normal directions were finally used to describe the paving block interaction within the numerical simulation tool. Additionally, a realistic description of all other parts of a paving block structure allowed for reliable stress

predictions within the whole superstructure. The accuracy of the finite element calculations, at least the response due to vertical loads, could be assessed by comparing the results to measurement data from full-scale accelerated pavement tests (APT) on two paving block test sections. These tests were conducted by an international cooperation consisting of two research institutes, the Vienna University of Technology (VUT) and the Swiss Federal Laboratories of Material Science and Technology (EMPA), and one industrial partner.

Publication B focuses on the influence of superelevated cross profiles of paving block structures on their load-bearing behaviour. Observations in practice suggest a strong influence of superelevated profiles on the overall performance of paving block structures. Many experienced engineers state that these effects should not be neglected within the design process. Therefore, a numerical simulation tool was developed which is able to capture the effect of such profiles on the load-bearing behaviour of paving block structures, qualitatively as well as quantitatively to a certain extent. Numerous parameter studies were performed to identify the influence of structural parameters, like the size of the superelevation, the number and dimension of paving blocks, the interaction between them, and the loading situation, on the structural behaviour.

In **Publication C**, the identification and assessment of horizontal deformation mechanisms of paving block superstructures were investigated by means of complex 3D finite element simulations, investigating 6 different laying patterns with 5 different types of paving blocks. The non-linear interaction behaviour between paving blocks was identified experimentally, implemented into the numerical simulation tool, and subsequently allowed for the reproduction of very realistic horizontal deformation mechanisms. Finally, the performance of several laying pattern and paving block type configurations were compared to each other, pointing out the strength and weaknesses of each superstructure and revealing which combinations are best performing.

The second part of the thesis (Publication D and Chapter E) comprises the investigation of mechanical mechanisms of paving block structures with mortar-filled joints. Particularly thermally induced stresses and the occurrence of cracks are observed.

Publication D aims at describing the response of paving block structures with mortar-filled joints due to temperature loading. Mechanical mechanisms in such structures were investigated especially concerning the occurrence of cracks, caused by thermally induced stresses. Therefore, a numerical simulation tool for such paving block structures under temperature loading was developed, which is able to take brittle failure mechanisms in-between paving blocks and paving blocks and the underlying mortar bed into account. By means of the proposed simulation tools, basic structural failure mechanisms of such paving block structures, due to different temperature events, could be identified.

In **Chapter E** the construction of three large paving block test fields in Waldegg, Austria, is discussed. Furthermore, a numerical simulation tool is proposed and numerical results are compared to data obtained from the test fields. By means of the simulation tool, basic structural failure mechanisms for rigid paving blocks structures on splitbed could be reproduced correctly. Finally, estimates for necessary friction coefficients between paving blocks and splitbed to prevent large cracks are given.

Chapter 1

Numerical simulation tool for paving block structures assessed by means of full-scale accelerated pavement tests (Füssl et al., 2016a)

Authored by   Josef Füssl, Herwig Hengl, Wolfgang Kluger-Eigl & Ronald Blab
Published in   *International Journal of Pavement Engineering*, pages 1-13, 2016

Block pavements are an attractive alternative to asphalt and concrete pavements, especially in communal areas. Architects and urban planners would like to take advantage of various shapes, colours and textures of paving blocks in order to achieve a higher quality of urban space if the performance of block pavements could be better predicted to avoid large horizontal displacements of chipped stone corners and rutting. Unfortunately, the computational performance prediction of paving block structures is more complex than that for flexible pavements with homogeneous surface layers of asphalt concrete. The influence of the large number of vertical joints between paving blocks on the overall mechanical performance has not been considered sufficiently within computational tools yet.

The proposed numerical simulation tool is able to take into account the complex mechanical behaviour of sand filled joints as well as the non-linear mechanical behaviour of the underlying base courses. Joints are modelled using a Mohr-Coulomb-type friction model with the normal stresses non-linearly related with joint opening. Three different experimental setups were developed for the identification of the model parameters. The base behaviour was modelled using the Drucker-Prager cap model. The paper shows that the proposed tool predicts reasonable deformations and stresses in block pavements. The results of the simulations were compared with measured stresses form the full-scale accelerated pavement testing and a good agreement was observed.

1.1   Introduction and motivation

Block pavements are an ecological, economical and visually appealing type of road surface. Especially in communal areas the large number of design possibilities they deliver, such as shape, colour, and texture, are greatly appreciated. Nevertheless, the use of block pavements is lower than one would expect. One of the reasons is a lack of adequate performance prediction tools, especially for predicting damage in areas with high vertical and horizontal loads due to brake and acceleration forces. Responsible for the performance of a paving block structure are (i) the material behaviour and the thickness of the base courses, (ii) the material quality and the shape/dimension of the paving blocks, and (iii) the type of vertical joints, defining the interaction behaviour between paving blocks. In many engineering design concepts this quite complex structural system is not captured realistically enough.

Since some design methods have evolved from, and hence are heavily based on, concepts for asphalt pavement structures, for the determination of relevant stress states in the base courses, blocks are modelled as continuous layer with an effective stiffness, e.g. in Janda (2004). In this procedure, stress states within the base courses are obtained on the basis of closed-form solutions for elastic half-space systems with infinite lateral dimension. The basic solution therefore was delivered by Boussinesq (Taylor (1963); Timoshenko and Goodier (1987)), which was extended by Burmister (1943, 1958) to multi-layered elastic systems. The solutions of Burmister can be found in a large number of software programs, e.g. in BISAR (1989); Everseries Pavement Analysis Programs (1999); Huang (2004). With these approaches stress states due to edge loading, especially in the upper base courses, can not be captured realistically. For this reason, numerical simulation tools based on the finite element method were developed. One of the first numerical tools was proposed by Huurman et al. (1992), in which rigid elastically bedded blocks are connected with springs and in a subsequent calculation the loaded concrete block is analysed. Further on, some similar models were developed, (Huurman (2006); Hassani (2006); Nishizawa et al. (1984); Nishizawa (2003)), which all had in common a linear elastic interaction behaviour between paving blocks and a rather simple material behaviour of the underlying base courses. An interesting model has been developed by Ascher (2003), where the non-linear elastic Dresdner model (Gleitz (1996)) has been assigned to the base course and the performance of the model was evaluated by experiments in Lerch (2005). Within these works also the horizontal resistance of paving block structures has been studied intensively.

This paper presents a finite element method-based numerical simulation tool for paving block pavements, with emphasis on characterization of the interaction behaviour between paving blocks. An orthotropic elasto-plastic material law in tangential direction and a non-linear elastic relationship in normal directions were finally used to describe the paving block interaction within the numerical simulation tool. Additionally, a realistic description of all other parts of a paving block structure allowed for reliable stress predictions within the whole superstructure.

The accuracy of the finite element calculations, at least the response due to vertical loads, could be assessed by comparing the results to measurement data from full-scale accelerated pavement tests (APT) on two paving block test sections. These tests were conducted by an international cooperation consisting of two research institutes, the Vienna University of Technology (VUT) and the Swiss Federal Laboratories of Material Science and Technology (EMPA), and one industrial partner, whose main activity is

the development, production and sale of concrete block and slab pavers.

In the following section, the APT, including the layout, instrumentation, test program and results, are described. The identification experiments for the mechanical behaviour of the vertical joints, the unbound base courses and the concrete blocks are proposed in Section 3. The identified material properties serve as input to a numerical simulation tool which is presented in Section 4. In Section 5, the simulation results are compared to measured values from the APT. Finally, a summary of the results is given and conclusions are drawn in Section 6.

1.2 Full-scale accelerated pavement test

Within full-scale accelerated pavement tests the whole traffic load of the expected service life of a pavement structure is simulated in real scale. This leads to two major advantages, namely, (i) the "total system" response is provided within (ii) a relatively short period of time, compared with mechanical testing at a smaller scale and the many years required for long-term monitoring, respectively. For this reason, full-scale accelerated pavement testing has a long tradition and has been conducted for almost 50 years (Powell (2012); Steyn (2012a)). A comprehensive overview of the so far performed APTs and the obtained significant findings can be found in the two NCHRP synthesis reports (F. Hugo (2004) and Steyn (2012b)), respectively. According to these reports, most of the APTs have been performed on asphalt pavements or dowelled concrete slab pavements. The few APTs performed on paving block structures have been carried out in Australia, New Zealand, South Africa, and Japan. A good overview of these developments together with insights on design and construction of paving block structures based on his extensive work in this field for decades has been given by Shackel (1990). Details of his performed heavy vehicle simulations on block pavements can be found in Shackel (1980b,a, 1982) and in the referenced publications therein. To the knowledge of the authors, the last APTs on block pavements were performed by Sharp around 2000. Some information about these experiments can be found in F. Hugo (2004) and Sharp et al. (1999). Within the present work, the Mobile Load Simulator (MLS10) has been applied for the first time to paving block superstructures. The MLS10 itself, the test sections and the testing program will be presented in the following.

1.2.1 Test sections

The APT sections and instrumentation were designed and constructed in Summer 2010. Four different pavements sections with paving slabs and three sections with paving blocks were built. Within this paper only the paving block sections, Section 5 to Section 7, will be considered (see Table 1.1).

test section	type of paving block	instrumentation
5	rectangular interlocking block 20/20/10 [cm]	4 SPC
6	double T block 10 [cm]	none
7 (porous concrete)	rectangular interlocking block 20/20/10 [cm]	2 SPC

SPC ... soil pressure cells

Table 1.1: Test sections

Each test section were 6.4 m long and 5.0 m wide, as illustrated in Figure 1.1 (a). The length of each test section was adjusted to the length between the corner jacks (7.2 m) of the MLS10 (see Figure 1.2), to avoid the machine standing on the pavement during traffic simulation. All sections were surrounded with a concrete foundation, serving as support for the MLS10 and as confinement for the pavement sections themselves. The

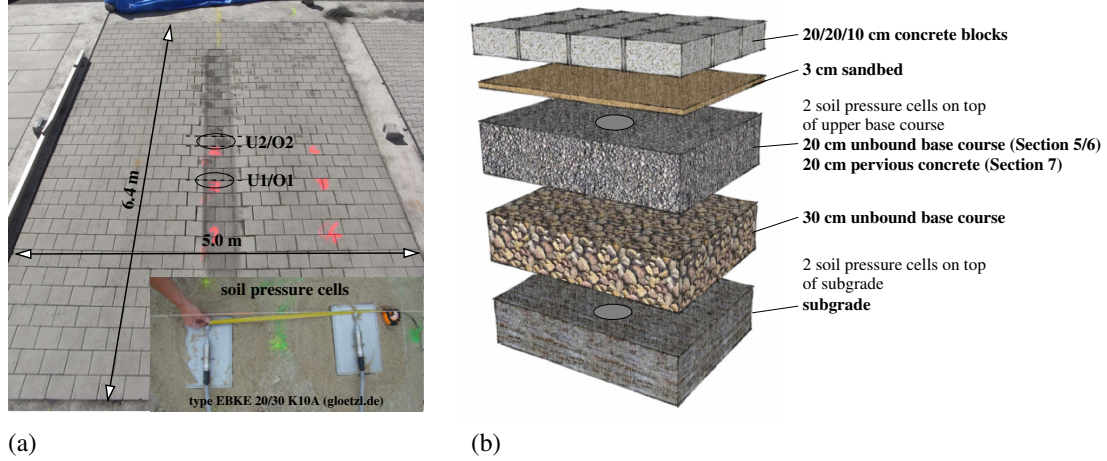(a)   (b)

Figure 1.1: (a) Layout of one test section (Section 5) including position of soil pressure cells, and (b) pavement structure.

superstructure of the test sections, illustrated in Figure 1.1 (b), was chosen according to the requirements in regulation RVS 03.08.63 (2008), describing block/slab pavements structures without compound effect on unbound base courses. Bedding sand (2/4 mm), jointing sand (0/4 mm), and base materials (0/63 mm and 0/32 mm) were chosen according to the requirements in regulations RVS 08.18.01 (2009) and RVS 08.15.01 (2008).

Test Sections 5 and 7 were instrumented in the main loading line of the MLS10 as shown schematically in Figure 1.1 (a). Soil pressure cells (SPC) of type EBKE 20/30 K10 A were installed on the surface of the subgrade and the upper base course (see Figures 1.1 (a) and (b)).

1.2.2 Accelerated Pavement Tests

For the traffic simulation, shown in Figure 1.2, the Mobile Load Simulator MLS10 from Switzerland (Partl (2008)) was used. The MLS10 was equipped with Goodyear 455/40 R22.5 super single tires, exhibiting a tire pressure of 1.06 N/mm^2 (10.6 bar) and able to apply a wheel load of 65 kN. At the beginning of the test procedure, this wheel load was adjusted with a calibrated static scale and controlled with a mobile weight in motion device (WIM), ensuring an exact wheel load of 65 kN. Before the traffic simulation a pre-loading phase with reduced wheel load and a speed of 7.2 km/h was performed on each test section for about 15 minutes (1,000 passes). After this initial phase the full load of 65 kN was applied and the speed increased to 22 km/h. During the tests no lateral wandering or application of water was carried out. The MLS10 was able to simulate 38,400 load rollovers per day. Table 1.2 gives the number of the projected and applied rollovers of each test section as well as the respective loading class according to the Austrian design standard RVS 03.08.63 (2008).
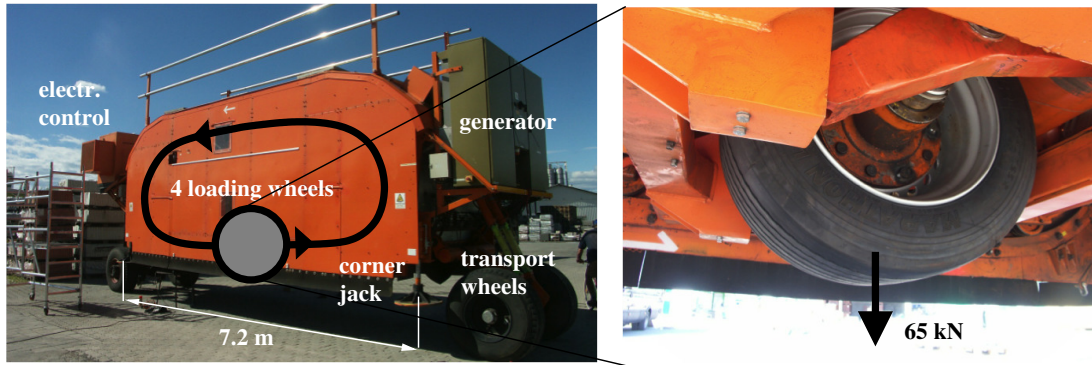
Figure 1.2: Mobile Load Simulator MLS10 with super single tires.

| test section | number of rollovers | | loading class[⋆] | max. rutting depth |
	projected	applied		[mm]
5	285.000	250.000	IV	> 25.0
6	285.000	285.000	III	19.5
7	285.000	285.000	III	3.5

[⋆]According to Austrian design standard (1)

Table 1.2: Test program (load 65 kN, 1.06 N/mm^2, super single tire

During testing the main problem was the rapid loss of jointing sand, since the sand joints within the newly constructed slab test sections had no time to consolidate and to develop conventional inter-locking status. Therefore it was necessary to add jointing sand during the maintenance stops of the MLS10. However, inspection and refilling of joints are regular maintenance actions for paving block structures during their lifetime. For further tests on these types of pavements it is, thus, recommended that new test sections are exposed to environmental conditions (rain, dust) for a few weeks before the start of the APT until the jointing material consolidates. Nevertheless, it can be stated that the execution of the APT and the projected load applications were completed successfully (see Table 1.2).

On Section 5 the APT was stopped before reaching the projected load passes because of a rut depth larger than 20 mm, which is the threshold value in Austria and also the maximum tolerance for the operating of the MLS10. The largest deformation was induced directly above the soil pressure cells installed at the formation level of the unbound base course. It was concluded that the compaction of the base course in the surrounding of the instrumentation was unsatisfactory. Although considerable deformation was measured, no blocks were broken and only minimal spalling on two loaded stones occurred. The width of joints in the middle of the load line after construction was less than the allowable tolerances, which may have contributed to the exhibited performance.

Section 6 exhibited a rut depth of 20 mm at the intended number of load passes, but no damaged blocks could be identified. Small horizontal deformations and contact between two pavers were observed in the touchdown of the super single tires. The joint

width of almost all joints in the middle of the load line decreased to below 1 mm.

The pavement structure with pervious concrete (Section 7) is a relatively new construction method in Austria for which only limited knowledge and experience is available. For this reason, it was interesting to observe that the performance of this pavement was excellent. Only small deformations could be measured and no visible damaged was observed.

In summary, it can be assumed that the performance of the test sections showed a realistic behaviour during the APTs compared to real traffic situations. A significant amount of time could be saved compared to test sections on public roads with high traffic volumes. The only shortcoming of the MLS10 is that no realistic breaking or acceleration forces, which often have a major impact on the performance of a pavement structure, can be applied on the road surface. In future, this disadvantage could be overcome by using a numerical simulation tool, where a variety of loads can be applied without much additional effort.

The obtained results from the installed measuring devices and their evaluation will be presented in the following section.

1.2.3   Results of APT

As mentioned before, Section 5 was equipped with 4 soil pressure cells (SPC), installed at the top surface of the subgrade (U1 and U2) and the top surface of the upper base course (O1 and O2) and Section 7 with 2 soil pressure cells at the top of the upper base course (O1 and O2). The position and arrangement of these measurement devices are shown in Figure 1.1. The SPC delivered measurement values with a frequency of 100 Hz during the whole test period. The obtained data within one illustrative second (100 measured values per SPC) is shown in Figure 1.3, for the SPC O1 and U1 of Test Section 5. It can be seen that the peak values of the compressive stresses due to a load pass can be captured with sufficient accuracy, even if a higher frequency could be recommended for the SPC O1. For further evaluation the maximum and minimum pressure values of
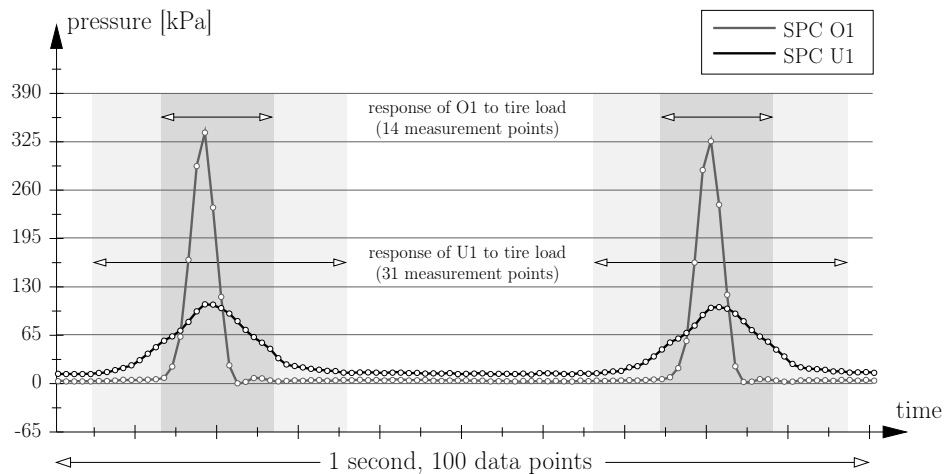

Figure 1.3: Data obtained within one illustrative second from soil pressure cells (SPC) O1 and U1 of Test Section 5.

each minute of the whole testing time were used. Figure 1.4 shows this data for the SPC U1 and U2 of Section 5. The obtained minute minima and maxima of the other SPC

can be found in Figure 1.15 and Figure 1.16 of the Appendix. In Section 5 the mean
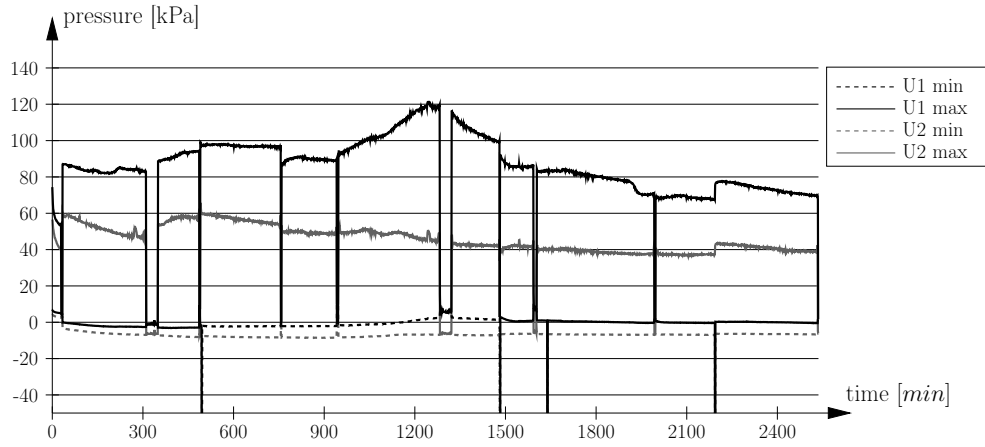

Figure 1.4: Data obtained from soil pressure cells (SPC) U1 and U2, installed on top of subgrade, of Section 5.

value and standard deviation of the pressure amplitudes (difference between minute maxima and minima) are compared to values obtained from finite element simulations.

1.3   Identification experiments

Responsible for the overall performance of a pavement structure with paving blocks are the following parts: (i) the joint behaviour between blocks, (ii) the mechanical properties of the blocks itself, and (iii) the behaviour of the base courses including the subgrade. For a reliable simulation tool the mechanical behaviour of all these parts needs to be characterised. For this reason, different identification experiments have been carried out which will be presented in the following.

1.3.1   Joint behaviour

For the determination of the joint behaviour three different new experimental setups were developed, which are illustrated schematically in Figure 1.5. From the first and second test setup (Figures 1.5 (a) and (b)) the frictional behaviour in vertical and horizontal direction, respectively, was obtained. By varying the confinement force in normal direction to the joint and by assuming a frictional behaviour according to Mohr-Coulomb, a vertical and horizontal friction angle describing the tangential joint behaviour could be determined from these experiments. Moreover, the amount of tangential deformation γ_e before plastic effects occur as well as a maximum shear stress τ_{max}, which is independent of the confinement stress, were identified. With all this information the tangential joint behaviour can be described by an anisotropic friction criterion, illustrated in Figure 1.6 and reading

$$\frac{|\tau_h|^2}{\tau_h^{crit2}} + \frac{|\tau_v|^2}{\tau_v^{crit2}} = 1, \tag{1.1}$$

with $\tau_v^{crit} = \varphi_v \sigma_n \leq \tau_{max}$ and $\tau_h^{crit} = \varphi_h \sigma_n \leq \tau_{max}$, where φ_v and φ_h denote the vertical and horizontal friction angle, respectively, obtained from experiments.

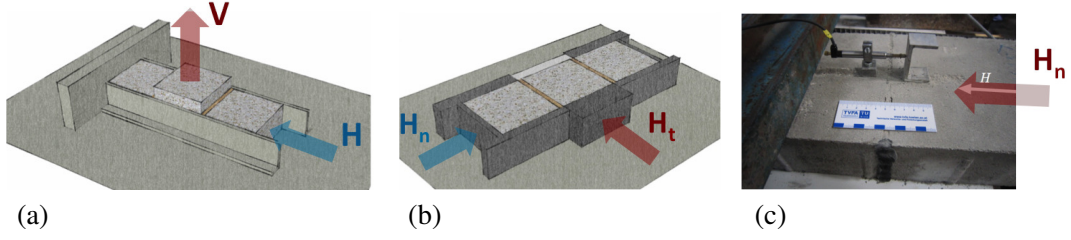(a)   (b)   (c)

Figure 1.5: Schematic illustration of identification experiments of mechanical
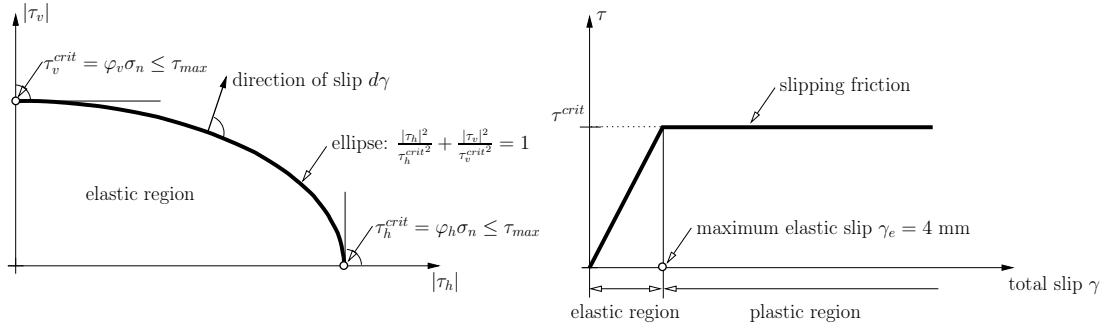joint behaviour in (a) horizontal, (b) vertical, and (c) normal direction.

Figure 1.6: Anisotropic friction model implemented in Abaqus to describe
the tangential behaviour between vertical joints.

From the third experiment (see Figure 1.5 (c)) a relationship between the joint normal stress σ_n and the joint deformation in thickness direction (direction of joint width) δu_n was obtained, reading

$$\sigma_n = E_0 \delta u_n^n, \tag{1.2}$$

where E_0 denotes a secant-bedding modulus and n is a dimensionless parameter.

A detailed description of the test-setup, the test program and the evaluation of all three experiments can be found in Füssl et al. (2016b). The identified parameters as input for the numerical simulation tool are finally: $\varphi_h = 1.21$, $\varphi_v = 0.58$, $\tau_{max} = 2.41$ N/mm^2 for the tangential joint behaviour, and $E_0 =$11.482 N/mm^3 and $n = 1.795$ for the normal joint behaviour.

1.3.2   Concrete paving block properties

The stiffness of the concrete slabs were obtained by ultrasonic measurements. The ultrasonic measurement setup and a concrete specimen with the two measuring directions are shown in Figure 1.7. By measuring the transit time T of the ultrasonic wave through the specimen, the wave velocity v was determined and further the modulus of elasticity E could be obtained by

$$E = \frac{\rho v^2 (1 + \nu)(1 - 2\nu)}{(1 - \nu)}, \tag{1.3}$$

where ρ denotes the mass density of concrete, which was measured for each sample (mean value 2.37 t/m^3), and ν is the Poisson's ratio assumed to be 0.15. From 24 measurements on 4 samples a mean value of the modulus of elasticity of 45,334 N/mm^2 with a standard deviation of 7.3 % was obtained.
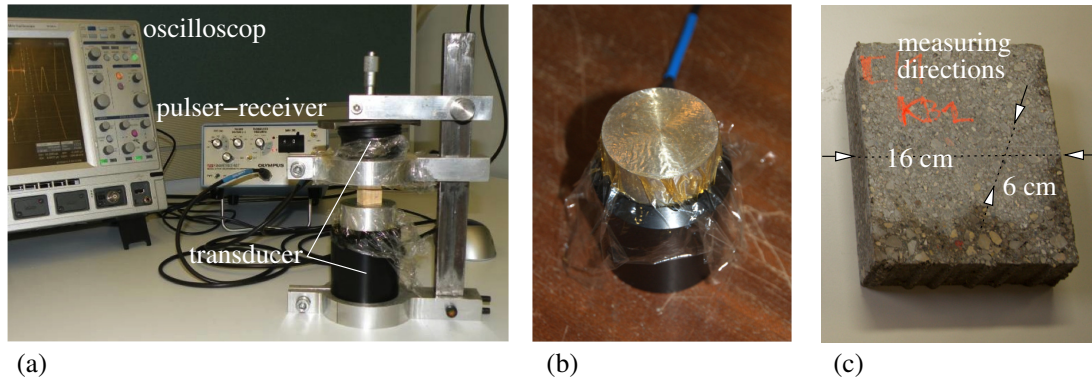
Figure 1.7: (a) Ultrasonic measurement setup with dummy sample, (b) ultrasonic transducer with honey as contact agent, and (c) tested concrete samples.

1.3.3 Behaviour of base courses

Unbound base course materials often exhibit non-linear elastic and plastic material behaviour that cannot be described with the linear elastic model. The non-linear (due to the granular material structure) elastic behaviour is often modelled by the simple two-parameter $k - \phi$ model (Hicks and Monismith (1971)), which suggests that the resilient modulus is proportional to the mean stress raised to a power, or further developed models like the three-parameter model according to Uzan (1985), the Dresden model (Gleitz (1996)) and the isotropic or anisotropic Boyce model (Boyce (1980); Hornych et al. (1998)). A good overview of the basic models for the resilient response of unbound layers is given in Lekarp et al. (2000). The plastic material behaviour is either described by classical failure criteria, according to Mohr-Coulomb or Drucker-Prager, or/and by the "shakedown" concept described in Werkmeister et al. (2001). A comprehensive model for granular layers, from non-linear elastic material behaviour up to plastic shakedown considerations, and the implementation into a finite-element code can be found in Chazallon et al. (2009). The drawback of such complex material models is the large number of material properties required for these models, which are mainly obtained from comprehensive static and cyclic triaxial testing programs, e.g. presented in COURAGE (1999).

For this reason and since the main focus of this work is on the interaction behaviour between paving blocks, a simple yet realistic approach was chosen to describe the constitutive relationship for the base courses in the proposed numerical simulation tool. Five conventional loading plate tests were carried out during the construction process on the top of the subgrade, the lower base course, and the upper base course. The experimentally obtained load deformation relationships were used to determine elasto-plastic material parameters of all three layers by reproducing the tests with a finite element model. In Figure 1.8 (a) the experimentally and numerically obtained load deformation relationships are compared with each other. It can be seen that by assigning a modified Drucker-Prager cap model to all base courses, a calibration of the material properties allows for a very good reproduction of the loading plate tests numerically. The modified Drucker-Prager cap model and the required parameters are described in the Appendix.

subgrade

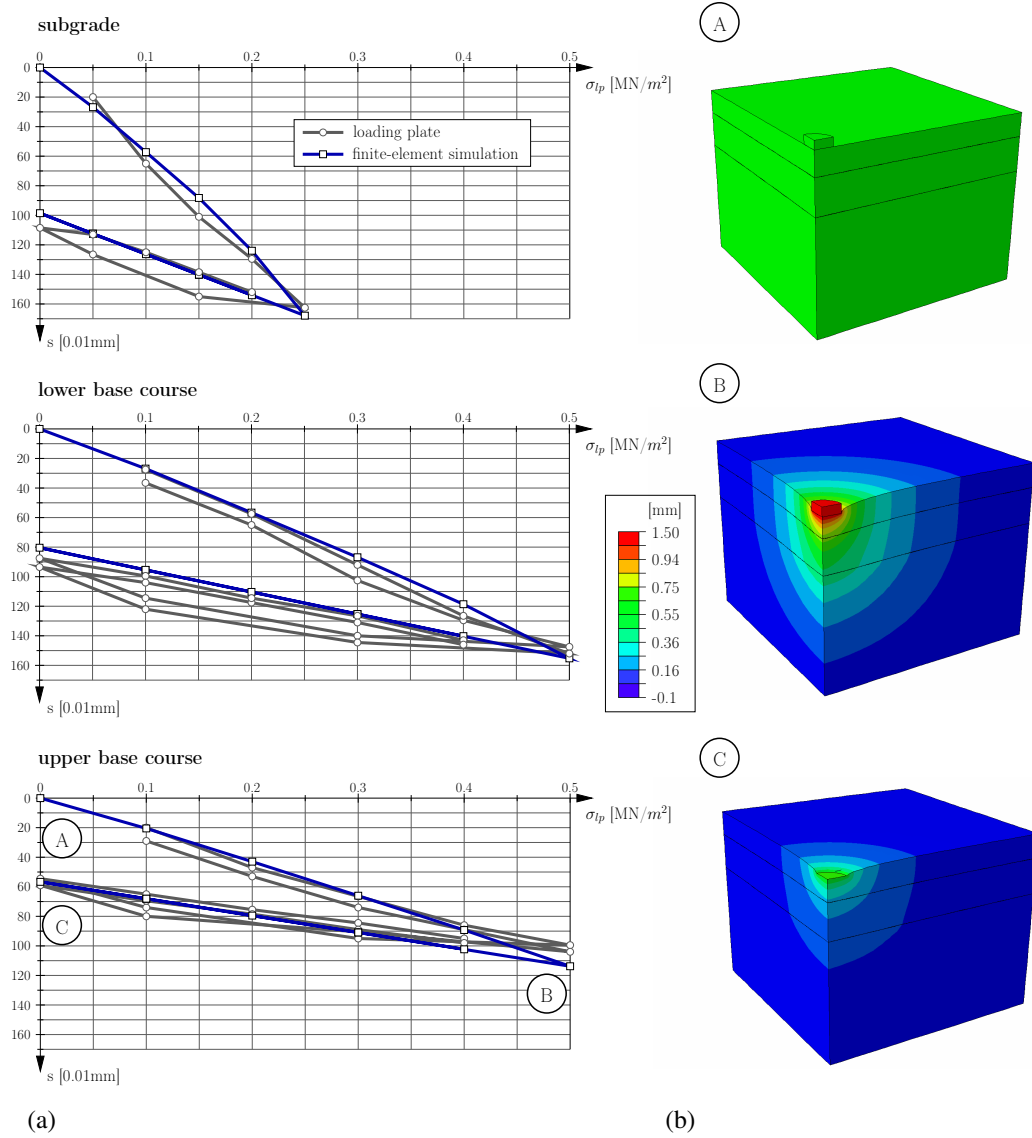**lower base course**

upper base course

(a)

A

B

C

(b)

Figure 1.8: (a) Loading plate test results on the top of the subrade, the lower base course and the upper base course compared to the corresponding numerical results, and (b) numerically obtained vertical deformation fields for a loading plate test at the top of the upper base course.

1.4   Finite Element Model

In this section a finite element model for the test sections on which the accelerated pavement tests (APT) have been carried out is presented. For the performance evaluation of the model, the obtained simulation results are then compared to the measurements taken during the APT.

The finite element model of Test Section 5 with the two investigated load cases and all boundary conditions is shown in Figure 1.9. Load case A represents a wheel load directly above a continuous transverse joint while the wheel load according to load case B is located exactly in-between two such joints. The dimensions of the analysed paving

tangential friction:
$\varphi = 0.6$
separation allowed

load cases A/B
380/80.7 mm load area
pressure $p = 1.06$ MPa

vertical joints:
tangential: anisotropic friction φ_h, φ_v
normal: nonlinear elasticity E_0, n

20/20/10 cm concrete paving stone
lateral modulus of subgrade reaction
$k_{st} = 500 MN/m^3$

4 cm sandbed
lateral modulus of subgrade reaction
$k_{sb} = 150 MN/m^3$

20 cm upper base course
lateral modulus of subgrade reaction
$k_{ubc} = 150 MN/m^3$

30 cm lower base course
lateral modulus of subgrade reaction
$k_{lbc} = 100 MN/m^3$

100 cm soil
lateral modulus of subgrade reaction
$k_{so} = 40 MN/m^3$

tied

tied

tied

dead weight
of all layers

elastic foundation
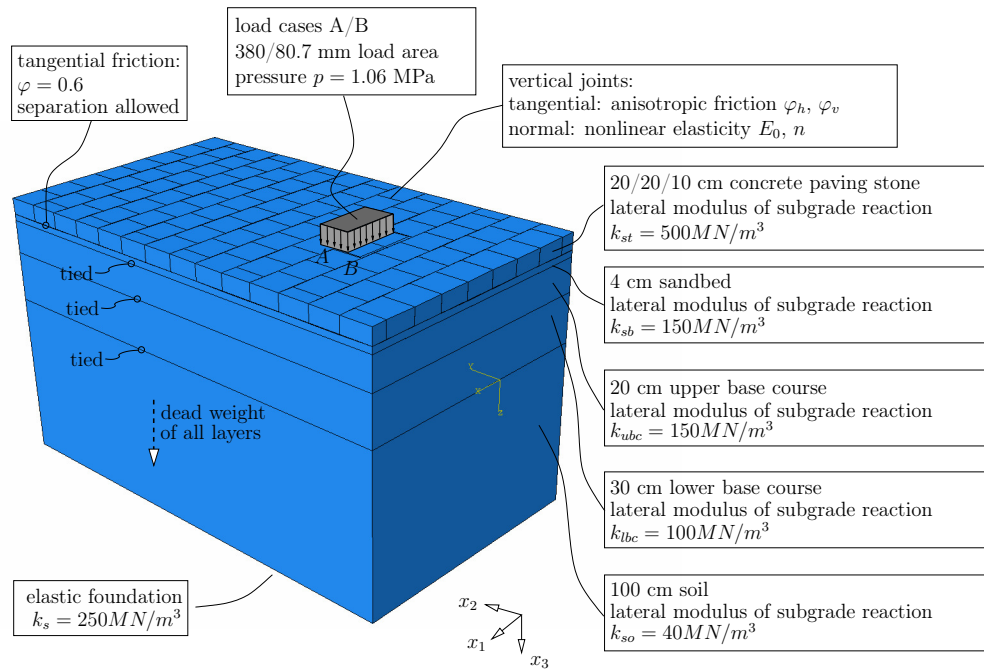$k_s = 250 MN/m^3$

x_2

x_1

x_3

Figure 1.9: Geometry, load and boundary conditions of finite element model.

blocks are 200/200 mm with a thickness of 100 mm. The elastic properties of the blocks were obtained from ultrasonic measurements as described in Section 1.3.2. The interaction between slabs (joint behaviour) is considered by an anisotropic friction criterion in tangential direction and with a nonlinear elastic relationship in normal direction. The identification of this interaction behaviour and the corresponding material properties were proposed in Section 1.3.1. To the upper as well as lower base course and the subgrade a modified Drucker-Prager cap model, described in Section 1.3.3, was assigned. Since for the sandbed no identification experiments were available, the same plastic behaviour as for the upper base course was assumed and a slightly stiffer elastic behaviour with an elasticity modulus of $E = 350$ N/mm^2 and a Poisson's ratio of $\nu = 0.3$. Between the paving blocks and the sandbed a friction coefficient of 0.6 was assigned and in normal direction lifting of the paving blocks was allowed. All other layers were tied together. The interaction with the surrounding base courses and subgrade material (lateral boundary of the modelled area shown in Figures 1.9 and 1.10, respectively) is roughly modelled by lateral elastic foundations with a lateral modulus of subgrade reaction according to suggestions of Austrian regulations. A lateral pressure is applied to

the concrete slabs, describing the restraining of the test sections and to activate a low cohesion within the vertical joints, as seen in joint experiments (Füssl et al. (2016b)).

The discretisation is done with 20-node hexahedron elements for the sandbed and 8-node hexahedron elements for all other parts. An exemplary mesh with the corresponding model parameters is shown in Figure 1.10.

model parameters:

number of concrete blocks: 119
number of contact surfaces: 313

total number of elements: 150,176
number of 3D linear elements: 78,272
number of contact elements: 71,904
total number of nodes: 252,033
total number of variables 540,387

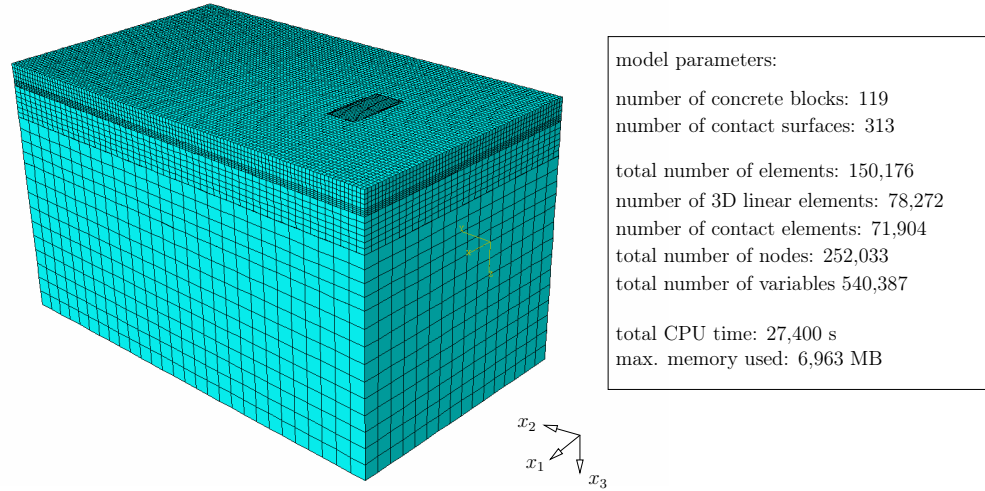total CPU time: 27,400 s
max. memory used: 6,963 MB

Figure 1.10: Exemplary finite element mesh, where the loaded blocks are finer discretised.

Subsequently, static calculations in Abaqus for different positions of the super single tire were performed. The wheel load of 65 kN was applied linearly within a maximum of 10 steps, and no more than 16 equilibrium iterations had to be carried out per step. The vertical deformation fields, obtained for the two load cases (A and B), are shown in Figure 1.11. An analysis of Figure 1.11 suggests that the model's predictions of the vertical displacements fields are reasonable. Mainly responsible for this is an appropriate implementation of the joint behaviour and the interaction between the slabs and the sandbed.
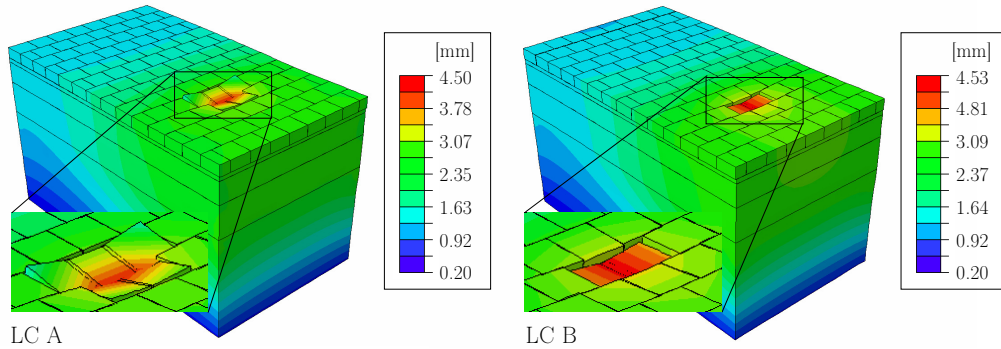

Figure 1.11: Vertical deformation fields of Section 5, for the two load cases (A and B) shown in Figure 1.9.

In the following, the relevant load cases and the resulting stress states obtained from the finite element simulations, which deliver extreme values at the positions of the SPC in the APT test sections, are presented. Figure 1.12 shows the relevant vertical

stress states at the top of the base courses and the subgrade. An influence of the load case on the distribution of vertical pressure can only be observed at the top of the upper base course. Under load case A, where the wheel load is directly above a continuous transverse joint (see Figure 1.11), the maximum vertical stress is slightly higher compared with the one under load case B. The same effect was also obtained from the APTs and can be seen in Figure 1.15. However, in contrast to concrete slab structures (investigated in Füssl et al. (2015b,a)), the load position has no major impact on the vertical stress distributions in the base layers.
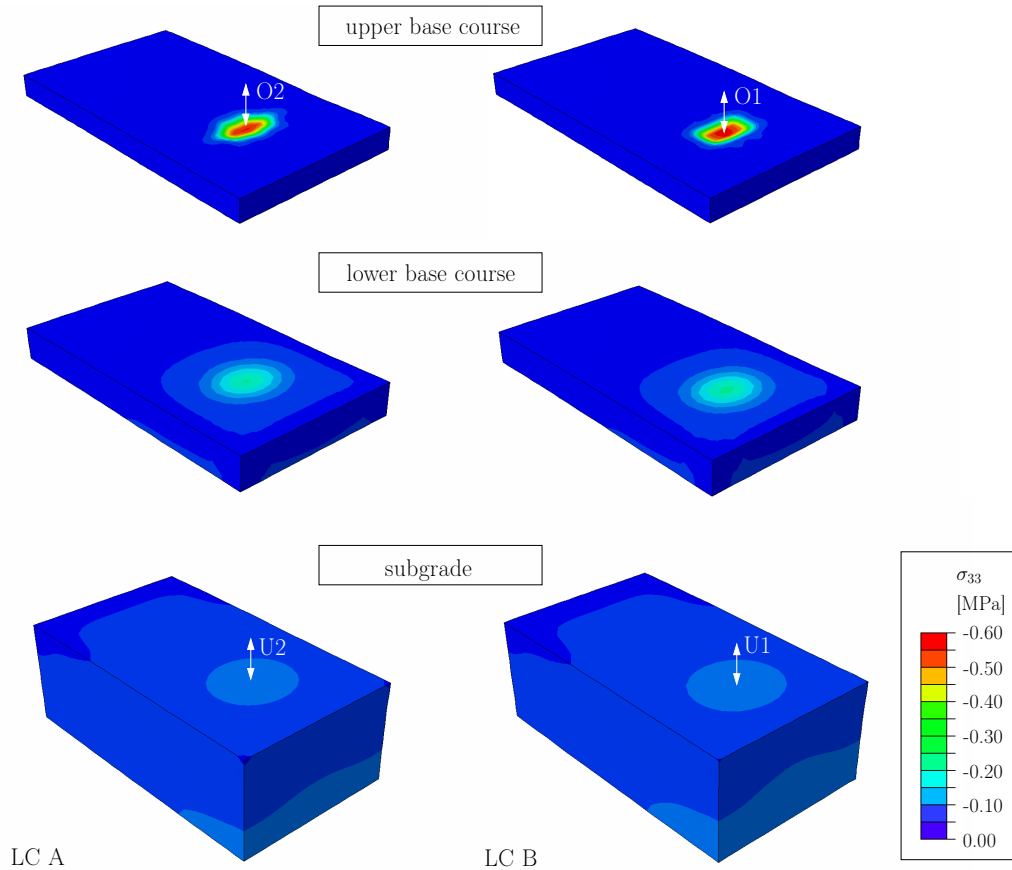

Figure 1.12: Relevant vertical stress states σ_{33} at the top of the base courses and the subgrade for Test Section 5, and the position of the relevant soil pressure cells (SPC).

In the next section, the measured stresses during the APT are compared to the numerically obtained results.

1.5   Comparison of experimental and numerical results

In the following, the results obtained from the two test sections (equipped with measuring devices) of the APT are compared to results from finite element simulations. Four soil pressure cells (SPC) were installed in Section 5, two at the top of the subgrade and the upper base course, respectively. At Section 7 two SPC were installed at the top of the subgrade. The measurement data was consolidated to mean values and the associated standard deviation of amplitude values (min/max values).

Figure 1.13 shows the comparison between the compressive stress values obtained from the SPC and the corresponding numerical results. The FEM values represent the mean vertical pressure over an area of 200/300 mm, equal to the measurement surface of the SPC. The individual lower values denote the mean pressure of a fictive SPC built-in with an eccentricity of 50/50 mm at the upper base course and 200/200 mm at the subgrade, respectively.
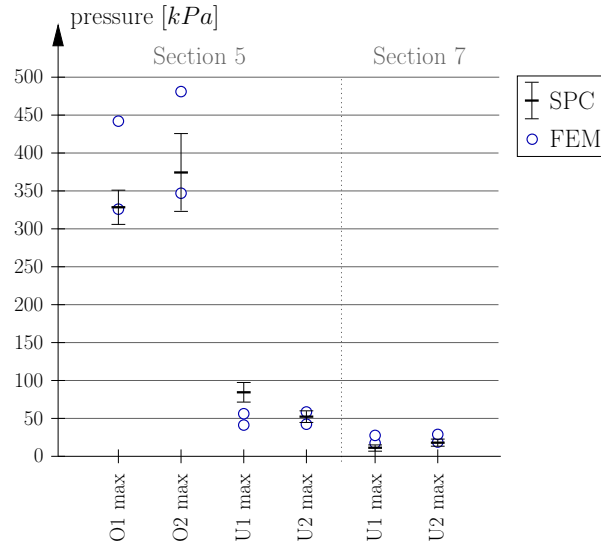

Figure 1.13: Mean values and standard deviation of maximum pressure values obtained from soil pressure cells compared to corresponding results from finite element simulations.

For all measuring points the experimentally and numerically obtained pressure values are in reasonably agreement. For a profound validation of the simulation tool, however, additional experimental data would be required.

1.6   Summary and concluding remarks

Within this paper, accelerated pavement tests (APT) using the Mobile Load Simulator (MLS10) on block pavements with sand filled joints were presented. Two test sections were equipped with soil pressure cells, allowing the recording of relevant pressure stress states in the base courses. These stress states were then compared to values obtained from a numerical simulation tool based on the finite element method, where the necessary material properties were acquired from different identification experiments. The main results and findings can be concluded as follows:

- The operation of the MLS10 on the three different test sections worked properly, and thus, this testing method can be recommended also for superstructures with paving blocks. The installed soil pressure cells (SPC) on the top of the upper base course and the subgrade were able to capture compressive stress peaks due to a tire rollover.

- On the basis of three different joint experiments, an appropriate characterisation of the tangential as well as normal mechanical behaviour of the sand filled joints was possible. The obtained mechanical behaviour could be implemented accurately

into the finite element model, using Mohr-Coulomb friction in tangential direction and a non-linear elastic material law in normal direction.

- For the first time, the complex bedding and interaction behaviour of paving blocks could be considered within a numerical simulation tool realistically. A comparison between the experimentally- and numerically-obtained pressure stress states in the base courses showed a reasonable agreement. Nevertheless, the punctual conducted pressure measurements cannot be considered as sufficient for a profound validation of the proposed numerical simulation tool.

In a next step, this simulation tool will be used to study two important load transfer mechanisms in block pavement structures which were not considered sufficiently so far: (i) the load transfer of horizontal loads into the structure (exemplarily shown in Figure 1.14(a)) and (ii) the influence of arch supporting effects on the load bearing capacity (exemplarily shown in Figure 1.14(b)). Basic numerical investigations of the latter mechanism have already been performed and can be found in Hengl and Füssl (2016). Both mechanisms are strongly influenced by the joint behaviour, the block shape and dimensions, and the laying pattern. All this can be considered very well with the developed simulation tool, and thus, meaningful results can be expected.
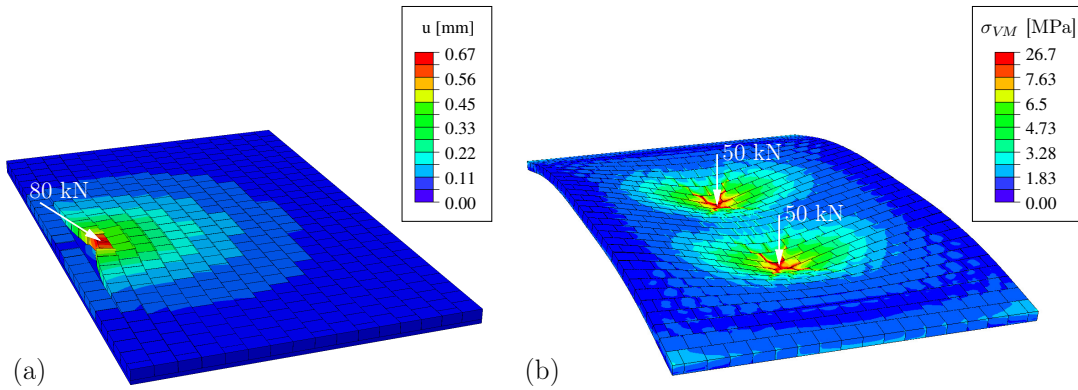
Figure 1.14: Future applications of the simulation tool: (a) study of the horizontal resistance of block pavement superstructures, and (b) determination of the influence of arch supporting effects on the load bearing capacity of paving block superstructures.

1.7 Appendix A: Data obtained from soil pressure cells (SPC)

Figure 1.15: Data obtained from soil pressure cells (SPC) O1 and O2, installed on top of upper base course, of Section 5.

Figure 1.16: Data obtained from soil pressure cells (SPC) U1 and U2, installed on top of subgrade, of Section 7.

1.8   Appendix B: Drucker-Prager cap model

The modified Drucker-Prager cap model is illustrated in Figure 1.17. It consists of a

Figure 1.17: Yield surface of the modified Drucker-Prager cap model (a) along the hydrostatic axis and (b) in the meridial plane.
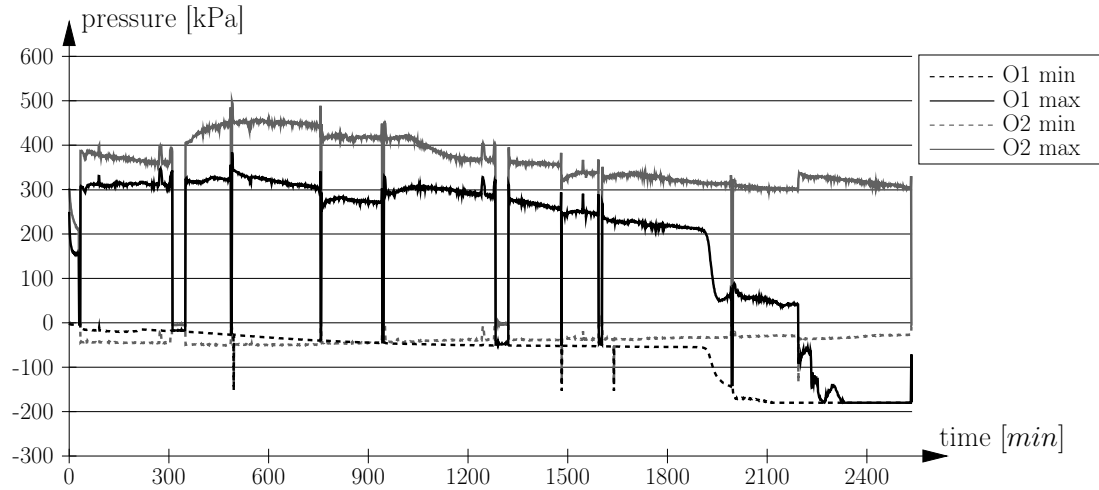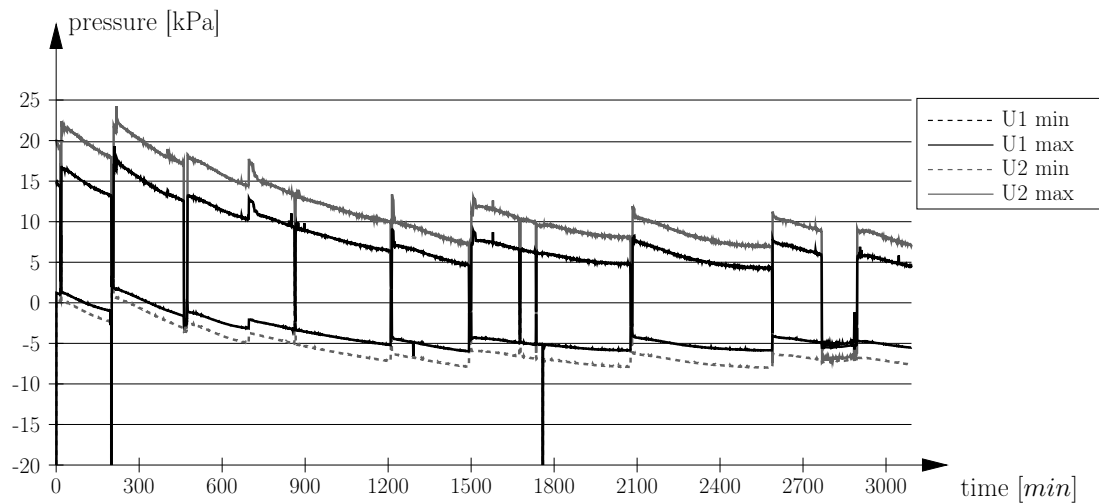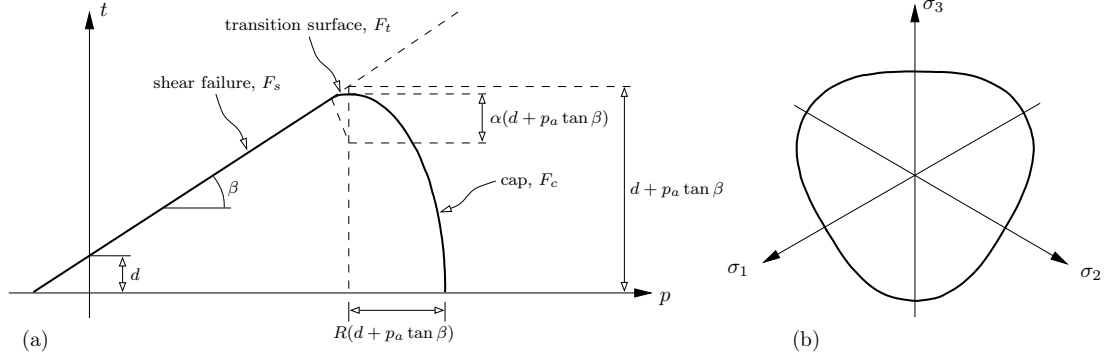
failure surface describing shear failure, which reads

$$F_s = t - p \tan \beta - d = 0 \qquad (1.4)$$

and a surface defining the plastic behaviour under predominantly volumetric compressive stress states, reading

$$F_c = \sqrt{(p - p_a)^2 + \left[\frac{Rt}{(1 + \alpha - \alpha/\cos \beta)} \right]^2} - R(d + p_a \tan \beta) = 0, \qquad (1.5)$$

where $p = -1/3\sigma_{ii}$ is the equivalent pressure stress, $q = \sqrt{3/2(\boldsymbol{\sigma}_d : \boldsymbol{\sigma}_d)}$ the Mises equivalent stress, and $r = (9/2\boldsymbol{\sigma}_d \cdot \boldsymbol{\sigma}_d : \boldsymbol{\sigma}_d)^{1/3}$ the third invariant of deviatoric stress with $\boldsymbol{\sigma}_d = \boldsymbol{\sigma} + p\mathbf{I}$. A deviatoric stress measure is defined as

$$t = \frac{q}{2} \left[1 + \frac{1}{K} - \left(1 - \frac{1}{K} \right) \left(\frac{r}{q} \right) \right]. \qquad (1.6)$$

The evolution parameter, p_a, reads

$$p_a = \frac{p_b - Rd}{(1 + R \tan \beta)}, \quad \text{and} \qquad (1.7)$$

the transition surface F_t between F_s and F_c is given by

$$F_t = \sqrt{(p - p_a)^2 + \left[t - (1 - \frac{\alpha}{\cos \beta})(d + p_a \tan \beta) \right]^2} - \alpha(d + p_a \tan \beta) = 0. \qquad (1.8)$$

The evolution of hardening is derived from the experimental results in Chiroux et al. (2005). The implemented relation between the hydrostatic yield stress and the volumetric plastic strain is given in Table 1.3.

Finally, with the parameters shown in Table 1.4 the loading plate tests could be reproduced very well.

hydrostatic yield stress [MPa]	volumetric plastic strain [–]	hydrostatic yield stress [MPa]	volumetric plastic strain [–]
0	0	0.10	0.0845
0.01	0.0141	0.15	0.1021
0.03	0.0373	0.30	0.1241
0.05	0.0551	0.40	0.1335
0.07	0.0690	0.50	0.1405

Table 1.3: Cap hardening stress/strain relationsship (derived from experimental data in Chiroux et al. (2005))

hydrostatic yield stress [MPa]	volumetric plastic strain [–]	hydrostatic yield stress [MPa]	volumetric plastic strain [–]
0	0	0.10	0.0845
0.01	0.0141	0.15	0.1021
0.03	0.0373	0.30	0.1241
0.05	0.0551	0.40	0.1335
0.07	0.0690	0.50	0.1405

Table 1.4: Material parameters

1.9 Acknowledgments

Chapter 2

The influence of superelevated profiles of paving block structures on their load-bearing behavior (Hengl and Füssl, 2016)

Paving block pavements are an ecological, economical and space forming valuable type of road surface, and therefore, the demand is continuously increasing. Nevertheless, immature design concepts often lead to unexpected performance, which reduces confidence in these structures. For example, positive effects on the load-bearing behavior due to superelevation of the cross profiles are not considered within existing design concepts, even though their influence on the performance of a block pavement structure is, according to the experience of skilled engineers, very large.

For this reason, this work focuses on the influence of superelevated cross profiles of paving block structures on their load-bearing behavior. A 3D finite element model has been developed, which is able to take the interaction behavior between paving blocks, in tangential as well as normal direction, accurately into account. Numerous parameter studies were performed to identify the influence of structural parameters, like the size of the superelevation, the number and dimension of paving blocks, the interaction between them, and the loading situation, on the structural behavior.

From these simulations, two different predominating structural failure mechanisms could be identified: (i) snap through buckling, for very small superelevations of the cross profile, and (ii) the formation of a kinematic chain, which is initiated very fast for high superelevations. At the transition from one to the other mechanism, the highest loading capacity of a paving block structure could be numerically observed. The corresponding superelevation, for a specific road width, changes interestingly only very low with changing boundary and interaction conditions. Therefore, based on comprehensive numerical calculations, it was possible to define an optimal region of superelevation-to-

road-width ratios. Moreover, a huge influence of the cross profile on the load bearing capacity of block pavement structures could be detected mechanically sound for the first time. Consideration of these effects within the design process may strongly improve the performance prediction of paving block constructions.

2.1   Introduction and Motivation

In recent years, concrete block pavements have become a favorite alternative to asphalt pavements, mainly in intra-urban regions due to their architectural design possibilities. Unfortunately, the design concepts are compared to asphalt pavement structures less sophisticated, which often leads to unexpected performance and, thus, reduces confidence in these structures. More knowledge about the support mechanisms of these systems and advanced prediction tools are necessary to exploit the potential of this type of construction and to serve as basis for a more extensive use and possible new areas of application. In the following, a brief overview of the rather low research activity regarding simulation tools for paving block structures is given.

Nishizawa (1984) was one of the first who investigated such structures with a finite element approach. For that, he developed a numerical model with 2D rectangular plate elements with joints modeled as a set of springs and the sub-base in form of a liquid foundation. Another 2D finite element analysis was carried out by Jacobs (1988), where linear spring elements were connecting indeformable rigid body block elements. Huurman (1992) assumed that the properties of the paving blocks have a minimal effect on the response behavior of the whole pavement structure. He used a finite element model with paving blocks interconnected by 4 sets of 3 springs for each joint, which was placed on four layers of bedding and was subject to a vertical loading.

The first 3D finite element approach can be found in Huurman (1992). Therein, the interactions between the paving blocks were again modeled by springs. Displacement, stress and strain information for the paving blocks, as well as for the baselayers and subgrade was obtained. Higher bending stresses were determined in case of higher joint stiffness. Hassani (2006) made use of shell elements to model the paving blocks as well as the joint sand between them. Lerch (2005) and Ascher (2006) modeled the interaction between the blocks with elements of zero thickness. To integrate a non-linear interaction behavior, the elastic as well as the shear modulus was adjusted iteratively during the analysis. Later, contact laws were implemented to model an elastic-plastic interaction behavior between the paving blocks, where the elastic part depends only on the contact pressure between elements and the plastic part depends on the number of load changes. Nejad (2006) chose contact elements to model interactions, finding out that the jointing width, as well as the shape, size and thickness of the paving blocks have a significant influence on vertical deformations of paving block structures. Mampearachchi (2010) used a 3D finite element model to perform a parametric study in order to determine necessary improvements for weaker support conditions of concrete block pavings. In the work of Oeser (2010) a sophisticated computational model is presented using elastic as well as plastic interaction properties. In Füssl (2015b,c, 2016) a 3D numerical simulation tool for concrete paving slabs is presented, in which both the joint behavior as well as the behavior of all base courses is modeled non-linear.

To the knowledge of the authors, paving block structures with superelevated profiles have never been investigated using numerical simulation tools. Even in design codes or guidelines for the design and construction of paving block structures, especially in the

Austrian design code RVS 03.08.63(2008), an superelevation of the cross profile of paving block structures is not considered. Nevertheless, observations in practice suggest a strong influence of superelevated profiles on the overall performance of such structures. Many experienced engineers state that these effects should not be neglected within the design process. The resulting motivation of this work is to develop a numerical simulation tool which is able to capture the effect of such profiles on the load-bearing behavior of paving block structures, qualitatively as well as quantitatively to a certain extent. Based on this motivation, the following objectives of this work can be formulated:

- The definition of an appropriate 'sub'-model of a paving block superstructure, being sufficient to depict the above mentioned effects, and an automated generation of the whole model geometry to allow for an efficient investigation of the influence of different cross profiles,

- an accurate description of the non-linear interaction behavior between paving blocks,

- the identification of the load-bearing mechanisms depending on the superelevation as well as the main failure mechanisms, and

- the influence of the load position, the boundary conditions, the number and dimension of paving blocks, and the joint properties on the structural performance.

Finally, a mechanically sound evidence for the positive influence of superelevated profiles on the performance of paving block structures should be provided.

In the following section, Section 2, the numerical simulation tool is proposed, while the identification of structural failure mechanisms based on the numerical results is subject of Section 3. Subsequently parameter studies are shown in Sections 4. A brief summary, concluding remarks and a future outlook are given in Section 5.

2.2   Simulation tool

Since normally a road is superelevated only in transverse direction, to capture the main influence of its superelevation on the mechanical performance and to analyze the structural behavior introduced by the banked cross profile, the consideration of only one paving block row, as shown in Figure 1, was considered sufficient. Moreover, to isolate the structural behavior of the paving blocks, the underlying base layers were not modeled. It is obvious that with such a model no direct quantitative assessment of the structural performance due to superelevated profiles is possible. Nevertheless, structural failure mechanisms can be investigated very well and, as it will be shown, the main parameters influencing the structural response can be identified. The superelevated profiles of all models have a parabolic shape with a maximum height H between 0 cm and 60 cm. The length of the paving block row L_R was set to a fixed value of 3 m, which corresponds to a typical single-track road width. The length L is the projection of the length L_R to the horizontal x_1-x_2 plane, and varies with the height H of the profile. In a first step, the dimensions of the paving blocks were set to an industry standard of 200/100/100 mm. Additional paving blocks with dimensions of 100/100/100 mm were used as curbstones. As illustrated in Figure 1, the basic model consists of 14 paving blocks and 2 curbstones. To the paving blocks a linear elastic material behavior is assigned, with an elastic modulus of 45 000 N/mm^2 and a Poissons ratio of 0.15. These
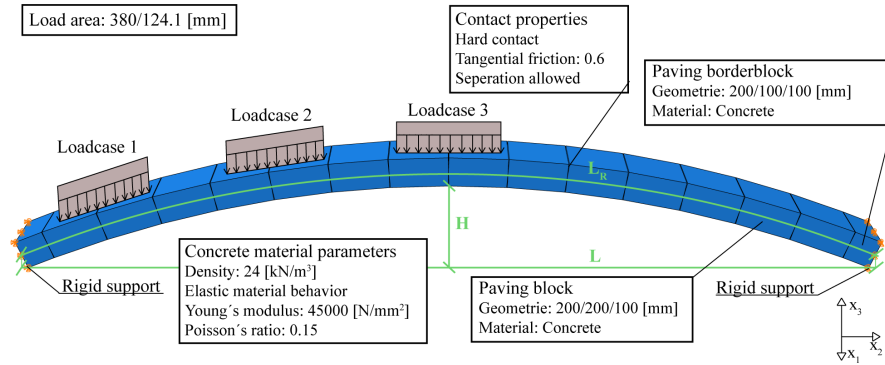
Figure 2.1: Geometry, boundary conditions, loading cases and material properties of the numerical model.

values were measured for concrete paving blocks using an ultrasonic measurement device in Füssl (2015b). Moreover, a density of 24 kN/m^3 is assigned to all paving blocks to take their dead load within the simulation into account. The interactions in lateral road direction, i.e. the interactions in normal direction to a blocks surface between paving blocks are defined as hard contact. The interaction behavior in tangential direction obeys the classical Mohr-Coloumb friction law, with a friction coefficient of 0.6, which was obtained from vertical shear tests in Füssl (2015a). The separation of surfaces is allowed, as well as no tensile force can be transferred through the joints between the paving blocks.

The displacements of the outer surface of the two curbstones are prevented, in all spacial directions, which prevents any translational and rotational movements of these two paving blocks at the boundary of the structure. All lateral paving block surfaces are supported in longitudinal road direction (x1-direction) by an elastic foundation with a bedding modulus of 15 N/mm^3, which is representative for the stiffness of the sand layer in the joint to the next row of paving blocks. Normal joint behavior experiments were carried out at the TVFA Vienna, confirming the magnitude of this value.

In a first analysis step the dead-load and in a second analysis step a fictitious wheel-load, on an area of 380/124 mm, were applied. The models are descretized with approx-
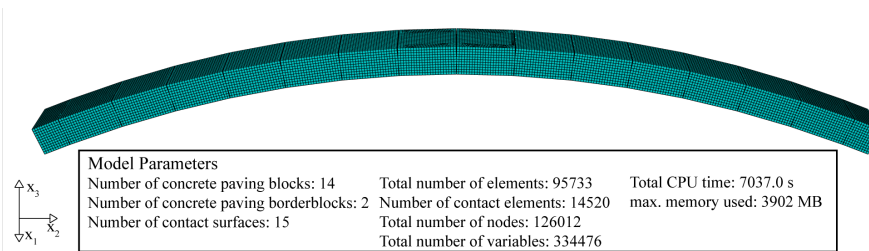

Figure 2.2: Exemplary finite element discretization of one numerical model and corresponding model parameters.

imately 95 000 elements, which is the result of a mesh size of 9 mm and a slightly finer mesh on the surface under the load area. Figure 2 exemplarily shows the discretization of one model. The finally chosen mesh is a compromise between computation time and result accuracy. As Figure 3 indicates, the influence of discretization is convergent with a raising number of elements.
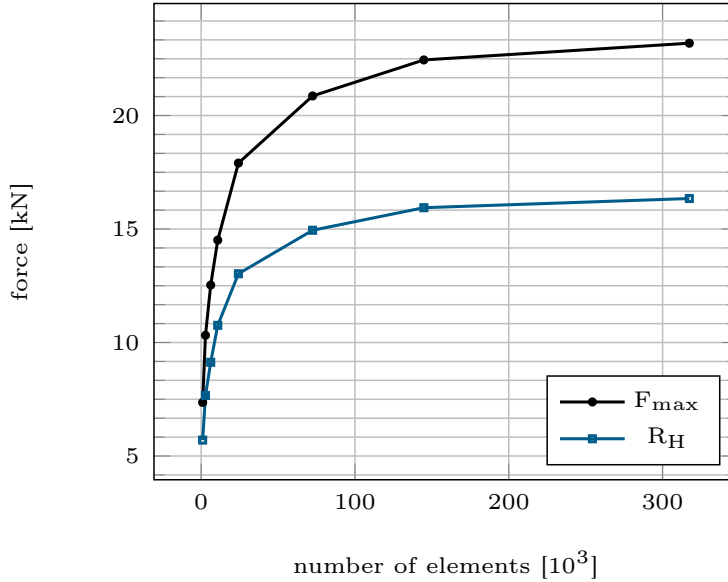

Figure 2.3: Maximum applicable wheel load F_{max} and corresponding horizontal reaction force R_H as a function of number of finite elements, determined at a model with a superelevated profile with H = 0.104 L.

For the generation of the finite element model and the further variations of parameters a python script was written, consisting of about 2 500 lines of code. Through a user interface, this script allows the definition of several parameters, such as the dimensions of the paving blocks, the banked profiles, the road width, the number of rows, as well as material and contact parameters. Next, this script runs an iterative procedure to create the geometry, and finally, all interaction are determined and the corresponding material parameters are assigned. This script enabled us to perform a high number of simulations, particularly as it was combined with a second script, which was varying the input parameters automatically.

2.3 Numerical results – identification of failure mechanisms

Within this section, first numerical results of the proposed simulation tool are presented and the basic structural failure mechanisms derived therefrom are explained. Typical load-deformation relationships for three different H/L ratios of the model geometry (shown in Figure 1) are illustrated in Figure 4. To be able to clearly determine the maximum wheel load F (black circles in Figure 4), later referred to as F_{max}, an arc length method based on the Riks-Wempner method was used to control the application of load increments. Thereby, the iterations are not performed at a constant external
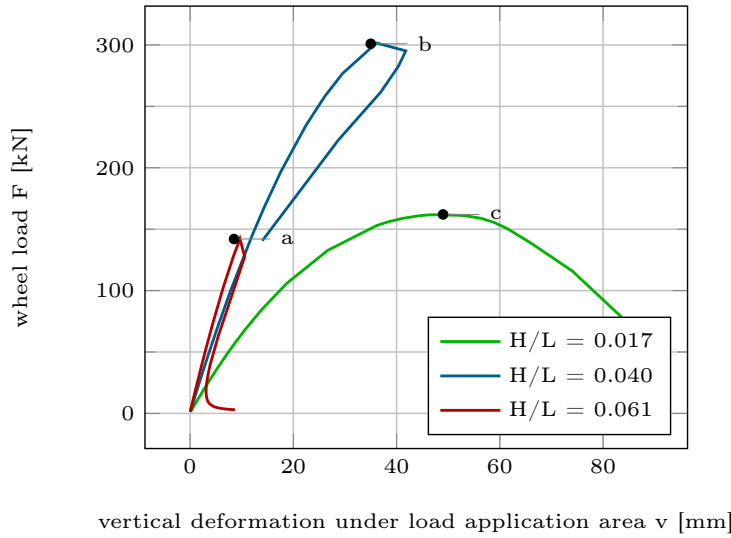
Figure 2.4: Typical load-deformation relationships for three different superelevations (H/L ratios of the model geometry) under LC2, obtained using an arc length method (Riks-Wempner-Method) controlling the application of load increments.

load, but at a generalized displacement vector, which gets extended by a load factor. With this approach it was possible to reliably determine the maximum wheel load F_{max} for H/L ratios from 0.003 to 0.15, shown in Figure 5.

As the paving blocks are not rigidly connected and there is no cohesive behavior assumed between the blocks, tangential forces can only be transmitted through friction. Therefore, for paving block structures with no elevation, no equilibrium state can be found. Starting at low superelevations, with increasing superelevation (H/L ratio) the maximum applicable load, F_{max}, increases quickly, reaching a maximum value at a certain superelevation and decreases quickly immediately thereafter. This highly non-linear distribution indicates a change in the structural failure mechanism over the investigated range of H/L ratios. Indeed, two basically different mechanisms could be observed by analyzing the corresponding deformation fields of all models. At low elevations H, 'snap through buckling' of the structure is the dominant failure mode, determining the ultimate load F_{max}. Tensile stresses due to bending of the structure are in large parts overpressed by compressive stresses resulting from the arch effect due to the elevation. With increasing superelevation (H/L ratio) the horizontal pressure force in the structure decreases, as shown schematically in Figure 6 (state $\bar{a}$ to state a), and for this reason 'snap through buckling' occurs at a higher force F. On the other hand, the bending moment introduced by the distance a (defining the difference between the structures' geometry and the ideal load transfer path), shown in Figure 6(a), increases and the main failure mechanism is dominated by the formation of a 'kinematic chain'. The term 'kinematic chain' refers to a system, where the number of support reactions is smaller, than the number of possible directions of movement, therefore at least one direction of movement counteracts no bearing reaction and the system can move or rotate freely in this direction.
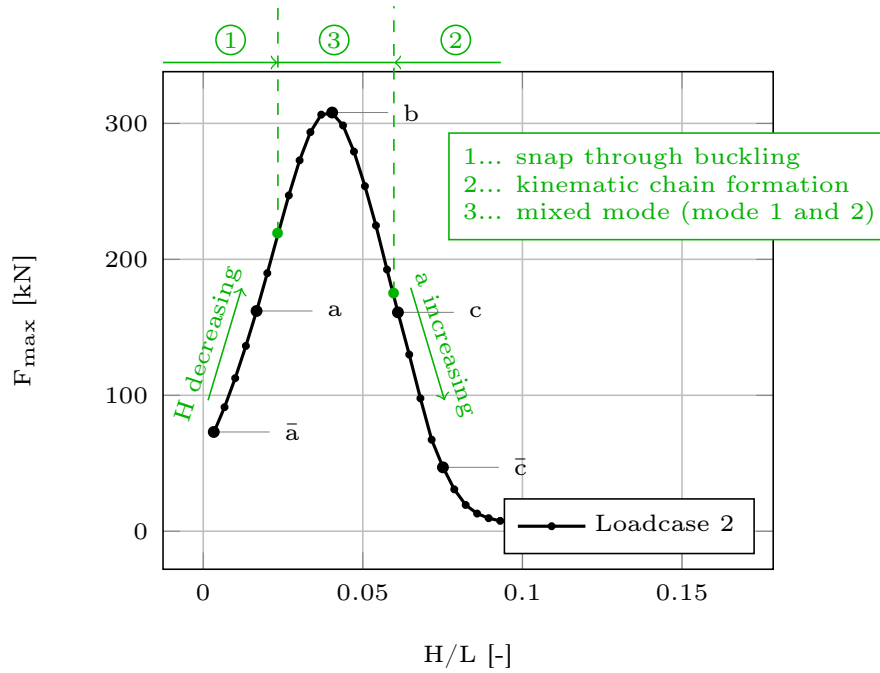
Figure 2.5: Maximum wheel load as a function of the H/L ratio
for LC2. Assignment of numerically-identified structural
failure mode (1, 2, or 3) to H/L ratio regions.

With a further increase of the superelevation H, the distance a also increases (as shown in Figure 6(c) to Figure 6($\bar{c}$)) and the formation of the 'kinematic chain' is introduced at a lower load F. Based on this evaluation of deformation fields, the dominating failure mechanisms are assigned to ranges of H/R ratios in Figure 5.

Representative deformation states (for points a, b, and c in Figure 5) at the ultimate load F_{max} are shown in Figure 7. The structures in Figure 7 (a) and (c) can resist about the same load but show a totally different failure mechanism. The former fails due to 'snap through buckling' while it comes to the formation of a 'kinematic chain' in the latter. Thereby the tensile stresses resulting from bending moments cannot be over-pressed entirely by the compressive stresses induced by the arc effect. Gradually gaps are opening between the blocks, initiating the afore mentioned transition to a unstable, statically under-determined system. The contacts where these gaping occurs behave similar to 'hinges', and thus, they are called as such subsequently. The occurring 'hinges' and their order of appearance are marked in Figure 7. Moreover, the load-deformation behavior is significantly different between these two failure modes, as can be seen in Figure 4. At lower elevations and 'snap through buckling', respectively, the effective stiffness of the structure is much smaller and the post-peak failure behavior is more stable.

So far, only loadcase 2 has been considered and the boundary conditions as well as the dimensions of the paving blocks and their interaction behavior have been kept constant. Within the following section, all these parameters are varied and the influence of these variations on the relationship presented in Figure 5 will be shown.
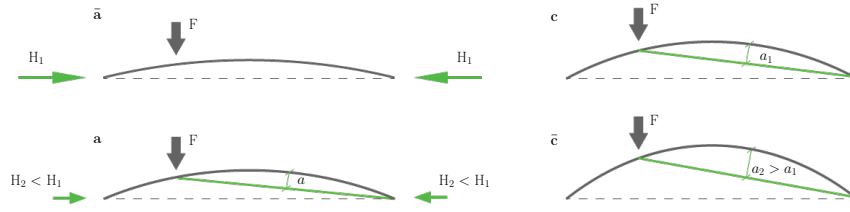
Figure 2.6:   Schematic representation of the most important variables to describe the structural behavior in principal.

(a) LC2, H/L=0.017, def. scale factor=1

(b) LC2, H/L=0.040, def. scale factor=3
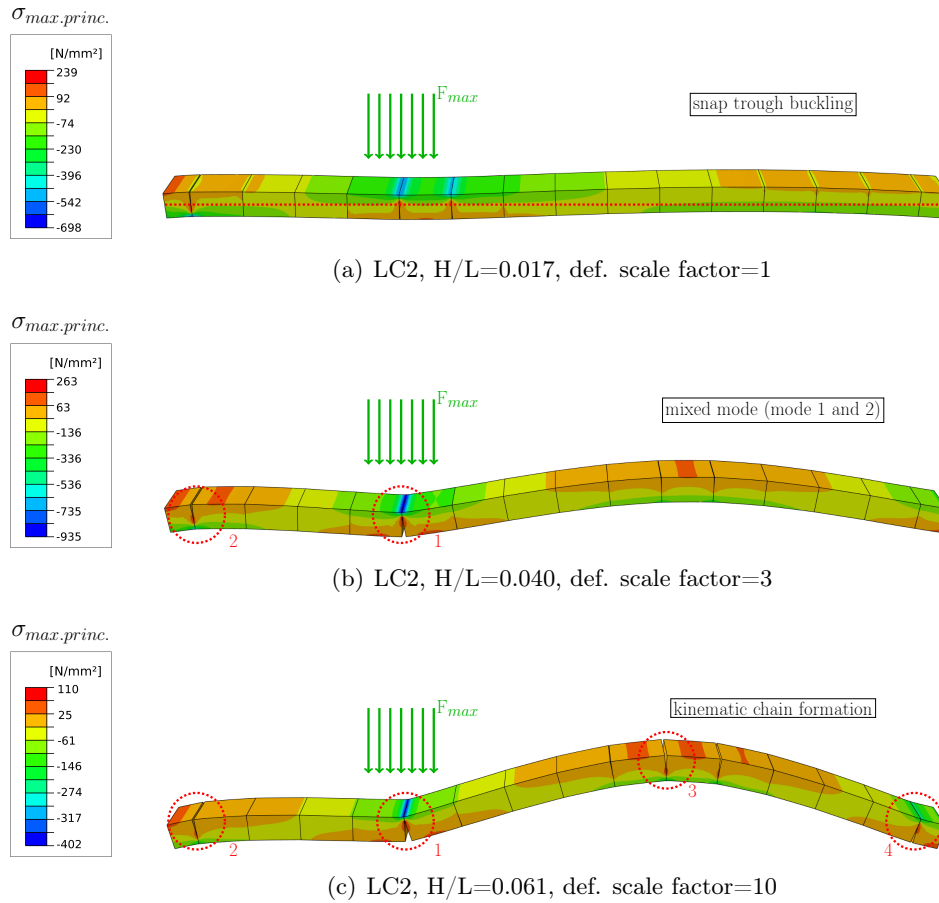

(c) LC2, H/L=0.061, def. scale factor=10

Figure 2.7:   Illustration of the three different failure mechanisms obtained: (a) Snap through buckling, (b) mixed failure mode, and (c) kinematic chain failure.

2.4   Numerical results – parameter studies

Figure 8 shows the relationship, presented in Figure 5 for LC2, between the ratio of the elevation H of the paving block structure and the road width L, H/L, and the maximum applicable wheel load F_{max} for the three different LCs defined in Figure 1. As the wheelload moves away from the center (LC3), the distance between the theoretically optimal supportline and the possible load transfer path increases and, for this reason, the structure experiences higher bending moments. Thus, the maximum applicable loads at almost all superelevations are smaller, but again increase when the load comes closer to the supports. If we consider the three chosen LCs as representative for the overall loading of the pavement structure, an optimum ratio H/L can be identified as the maximum value of the area enclosed by the three graphs in Figure 8. Selected numerical
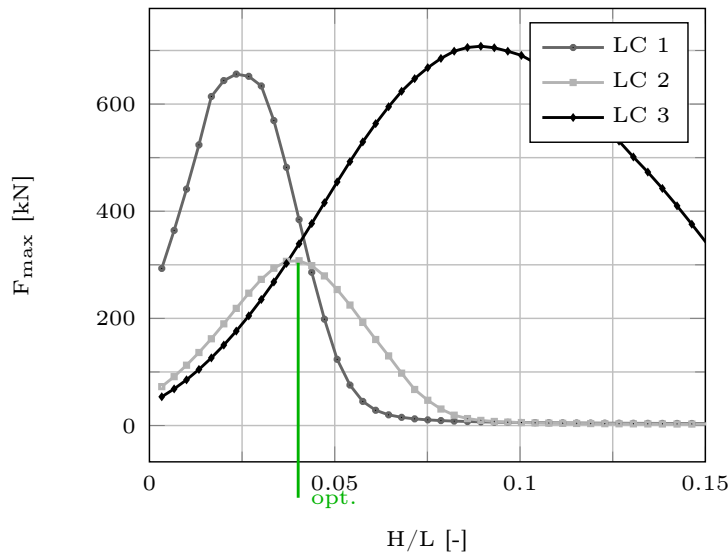
Figure 2.8: Maximum applicable wheel load F_{max} as a function of the superelevation (H/L ratio), for all three considered LCs.

results for an H/L ratio of 0.15 and for four different LCs are shown in Figure 9, giving a good impression of the arising 'kinematic mechanisms' at the point of structural failure. Figure 9(a) shows that paving blocks can shear off in combination with the 'kinematic chain' failure when the load application is located near a support of the structure. In a next step, the question will be answered how the optimum H/L ratio is affected by the following structural properties:

1. The horizontal stiffness of the boundary conditions, representing the horizontal stiffness of the whole structure,

2. the number of paving blocks,

3. the frictional behavior of the vertical joints,

4. the height of the paving blocks, and

5. the material strength of the paving blocks.

(a) LC1, H/L = 0.15, deformation scaling factor = 450

(b) LC2, H/L = 0.15, deformation scaling factor = 450

(c) LC3, H/L = 0.15, deformation scaling factor = 15

(d) LC4 (two wheels), H/L = 0.15, deformation scaling factor = 400

Figure 2.9:   Illustration of the kinematic chain formations for a structure with a very high H/L ratio of 0.15, for four different LCs.
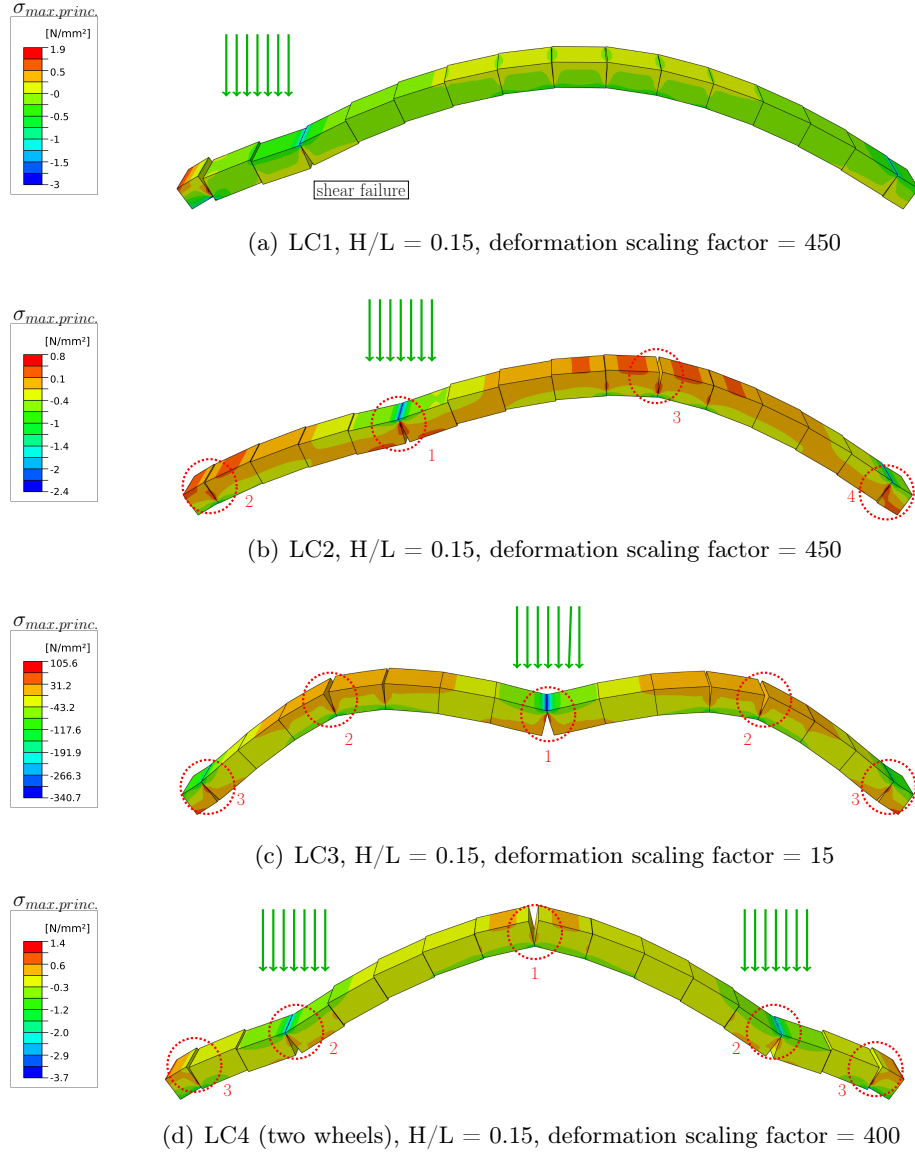
1. Horizontal support stiffness

Figure 10 shows the maximum applicable wheel load F_{max} (for LC2) as a function of the horizontal support stiffness of the structure, for two different H/L ratios. As expected, F_{max} decreases with decreasing horizontal support stiffness, until no structural resistance is available at zero horizontal support stiffness. This trend was observed for all elevations in a similar manner. Whereas for superelevations associated with the failure mode 'snap through buckling', the increase of F_{max} with increasing horizontal support stiffness is steeper. This means, conversely, that pavement structures with a low superelevation are slightly more sensitive, within the practical relevant region of support stiffnesses from 0 to 50 N/mm^3, with respect to a reduction of the horizontal structural stiffness than strong superelevated structures.
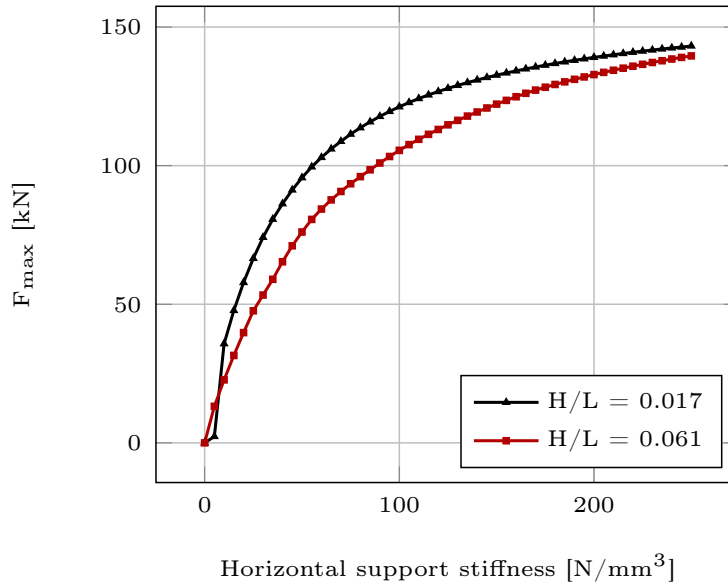
Figure 2.10: Maximum applicable wheel load F_{max} (for LC2) as a function of the horizontal support stiffness, for two different H/L ratios.

To determine how the optimum elevation, defined before and shown in Figure 8, depends on the horizontal support stiffness, the same relationships as shown in Figure 8 were determined for two additional boundary conditions, a support stiffness of 5 and 50 N/mm^3. The results for all three boundary conditions are illustrated in Figure 11. While the overall level of structural resistance strongly decreases with 'softer' lateral support, the optimum H/L ratio interestingly changes very little. Taking into account the horizontal support stiffness of such a structure, the range of the optimum elevation can now be defined as 0.030 to 0.039 L.
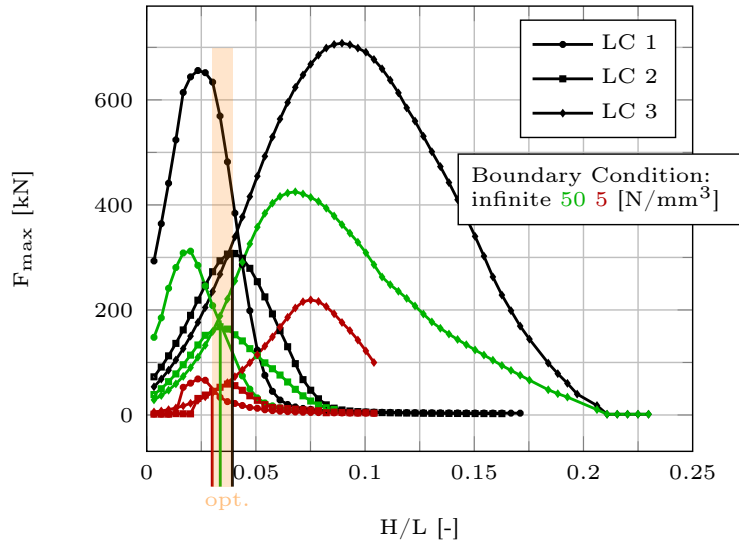
Figure 2.11: Maximum applicable wheel load F_{max} as a function of H/L ratio, for three different LCs and for three different horizontal support stiffnesses (5 N/mm^3, 50 N/mm^3, and 'rigid').

2. Number of paving blocks

Next, the influence of the number of paving blocks per meter arc length on the load-bearing behavior of the structure is investigated (see Figure 12). With an increasing number of paving blocks the system becomes weaker. This effect is more pronounced at high elevations, as can be clearly seen in Figure 12 by comparing the relationships for H/L ratios of 0.017 and 0.061. At elevations where 'kinematic chain' failure can be expected, more paving blocks increase the structural degrees of freedom and, thus, the structural resistance is decreased. This can also be seen in Figure 13, where F_{max} is plotted over the H/L ratio of structures with 5 and 15 paving blocks per meter arc length, which represents the range of practical application. The corresponding area of optimum elevation is between 0.028 and 0.039 L.

3. Joint behavior

Another important parameter which has to be considered is the friction coefficient between the paving blocks, representing the maximum frictional resistance between paving blocks defined by the product of the compressive stresses between the paving blocks and the friction coefficient: $\tau_{res} = \sigma_n \cdot \mu$. When the frictional shear stress exceeds the frictional resistance in all points of a surface to surface contact, sliding occurs till equilibrium is found again or the system collapses. Models with frictionless joint behavior can not resist any load, they turn kinematic and collapse. On the other hand, friction coefficients higher than 0.2 do not contribute to the maximal applicable load anymore, because the maximum occurring frictional shear stress is already covert, as the results in Figure 14 in-
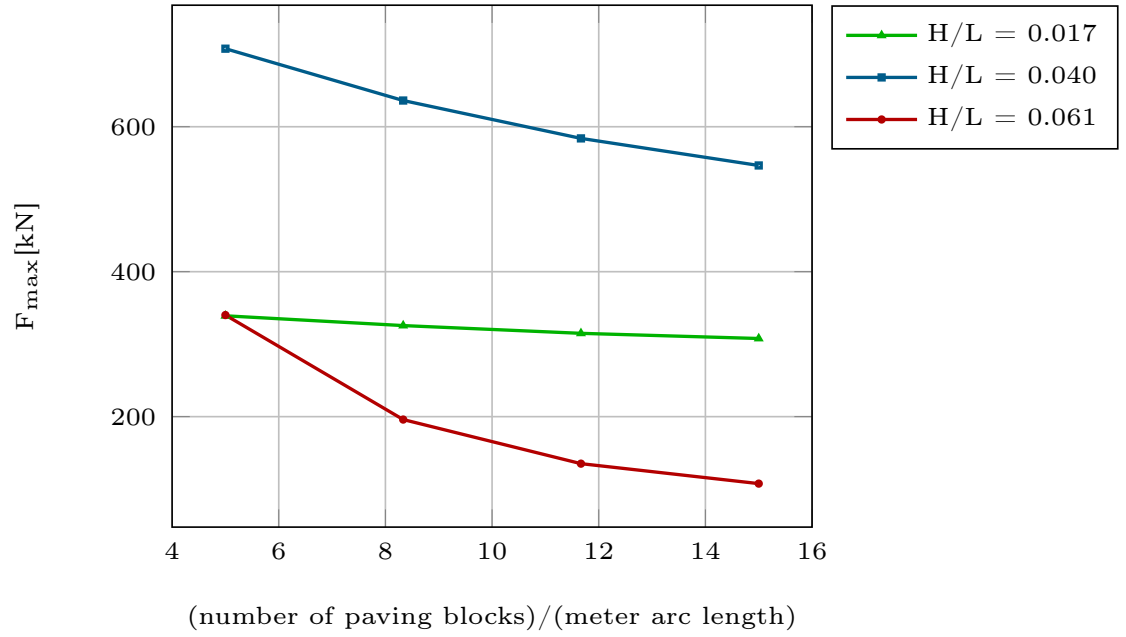
Figure 2.12:   Maximum applicable wheel load F_{max} (for LC2) as a function of the number of paving blocks per meter arc length, for three different H/L ratios.
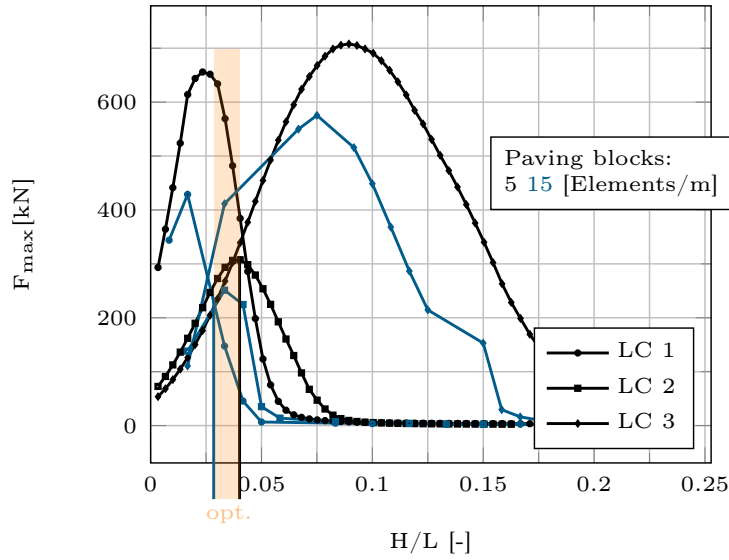

Figure 2.13: Maximum applicable wheel load F_{max} as a function of H/L ratio, for three different LCs and for two different number of paving blocks per meter arc length (5 and 15 paving blocks / meter).

dicate. As the friction coefficient of 0.2 is already exceeded by most paving block structures customary in the market, no further simulations were run regarding the joint behavior.
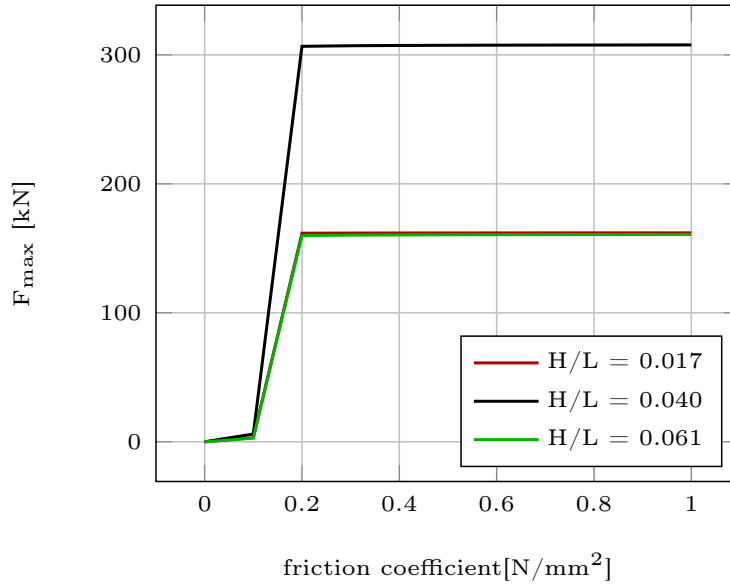
Figure 2.14:   Maximum applicable wheel load F_{max} as a function of the friction coefficient in vertical joints.

4. Height of paving blocks

Further, the height of the paving blocks directly influences the stresses present in the simulated pavement structures. Figure 15 shows the simulation results for different H/L ratios and paving block heights of 80, 100, and 120 mm. Again the range of optimum elevations was found to be in a similar range as for the structural properties investigated before, between 0.030 and 0.040 L.

5. Material strength of paving blocks

As all of these simulations were not restricted by material strength parameters, very high loads could be applied to the structures. To obtain more realistic values for the load bearing capacity of the investigated structures and to identify the impact on the optimum superelevation, F_{max} was determined as the wheel load under which the maximum principal stress in the paving block reaches a strength value of 50 N/mm^2, which represents the upper boundary of the common block pavement material strength range. The results from this evaluation, illustrated in Figure 16, show that the optimal elevation lies at 0.042 L.
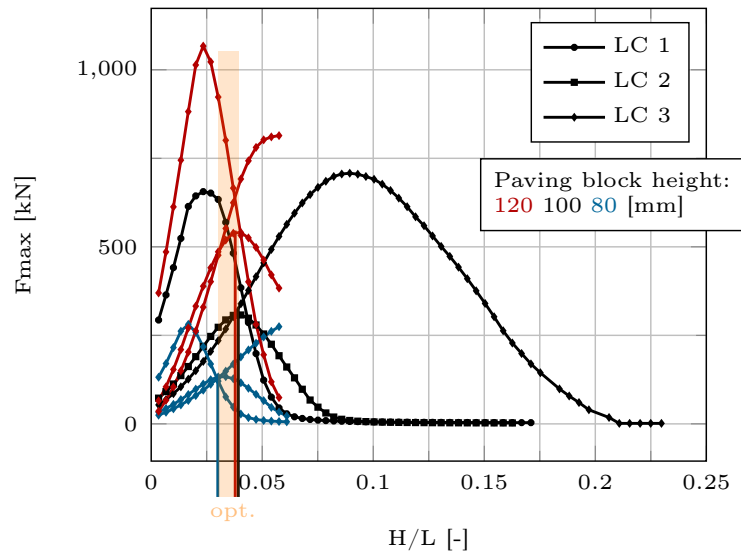
Figure 2.15: Maximum applicable wheel load F_{max} as a function of H/L ratio, for three different LCs and for three different paving block heights (120, 100, and 80 mm).
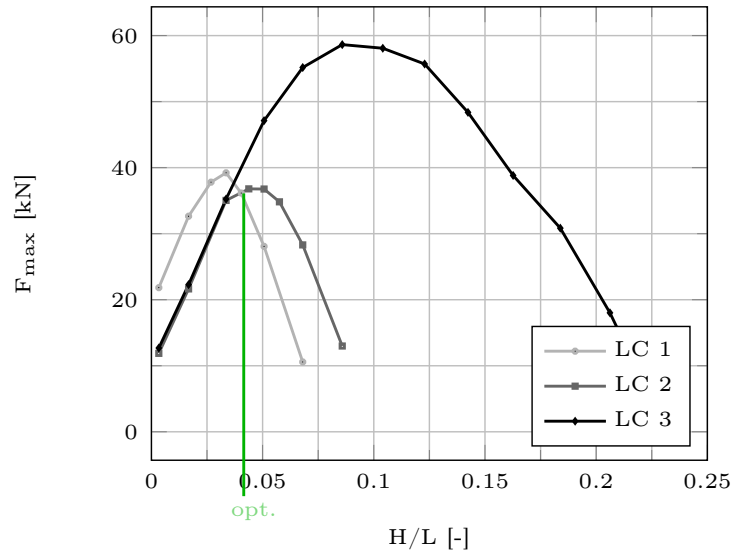

Figure 2.16: Maximum applicable wheel load F_{max} as a function of H/L ratio, taking into account a maximum principal stress of 50 within the paving blocks.

2.5   Conclusion and Outlook

Within this work, the effect of superelevated profiles of paving block structures on their load-bearing behavior has been investigated using a numerical model. The modeling of only one paving block row was considered to be sufficient to capture the main structural failure modes. Hundreds of non-linear numerical simulations have been carried out, with an average of 335 000 degrees of freedom and an average calculation time of 3.5 hours. The generation of all models as well as the calculations themselves were controlled by a phython script, allowing for an efficient processing of the simulation program, especially with regard to the creation of the different model geometries.

Based on the obtained results from this comprehensive simulation program the following conclusions can be drawn:

- With the developed simulation tool the load-bearing behavior of superelevated paving block structures could realistically be reproduced. The use of an arc length method to control the application of load increments allowed for a reliable determination of limit loads for different paving block structures, and, thus, allowed for a mechanically-sound analysis of such structures.

- The load carrying capacity of the investigated paving block structures is activated by compressive stresses at the contact surfaces between paving blocks, depending on the shape of the superelevated profile. These compressive stresses allow tangential forces to be transmitted between paving blocks by frictional resistance and occuring bending moments are suppressed until it comes to structural failure.

- Through an accurate description of the non-linear interaction behavior between paving blocks, taking into account the frictional behavior in tangential direction and the separation in normal direction, the structural behavior of superelevated paving block structures could be simulated realistically. Two main failure mechanisms could be identified, 'snap through buckling' and a mechanism characterized by the development of a 'kinematic chain'. The maximum applicable wheel load as well as the occurring failure mechanism depends on the size of the superelevation.

- Considering three different loading situations and a large number of different superelevations, a range of optimal superelevations could be identified. Interestingly, the effect of different structural properties, such as horizontal support stiffness, paving block dimensions, number of paving blocks, etc., on this range is smaller than expected. For all investigated structures, the optimum superelevation lies between 0.028 and 0.042 times the road width. This optimum superelevation seems steep, especially compared to the recommended lateral elevation for surface drainage which lies between 2% and 2,5% as in RVS (2009). But even a lower superelevation will show positive effects on the structures behavior.

- In order to make reliable quantitative statements with respect to the load carrying capacity larger sub-models, including several paving block rows and base layers, probably need to be investigated. Nevertheless, based on these results, the positive influence of superelevated profiles on the load-bearing behavior of paving block structures can be confirmed.

In order to investigate the influence of different laying patterns of paving blocks on the structural response, larger models are considered in a follow-up study, as shown

in Figure 17(a) and Figure 17(b). Both structures represent a conventional stretcher bond, with the difference that the laying pattern is 90 degree twisted between these two structures. Both models consist of 17 rows, each comprising 31 paving blocks with dimensions 200/200/100 mm, leading to a pavement width of 620 cm. In lateral direction, the structures are clamped and the side faces in driving direction are elastically bedded (bedding modulus of 15 N/mm^3). As loading a truck axle with 2.75 m wheelbase was applied, with a tire contact area of 380/124 mm. The reaction forces at the rigid lateral support are shown in Figure 17(c) and Figure 17(d). The laying pattern on the left side of Figure 17 is characterized by continuous joints transverse to the driving direction, resulting in a more concentrated load introduction into the lateral supports. A further consequence is a larger vertical deformation, as can be seen by the comparison of Figure 17(e) and Figure 17(f).

A sophisticated and automated model generation allows the study of such complex model geometries with a large number of interactions. For this reason, future work is devoted to the extension of the modelling capabilities together with an easy to use interface, to make this numerical simulation tool accessible for engineers.

(a) Mises stress

(b) Mises stress

(c) Reaction forces at rigid support

(d) Reaction forces at rigid support
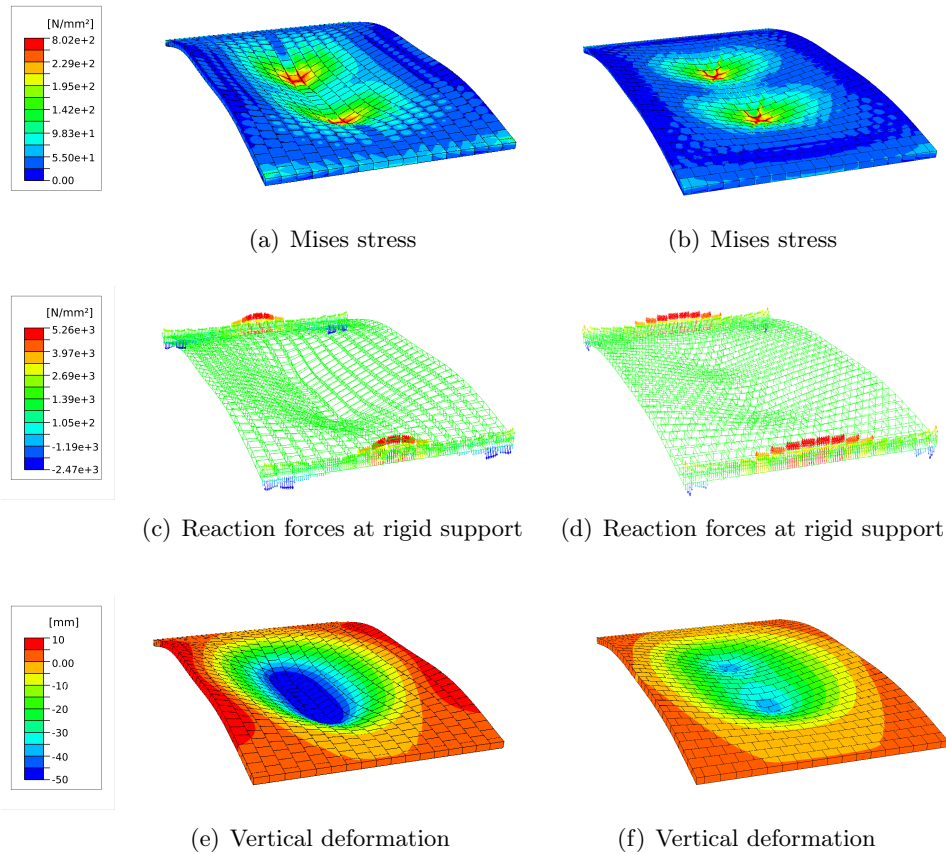

(e) Vertical deformation

(f) Vertical deformation

Figure 2.17:   Example of a superelevated block pavement (no underground) with a simulated axle loading (2 weels: 380/124.1 mm), Def. scale factor=10

Chapter 3

Horizontal deformation resistance of paving block superstructures - influence of laying pattern and joint behavior (Hengl et al., 2017a)

Authored by   Herwig Hengl, Wolfgang Kluger-Eigl, Ronald Blab & Josef Füssl
Submitted to *International Journal of Pavement Research & Technology*

Paving block structures are experiencing an upswing in urban areas, mainly due to their ecological, economical and space forming qualities. Unfortunately, this trend is being weakened by damages which occur even if all design standard were met. Very often unsightly horizontal relative deformations between paving blocks are observed, a failure mechanism which is not taken into account in standards sufficiently.

The identification and assessment of such horizontal deformation mechanisms of paving block superstructures represents the main objective of the present work. This is realized by means of complex 3D finite element simulations, investigating 6 different laying patterns with 5 different types of paving blocks. The non-linear interaction behavior between paving blocks was identified experimentally, implemented into the numerical simulation tool, and subsequently allowed for the reproduction of very realistic horizontal deformation mechanisms.

Finally, the performance of several laying pattern and paving block type configurations were compared to each other, pointing out the strength and weaknesses of each superstructure and revealing which combinations are best performing.

3.1   Introduction and Motivation

Paving block structures are experiencing an upswing in urban areas due to their ecological, economical and space forming qualities compared to common asphalt pavements. Even in areas with high traffic volumes paving block structures are expected to represent a suitable alternative to common pavement building systems in future. This trend is, however, continuously weakened by unexpected damage of newly built paving block pavements. The reason for this are immature design concepts and standards, which are heavily based on the concepts for asphalt pavements and do not take the special characteristics of this block-like structures sufficiently into account. The success of a project is therefore strongly dependent on the quality of planning and construction provided by experienced engineers and executing companies, rather than on reliable scientific knowledge implemented into design concepts and standards.

Figure 3.1:   Damage in a paving block structure because of too little horizontal loading resistance.

A brief overview of the rather modest research activities concerning paving block structures is given in the following. One of the first investigations on paving block structures with finite element simulations were done by Nishizawa et al. (1984) in 1984. He developed a numerical model with the joints modelled through a set of springs and 2D rectangular plate elements. In 1988 Jacobs and Houben (1988) undertook further investigations using 2D rigid block elements connected with linear springs. The first 3D finite element approach can be found in Huurman et al. (1992), where the numerical model contains paving blocks interconnected by four sets of three springs for each joint. The paving block superstructure is placed on four layers of bedding and subject to vertical loading. Displacement, stress, and strain information for the paving blocks, as well as for the baselayers and subgrade could be obtained. Higher bending stresses were determined in case of higher joint stiffness. Hassani (2006) used shell elements to model paving blocks and the joints between them. Lerch (2005) and Ascher et al. (2006) implemented a non-linear interaction between paving blocks, represented by zero-thickness elements in their simulations, where elastic as well as shear moduli were adjusted iteratively during the analysis. Later, this interactions were

substituted by non-linear contact laws, allowing for elastic-plastic interactions between paving blocks. Also Nejad and Shadravan (2006) modelled interactions with contact elements and found out that jointing width, shape, size, and thickness of the paving blocks have a major impact on the vertical structural deformations. Mampearachchi and Gunarathna (2010) performed a parametric study under usage of a 3D finite element model to determine necessary improvements for weaker support conditions of paving block structures. In the work of Oeser and Chandra (2010) a 3D Cosserat theory is applied to a sophisticated computational model using elastic as well as plastic interaction properties. A 3D numerical simulation tool for concrete paving slabs is presented in Füssl et al. (2015a), Füssl et al. (2015b) and Füssl et al. (2016a), where non-linear and plastic behavior between paving slabs and between slabs and sandbed is taken into account. In Hengl and Füssl (2016) various parameter studies were carried out on comprehensive numerical models to define an optimal region of superelevation-to-road-width ratios for superelevated profiles of paving block structures.

The main focus of all these research lied on the vertical structural response of paving block structures and the critical stresses and strains in the underlying baselayers. In addition to the vertical resistance, however, the structural resistance to horizontal loads is assumed to represent an equally important performance characteristic, especially for paving block structures. According to experienced engineers, it is often observed in practice that due to braking and steering maneuver of heavily loaded trucks or buses damage is introduced into paving block structures. Such loadings are normally not part of design approaches and also hardly treated in scientific literature. Neglecting these horizontal loadings can cause damage in form of permanent shiftings in the superstructure and chipped edges of paving blocks, as can be seen in Figure 3.1.

For example, the Austrian regulation for paving block pavements RVS 03.08.63 defines the admissible paving block structure as well as the thickness of the base courses only based on the expected traffic volume. However, it is obvious that the paving block surfaces, the shape, as well as the laying pattern must have a significant impact on the horizontal shifting resistance (responsible for frequently observed shortcomings) of the superstructure. This represents the main motivation for this work, which aims at a numerical simulation tool able to capture the effect of different laying patterns as well as different types of paving blocks on the horizontal shifting resistance of the related paving block superstructure. Based on this motivation, the following main objectives had been defined:

- The definition of sufficiently large and suitable sub-models of paving block superstructures allowing for the determination of the horizontal shifting resistance of these structures without significant influence of the boundary conditions. Furthermore, an automated generation of the whole superstructures geometry, to allow for an efficient investigation of several paving block geometries as well as laying patterns.

- An appropriate description of the non-linear interaction behaviour, in tangential as well as normal direction of the vertical joints, between paving blocks. Shear failure in the joints and the opening of joints should be reproduced realistically.

- Finally, the finite-element-based determination of the horizontal shifting resistance as well as the corresponding deformation (failure) mechanisms of different paving block superstructures.

The 5 types of paving blocks and the 6 different laying patterns investigated in this work are shown in Figure 3.2. To get realistic interaction properties, describing the contact behaviour between paving blocks, two types of experiments on paving blocks were carried out. The experimental setup as well as the results are given in Section 2. In Section 3, the developed simulation tool is described in and the corresponding numerical results are presented in Section 4. Thereby, each paving block was examined in every type of laying pattern. Finally, concluding remarks are given in Section 5.
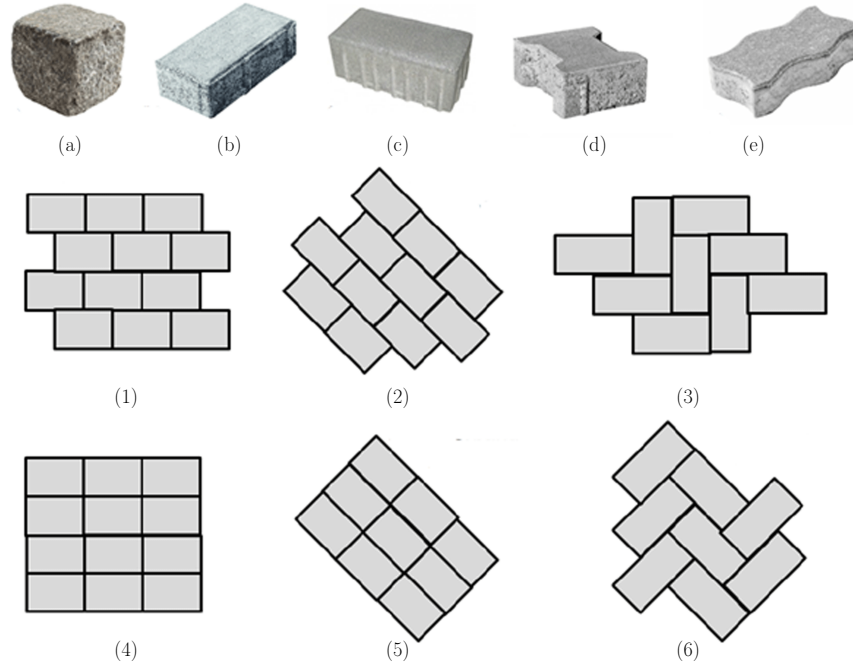
Figure 3.2:   Paving block types and laying patterns investigated in this work: (a) Granite Cube, (b) Concrete Block, (c) Concrete Interlocking Block (CIB), (d) Double-T Block, (e) Wave Block, and (1) Stretcher Bond, (2) Stretcher Bond 45°, (3) Herringbone, (4) Stacked Bond, (5) Stacked Bond 45°, (6) Herringbone 45°

3.2   Identification experiments for the vertical joint behaviour

The transmission of forces between paving blocks through the vertical joints of the paving block structure strongly affect, not to say define, the overall structural behaviour in horizontal direction. For this reason, special focus was laid on the identification of these properties. Two different kinds of experiments were carried out at the TVFA Vienna to obtain shear and normal properties for all of the 6 paving block types aforementioned. The experiments and the results are presented in the following two subsections. Additional information about such experiments can be found in Füssl et al. (2016b), where similar tests were performed by the authors.

Deformation u_n [mm]	Pressure σ_n [MPa]
-0.5	0
0	0.0001
0.05	0.15143
0.1	0.35921
0.15	0.62114
0.2	0.93722
0.25	1.30745
0.3	1.73183
0.35	2.21036
0.4	2.74304
0.45	3.32987
0.5	3.97085
0.55	4.66598

Table 3.1: Average normal joint behaviour extracted from the experimental results shown in Figure 3.4, used as input to the numerical simulation tool.

3.2.1 Normal joint behavior experiment

The experimental setup for the identification of the joint behaviour in normal direction is illustrated in Figure 3.3. Thereby, two paving blocks are placed on a wooden multilayer
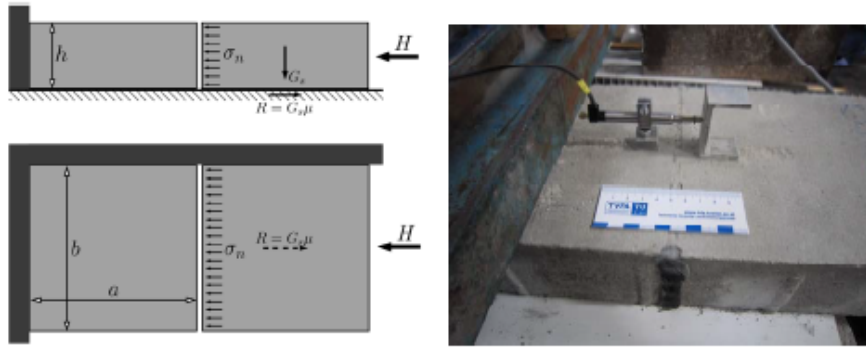
Figure 3.3: Experimental setup for the identification of the joint behaviour in normal direction.

board and the 5 mm thick joint between them is filled with sand (0/2) and manually compacted. One paving block is completely clamped while to the other one a horizontal force H is applied and the relative normal displacement u_n between these two blocks is measured with an LVDT. The obtained relationships between the normal stress σ_n and the displacement u_n for 5 performed tests are plotted in Figure 3.4. Since this information was assumed not to be as decisive as the shear behaviour and less dependent on the type of paving block, this experiment were only conducted with Concrete Blocks and Concrete Interlocking Blocks. Finally, an average response was evaluated (red graph in Figure 3.4), from which the input data for the numerical simulation tool was extracted (given in Table 1).

Figure 3.4:   Relationships between the normal stress σ_n in the vertical joints and the relative displacement u_n between paving blocks (Concrete Blocks and Concrete Interlocking Blocks) obtained from experiments.

3.2.2   Tangential joint behaviour

The experimental setup to identify the tangential joint behaviour is illustrated in Figure 3.5. Thereby, three paving blocks are arranged in a row on a wooden multilayer board and the 5 mm thic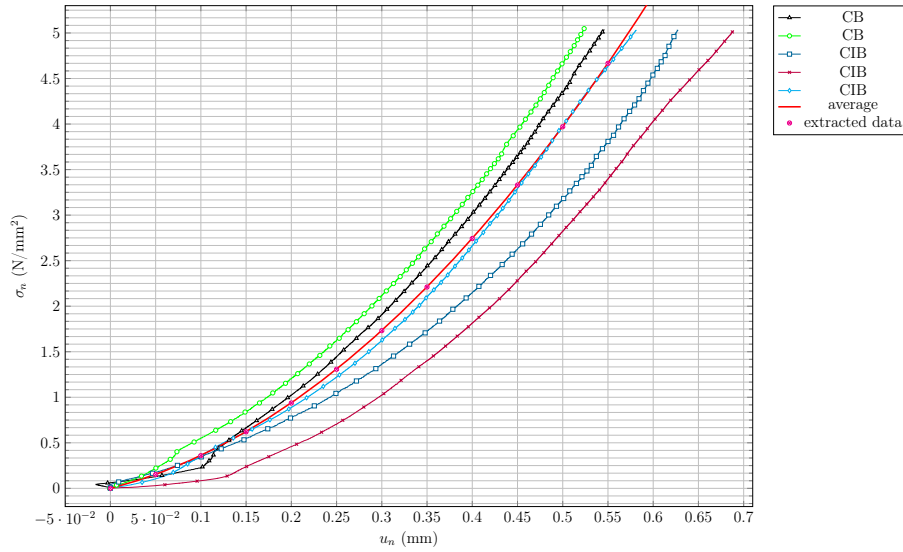k joints in-between are filled with sand (0/2), which is mechanically compacted under dry conditions. Then, in a first step, a constant load H is applied in "row"-direction (horizontal direction in Figure 3.5), allowing frictional forces to be activated in the joints. In a second step, an increasing load F is applied to the middle paving block transversely to the "row"-direction up to the point of shear failure (see, e.g., Figure 3.5 (b, d, f)). The relative displacements in "row"-direction as well as the force F were measured continuously. This experiment was carried out for all 5 types of paving blocks, at each for up to 5 different constant loads H and with at least two tests per configuration to ensure repeatability. For all these tests the maximum (average) shear stress in the joint as a function of the average normal stress in the joint, defined through the load H, is plotted in Figure 3.6.

The data of each paving block type can be connected through a Mohr-Coulomb friction law quite well (linear graphs in Figure 3.6). The resulting Mohr-Coulomb friction parameters (cohesion and friction angle) for each paving block type are given in Table 2, and were subsequently used as input to the numerical simulation tool.

3.3   Numerical simulation tool

Exemplarily for all models of different laying patterns, the model for a stretcher bond 45° is displayed in Figure 3.7. It only consists of the paving blocks and the underlying sandbed. The other base layers were not modelled explicitly, since it can be assumed that they contribute only little to the horizontal shifting resistance of the whole paving block structure. At least they would not influence the performance comparison between
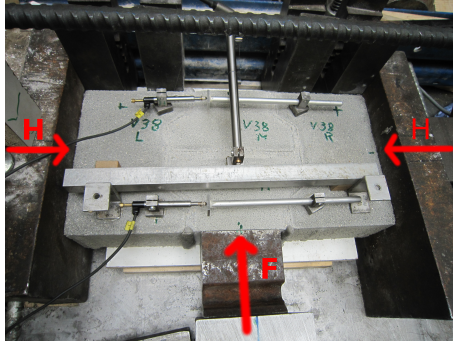
(a) Double-T Block, Initial (undeformed) configuration.

(b) Double-T Block, Exemplarily state after failure.
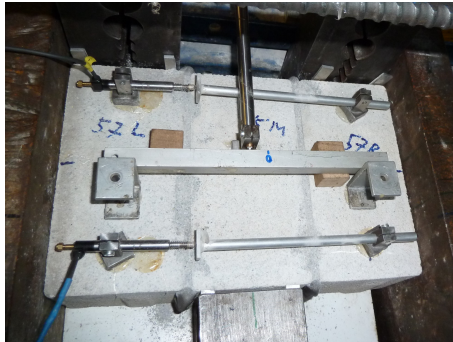
(c) Concrete Block, Initial (undeformed) configuration.

(d) Concrete Block, Exemplarily state after failure.

(e) Wave Block, Initial (undeformed) configuration.
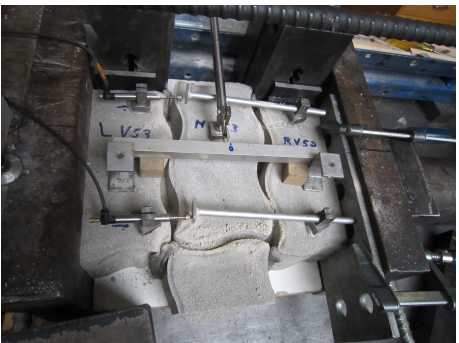
(f) Wave Block, Exemplarily state after failure.

Figure 3.5: Experimental setup to identify the tangential joint behaviour for (a,b) the Double-T Block, (c,d) the Concrete Block, and (c,f) the Wave Block.
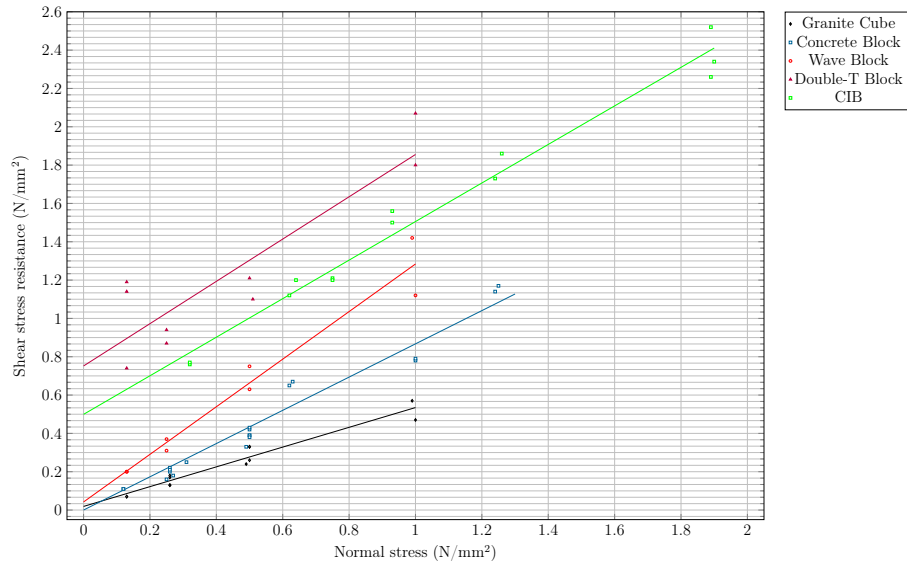
Figure 3.6:   Shear stress resistance - Results of horizontal displacement
                experiments

Specimens	dimension [cm]	cohesion c [MPa]	friction angle [°]
Concrete Block	20/10/8	0	49.69
Granite Cube	18/18/18	0.0189	29.56
Wave Block	21.5/10.5/8	0.0422	71.15
CIB	20/10/8	0.4994	57.64
Double-T Block	19.5/16/7.6	0.7519	63.23

Table 3.2: Mohr-Coulomb friction parameters for all 5 paving block types
            obtained from identification experiments.

different paving blocks and laying patterns, which is the main focus of this work. For all
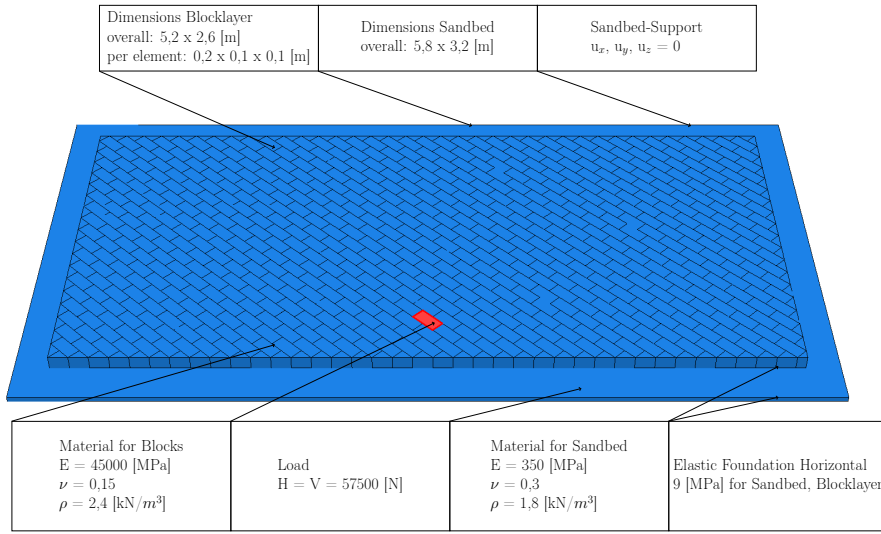
Figure 3.7:   Geometry and boundary conditions of the numerical model
                illustrated by means of a stretcher bond 45° model.

models the chosen modelling area is rectangular with an approximate dimension of 5.8 m
to 2.6 m. Small deviations to this dimensions result from the different laying patterns.
The dimensions of the paving blocks are set, according to an industry standard, to
200/100/100 mm. Paving blocks with different geometry and dimensions are used as
border stones to provide a straight boundary. Linear elastic material behaviour is
assigned to the paving blocks, with an elastic modulus of 45 000 MPa, which was
obtained by ultrasonic experiments on similar paving blocks in Füssl et al. (2015b), and
a poisson's ratio of 0.15. Furthermore, a specific weight of 24 kN/m^3 was assumed for
the paving blocks, allowing to take their dead load within the simulations into account.

The interaction between paving blocks in normal direction is defined as a tabular
pressure-overclosure relationship according to the normal joint behaviour experiments
described in Section 2, whereas the exact values used can be found in Table 1. The
interaction behaviour in tangential direction between paving blocks is described by
a Mohr-Coulomb friction law, with the cohesions and friction angles obtained from
the tangential joint behaviour experiments described in Section 2. For all investigated
paving blocks these strength values can be found in Table 2. The default Mohr-Coulomb
friction criterion in Abaqus is not able to take a cohesion not equal to zero into account.
For this reason, this criterion has been adapted and implemented as a user subroutine
written in Fortran. More details of the implementation of this tangential behaviour
will be given in a following subsection. At the lateral boundary all paving blocks are
supported by an elastic foundation with a bedding modulus of 9 MPa/mm, which is
an extrapolated value obtained from the normal pressure-displacement relationship in
Figure 3.4. This bedding modulus approximately represents the stiffness of a vertical
sand joint adjacent to a rigid border block.

To the underlying sandbed also a linear elastic material behaviour has been assigned,
with an elastic modulus of 350 MPa, a Poisson's ration of 0.3 and a specific weight of
18 kN/m^3. Since the vertical structural response of the paving block structure was

not investigated in this work it seemed not to be necessary to model a more complex behaviour. For this reason, also the displacements of the lower surface of the sandbed were simply prevented in all spacial directions. Between the sandbed and the paving blocks a "hard" contact was assumed in normal direction, allowing the paving blocks to lift off unstressed while stresses are transmitted fully under pressure. In tangential direction classical Mohr-Coulomb friction is modelled with a frictional coefficient of 0.6 and no cohesion.

The whole model is discretised with 8-node hexahedron elements, except some of the border blocks with non-rectangular geometry where wedge elements are used. Exemplarily, the discretised version of the stretcher bond 45° model is shown in Figure 3.8. A characteristic mesh size of 25 mm is used for the paving blocks, whereas the mesh is
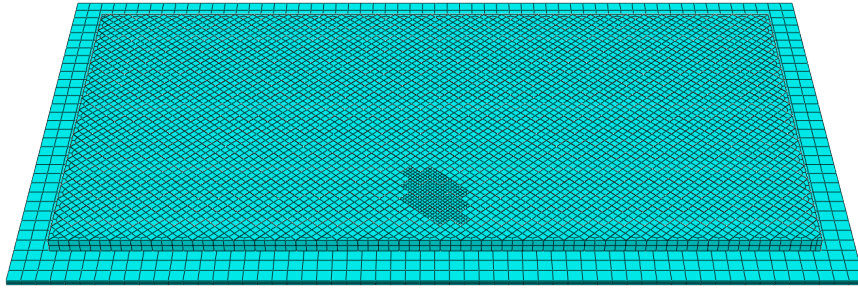

Figure 3.8:   Discretisation of the stretcher bond 45° model with 8-node hexahedron elements.

refined (12.5 mm characteristic mesh length) in the area where the wheel-load is applied. The horizontal element lengths of the mesh of the sandbed is 50 mm, finally resulting in a total number of elements for each model of around 100 000.

The simulations were carried out as follows: In a first analysis step the dead load and in a second analysis step a fictitious braking performance of a single tire was applied to a single paving block. This fictitious loading consists of a standard vertical tire load of 57.5 kN and of a horizontal loading of equal size, representing an absolute upper limit of possible braking forces. The finite element analysis was carried out with the Abaqus/Standard solver on a HPC computing cluster at TU Wien, using unsymmetrical matrix storage and including non-linear effects of large displacements.

To improve the stability of the numerical simulations an elastic slip at all tangential contact interactions was allowed. However, this elastic slip was restricted to 0.0005 times the adjacent characteristic element size l_{el} and therefore has no significant influence on the numerical result. The ideal frictional behaviour, where no relative motion Δu_t is allowed for $|\tau| < \tau_{crit}$, as displayed in Figure 3.9 (a) is thus approximated with the relationship shown in Figure 3.9 (b). So, a small amount of elastic motion, related to the frictional shear stress through:

$\Delta u_{el} = \frac{\tau_{crit}}{\Delta u_{el,max}} \cdot \Delta u_t = \frac{0.6 \cdot \sigma_n}{0.0005 \cdot l_e} \cdot \Delta u_t : \{\Delta u_t \in \mathbb{R} \mid |\Delta u_t| \leq \Delta u_{el,max}\}$,

where σ_n represents the pressure between paving block and sandbed, is allowed. For

more detailed information about the numerical implementation of Mohr-Coulomb friction using the penalty method, which was used in this work, the reader is referred to Corp. (2016).
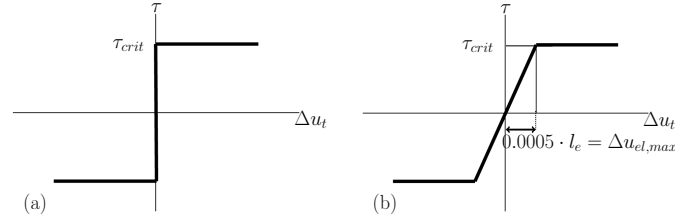

Figure 3.9: (a) Ideal frictional behaviour and (b) the approximation allowing a small amount of elastic slip used in this work.

3.3.1   Creation of different model geometries

Due to the large number of paving blocks modelled for each laying pattern (as can be seen in Figure 3.7) and to be able to flexibly adjust geometric parameters the models were generated by an extensive python script consisting of more than 1000 lines of code. The script offers a GUI through which future users can define a variety of parameters, such as the dimensions of the paving block, the size of the model region, the material and contact properties, as well as the type of laying pattern. Subsequently, the whole model is generated automatically, including the geometry of the border stones and all the contact interactions between the paving blocks and the paving blocks and the sandbed. Furthermore, in combination with a bash script this automated model generation provides a powerful tool for conducting parameter studies.

3.4   Numerical simulation results

As already mentioned within the introduction, numerical simulations have been performed for each configuration of the 5 different paving blocks and the 6 different laying patterns proposed, with the intention to determine the effect of those on the horizontal shifting resistance of the corresponding paving block superstructure. Trying to present the results in a structured way, in the first subsection the performance of all 5 paving blocks is compared by means of two laying patterns, while the performance of the 6 different laying patterns is compared in the second subsection by means of only the Concrete Block and the Concrete Interlocking Block. Finally, a results overview of all simulations conducted is given in the third subsection.

3.4.1   Performance of different paving blocks arranged in the same laying pattern

Figure 3.10 shows the horizontal deformation fields for all 5 different paving blocks layed in a stacked bond. For comparison reasons all paving blocks were modelled with the same dimensions. In addition, it should be noted here that since the non-planar

side surfaces of the Double-T Block as well as the Wave Block are already considered within the identified strength parameters obtained from experiments, the real geometry of these paving blocks doesn't need to, or even must not, be modelled at this structural scale.

(a) Stack - Concrete Block, u_{max}=6.11 [mm]

(b) Stack - Granite Cube, u_{max}=5.68 [mm]

(c) Stack - Wave Block, u_{max}=2.00 [mm]

(d) Stack - CIB, u_{max}=1.15 [mm]

(e) Stack - Double-T Block, u_{max}=1.08 [mm]
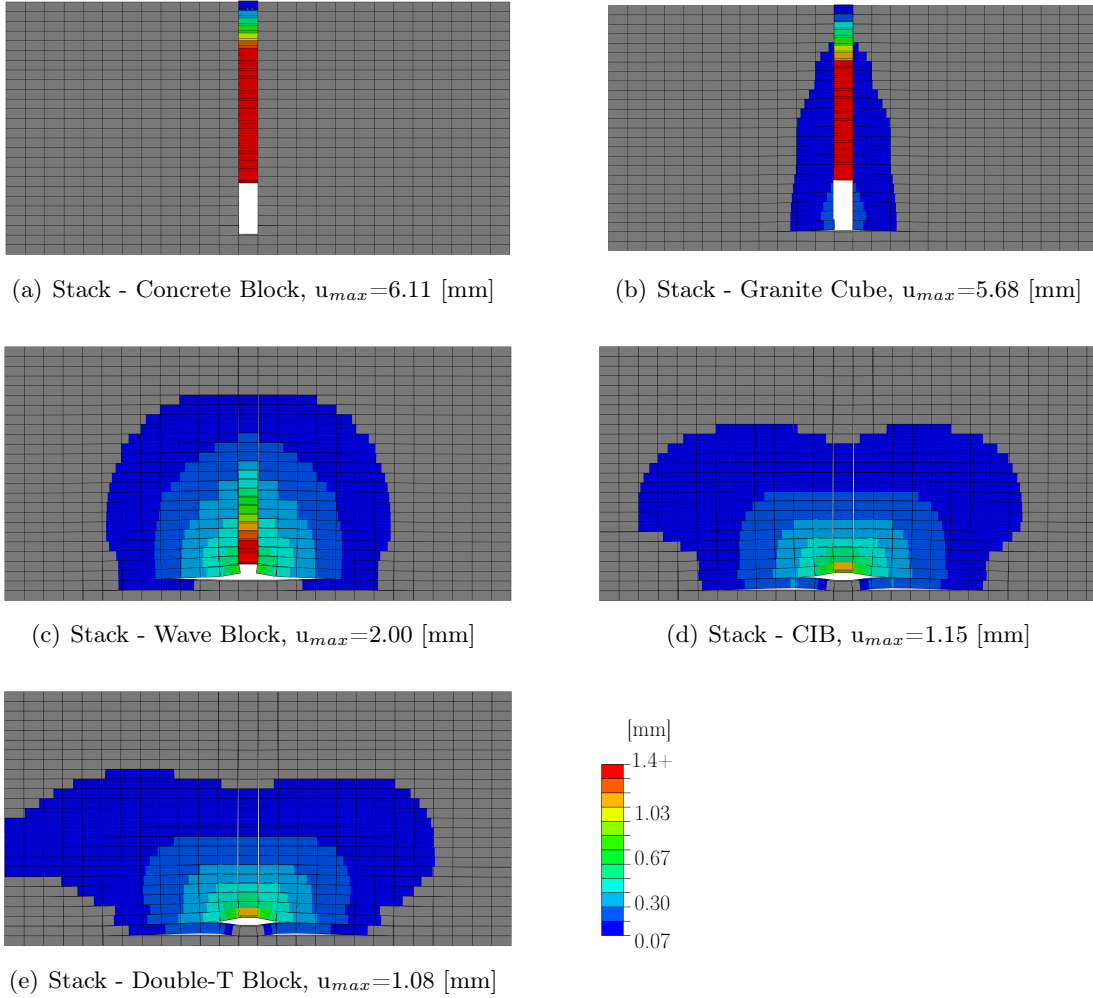
Figure 3.10:   Horizontal deformation fields of the 5 investigated paving blocks arranged in a stacked bond. A vertical and horizontal load of 57.5 kN each is introduced on one paving block. Scaling of deformations: 100.

For the visualisations in Figure 3.10 the sandbed was excluded and the deformations were scaled by a factor of 100. All deformation fields are related to the same fictitious loading state as described before and, thus, show an impressive performance difference between these five different paving blocks. For the Concrete Block, exhibiting zero cohesion between paving blocks, about six times the deformation was obtained compared with the best-performing Double-T Block. Since there are no compressive stresses in transverse direction, the Concrete Block is not able to transfer shear stresses to adjacent rows and, thus, only the loaded row is shifted in load direction. The maximum displacement could be obtained by simply summing up the overlaps of the paving blocks in this row, which can be interpreted as the compression of the sand joints plus the displacement of the border block of the structure, which is kept quite small by a relatively stiff

elastic foundation on the boundary. It can be assumed that the maximum displacement would be even larger if more paving blocks were modelled in load direction. A similar picture is drawn by the Granite Cube, also exhibiting only a very small cohesion of 0.019 MPa. For this reason, as expected, paving blocks with no interlocking effect (cohesion) are not suitable for this laying pattern. A completely different system response was obtained for the three paving blocks having significant interlocking capabilities, the Wave Block, the Concrete Interlocking Block, and the Double-T Block. For all three, the obtained displacement field was proven to be independent on the boundary conditions, and without any compressive force in transverse direction they are able to activate a large amount of paving blocks counteracting the very concentrated introduced load.

This can also be seen very clearly in Figure 3.11, in which the normal and shear contact forces between paving blocks are vividly illustrated, for the Concrete Blocks and the Concrete Interlocking Blocks.

The great decrease of contact forces in the surrounding of the load introduction comes from the great shear forces which can be transferred to the sandbed by the paving blocks which experience a substantial vertical loading. At a certain distance from the load introduction a constant decrease of contact forces can be observed, reflecting the shear transfer capability of the paving blocks to the sandbed only due to their dead weight.

These large areas of constant shear transfer to the sandbed (for the Concrete Interlocking Blocks) can be nicely seen in Figure 3.11(f). Interestingly, between these areas and the load introduction zone where very high shear forces are introduced into the sandbed, an area with no force transmission becomes visible. A deeper look at the simulation results revealed that in these areas the paving blocks are lifted and, thus, are having no contact to the sandbed.

A far lesser impact of the typ of paving block on the horizontal deformation was obtained for the stretcher bond laying pattern, as can be seen in Figure 3.12. Clearly, this laying pattern allows for a natural distribution of the introduced load into the transverse direction for all types of paving blocks. This is illustrated by means of the nodal normal contact forces plotted in Figure 3.13 for the Concrete Block superstructure.

Nevertheless, still a significant influence of the joint properties remain, leading to a 2.5 times higher deformation of the Concrete Block structure compared to the Double-T Block structure. Anyways, the appropriate choice of the size of the modelling region, to avoid a strong influence of the boundary conditions, can be seen well here. Only for the Double-T Block superstructure an even smaller maximum deformation would probably be obtained with a larger transverse modelling length.

3.4.2 Performance of different laying patterns with the same paving blocks

In the following, horizontal deformation fields are shown for the 6 different laying patterns and for the Concrete Block as well as the Concrete Interlocking Block.

The results for the stacked bond, the stretcher bond, and the herringbone are illustrated in Figure 3.14. Figures 3.14 (a) to (d) have already been shown before, but only in this comparison it becomes obvious that the stretcher bond represents the ideal laying pattern for conventional concrete paving blocks. The maximum horizontal deformation is only slightly higher than that of the concrete block with interlocking effect in the stretcher bond, and it is smaller than the maximum deformation in all other laying pat-

(a) Normal contact forces between Concrete Blocks

(b) Normal contact forces between Concrete Interlocking Blocks

(c) Shear contact forces between Concrete Blocks

(d) Shear contact forces between Concrete Interlocking Blocks

(e) Concrete Blocks: Shear contact forces in loading direction

(f) Concrete Interlocking Blocks: Shear contact forces in loading direction
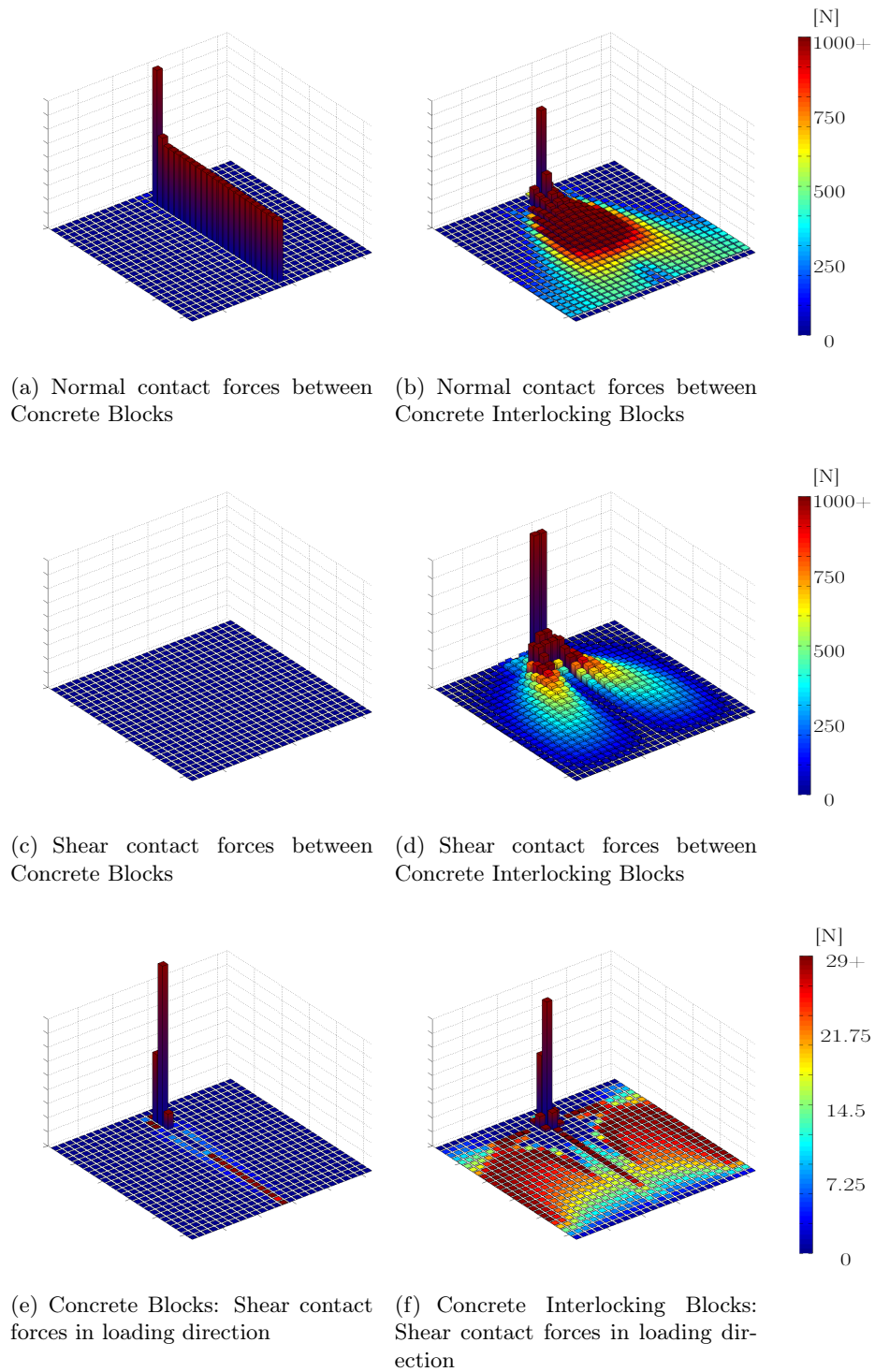
Figure 3.11:   Visualisation of contact forces (in loading direction) between paving blocks, for the stacked bond laying pattern.
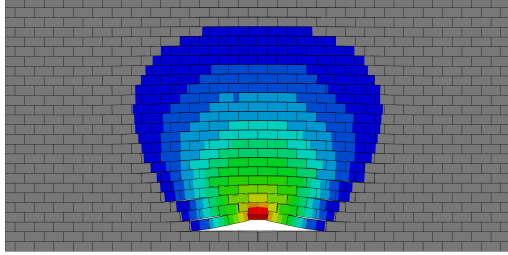
(a) Stretcher - Concrete Block, $u_{max} = 2.44[mm]$
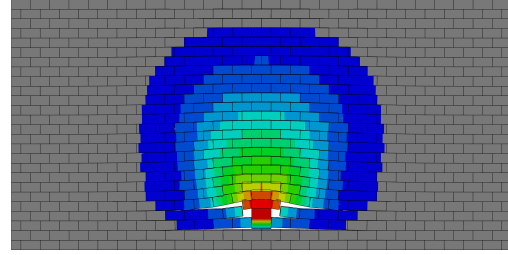
(b) Stretcher - Granite Cube, $u_{max} = 1.77[mm]$
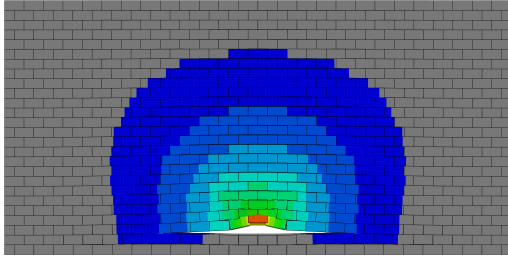
(c) Stretcher - Wave Block, $u_{max} = 1.28[mm]$
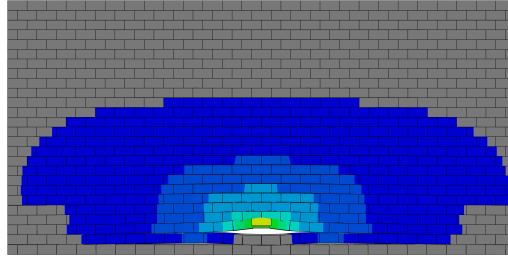
(d) Stretcher - Concrete interlocking block, $u_{max} = 0.98[mm]$
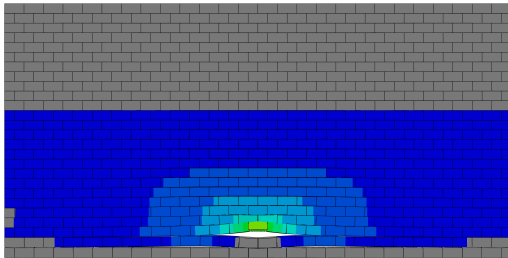
(e) Stretcher - Double-T Block, $u_{max} = 0.90[mm]$
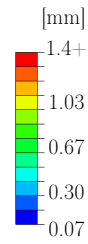
Figure 3.12: Horizontal deformation fields of the 5 investigated paving blocks arranged in a stretcher bond. A vertical and horizontal load of 57.5 kN each is introduced on one paving block. Scaling of deformations: 100.
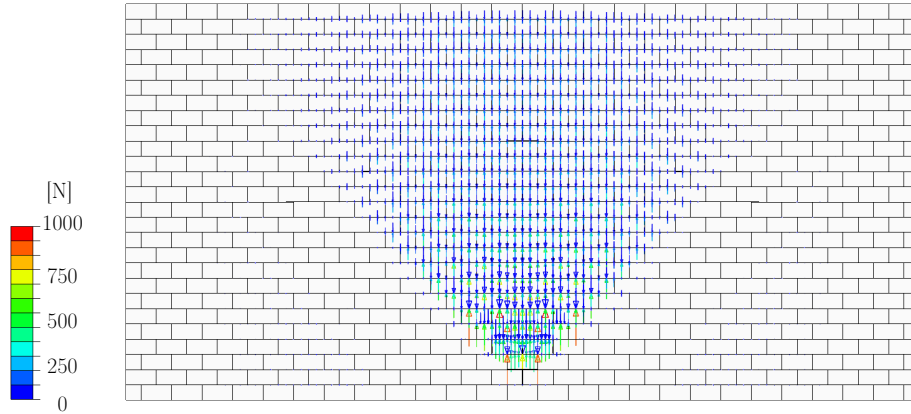
Figure 3.13: Nodal normal contact forces in load direction for a
stretcher bond with Concrete Blocks.

terns. Conversely, CIBs are ideally suited for a stacked bond, because their interlocking capabilities fully compensate the non-interlocking nature of this laying pattern.

It is also interesting to see that the performance of the Concrete Block is getting worse when laid in a herringbone laying pattern instead of a stretcher bond while the performance of the CIB is getting even better. This is because the interlocking capability of the herringbone can only be activated ideally if the vertical joints exhibit cohesive behaviour (as can be seen in Figures 3.14 (e) to (f)).

The deformation fields of the three remaining laying patterns, the 45° rotated ones, are shown in Figure 3.15.

As can be seen, even for this complex arrangements of paving blocks the numerical simulation tool is able to deliver plausible shifting mechanisms. The mechanisms themselves are strongly characterised by the 45° orientation of the laying patterns. Looking at the conventional Concrete Block, only for the stacked bond a significant performance improvement can be identified compared to its not rotated counterpart, while for the other two laying patterns similar maximum deformations are obtained. For the stretcher bond an even worse performance can be observed, which is caused by a very concentrated, and thus bad, force distribution into the superstructure. This is illustrated in Figure 3.16, showing the rather narrow bands of nodal normal contact forces in this laying pattern.

Considering the Concrete Interlocking Blocks, the performance is better for all three laying patterns. This has essentially two reasons: First, due to the 45° rotation more joints are heavily loaded by shear forces and, thus, the interlocking capability of the joints get highly activated and, secondly, also paving blocks behind the load introduction are getting involved into the load transfer mechanism.

3.4.3   Overview of simulation results

Figure 3.17 finally shows the maximum horizontal deformation in loading direction u_{max} for all configurations of the 6 laying patterns with the 5 investigated paving blocks. In general it can be said that both the type of laying pattern as well as the type of paving block have a significant influence on the horizontal shifting resistance. However,

(a) CB in stacked bond, $u_{max} = 5.68$ mm

(b) CIB in stacked bond, $u_{max} = 1.15$ mm

(c) CB in stretcher bond, $u_{max} = 1.77$ mm

(d) CIB in stretcher bond, $u_{max} = 0.98$ mm

(e) CB in Herringbone, $u_{max} = 1.94$ mm

(f) CIB in Herringbone, $u_{max} = 0.64$ [mm]

Figure 3.14:   Horizontal deformation fields for three different laying patterns and two different paving blocks. A vertical and horizontal load of 57.5 kN each is introduced on one paving block. Scaling of deformations: 100.

(a) CB in stacked bond 45°, $u_{max} = 2.60$ mm

(b) CIB in stacked bond 45°, $u_{max} = 0.73$ mm

(c) CB in stretcher bond 45°, $u_{max} = 2.08$ mm

(d) CIB in stretcher bond 45°, $u_{max} = 0.55$ mm

(e) CB in herringbone 45°, $u_{max} = 1.83$ [mm]
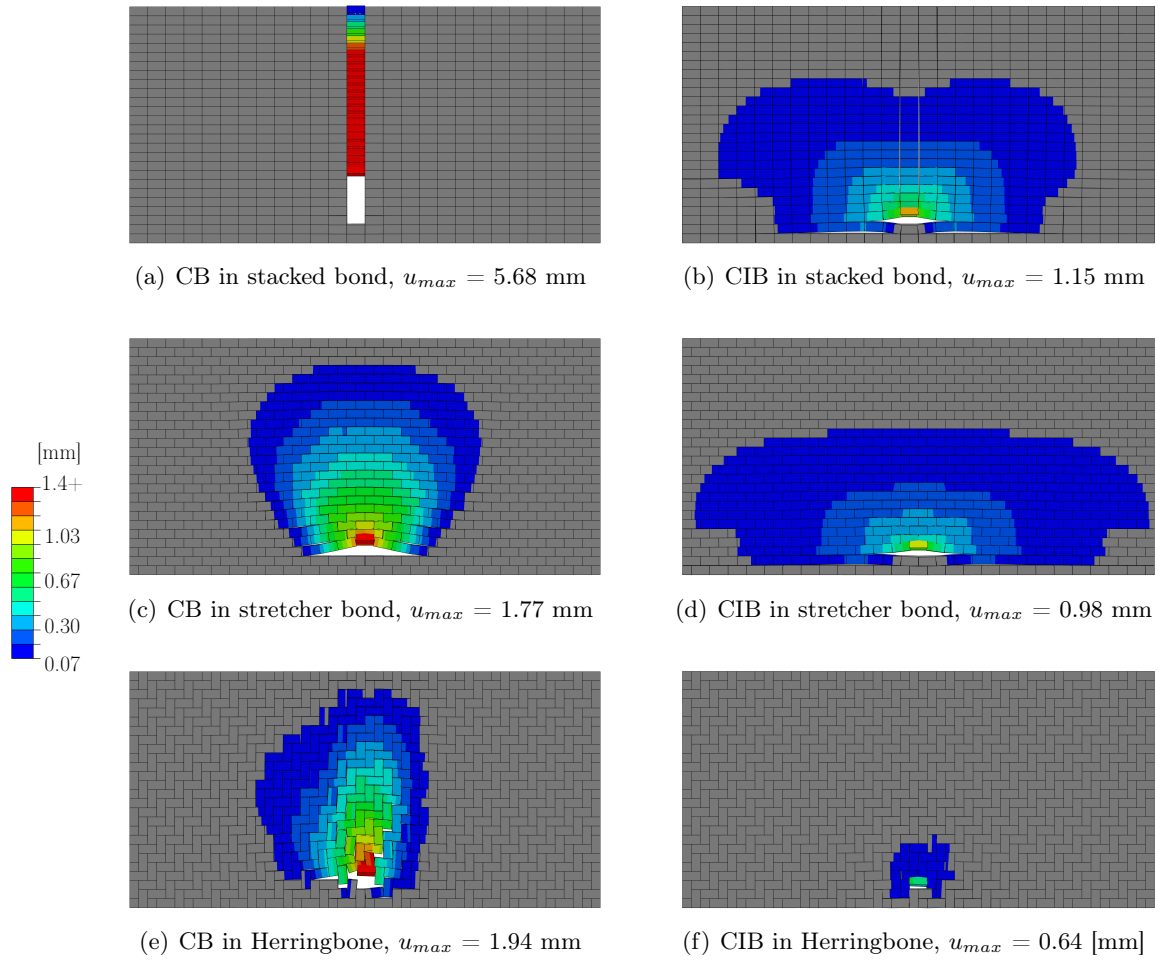
(f) CIB in herringbone 45°, $u_{max} = 0.47$ mm
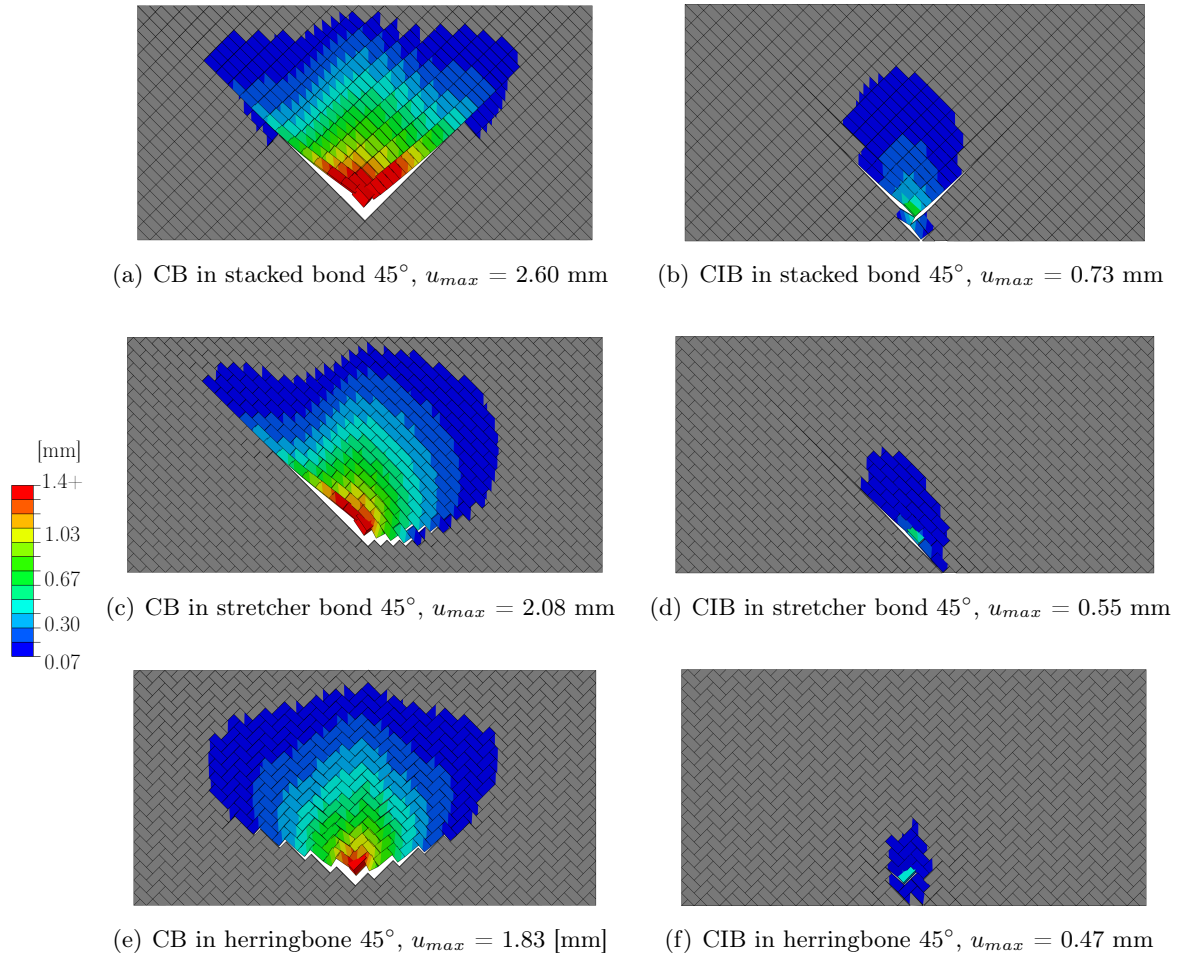
Figure 3.15: Horizontal deformation fields for three different laying patterns and two different paving blocks. A vertical and horizontal load of 57.5 kN each is introduced on one paving block. Scaling of deformations: 100.
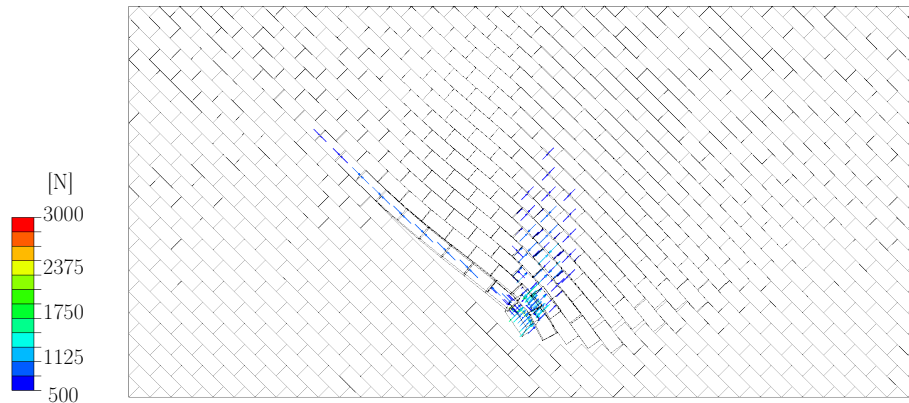
Figure 3.16:   Rather bad distribution of nodal normal contact
forces in a stretcher bond 45° with Concrete Blocks, leading
to high horizontal deformations.

disregarding the stacked bond, the paving block type seems to play a more important role and cannot be compensated by the type of laying pattern easily. On average paving blocks with joints providing a decent interlocking effect perform three times as good as paving blocks in the same laying pattern without interlocking capabilities. This may lead to huge performance differences also in practical applications and shouldn't be ignored by design concepts and standards.

Of course, there are still a lot of other parameters influencing this horizontal deformation resistance, such as the paving block height, the joint filling (which can partly be described by the paving block height), the contact stiffness (which could be reduced in case of poorly compaction), and so on. The presented numerical simulation tool is capable of taking all this parameters into account. Two relationships are exemplarily given in Figure 3.18, showing the significant influence of the paving block height as well as the normal contact stiffness in the vertical joints. A doubling of this stiffness can reduce the maximum horizontal deformation by almost half.

Figure 3.17:   Maximum horizontal deformation in loading direction u_{max} for the investigated 6 different laying patterns and 5 different paving blocks.

Figure 3.18:   Influence of the paving block height and contact stiffness in normal direction on the maximum horizontal deformation.

3.5 Conclusions

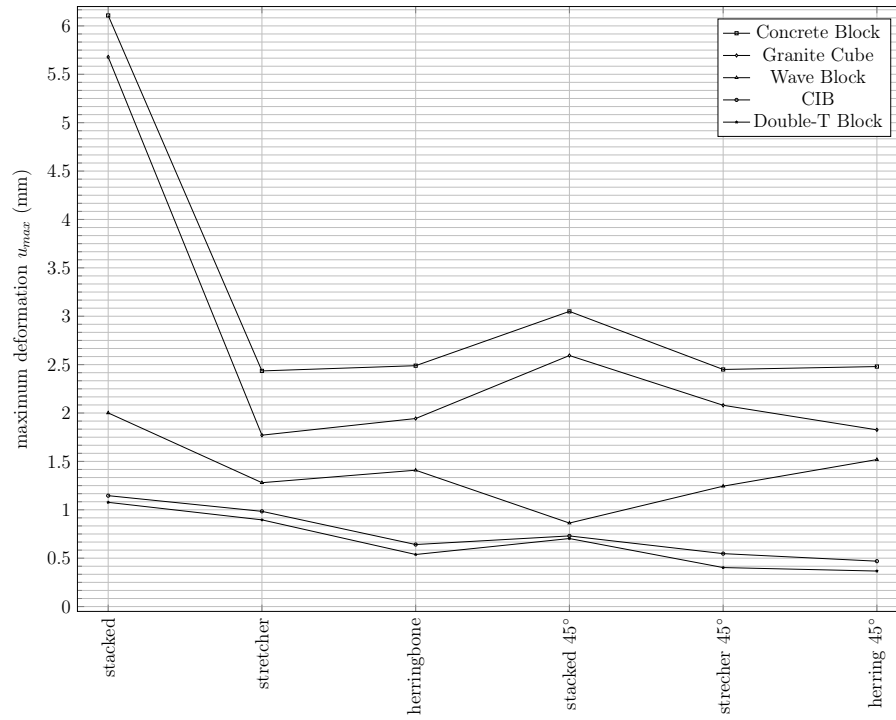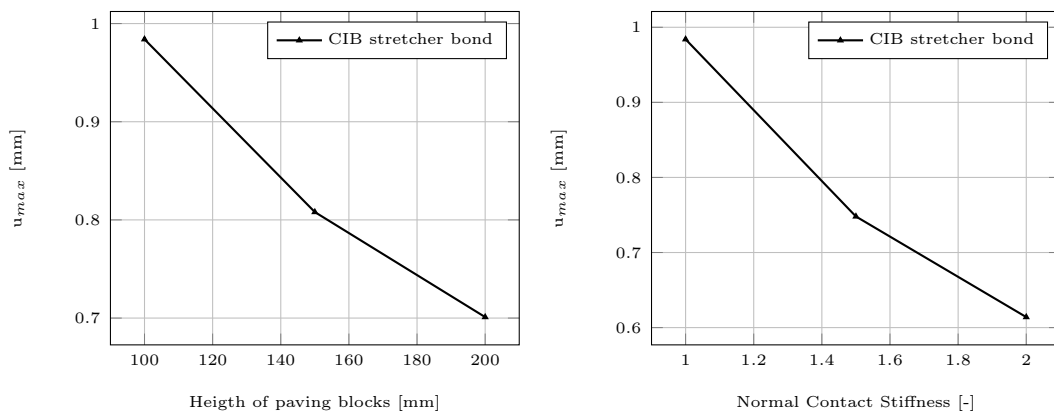In this paper, a numerical simulation tool has been proposed allowing for a realistic reproduction of resistance mechanisms of paving block superstructures under horizontal loading. To accomplish that, numerical models with more than 2000 non-linear interactions, with their behaviour defined through a user subroutine written in Fortran, had to be run. The required strength properties to define the non-linear joint behaviour of all 5 investigated paving block types were obtained by special tangential shear experiments. Based on these investigations, answers to the three questions raised in the introduction can now be formulated:

- The fully automation of the model creation, enabled by a complex Python script, allowed us to run a huge amount of simulations to finally identify an appropriate model size for which the influence of boundary conditions is not significant for the majority of the investigated configurations. Furthermore, much attention was paid to any kind of numerical regularisation mechanism, like artificial stiffnesses and viscous damping. Many parameters studies were conducted to ensure that such influences are negligible.

- The non-linear behaviour of the vertical joints, in normal as well as tangential direction, could be reproduced quite accurate. Therefore, information from two kind of joint experiments were used and implemented into the numerical simulation tool.

- Mainly for this reason, very plausible 3D deformation mechanisms could be obtained for several laying patterns with different types of paving blocks. Interesting insights into load transfer mechanisms could be gained, showing a huge variety depending on the combination of laying pattern and type of paving block. Finally, this allowed for a comprehensive performance evaluation of several paving block pavements with respect to their horizontal shifting resistance.

In short, the simulation results have confirmed the high performance expectations of paving blocks with interlocking effects. On average these paving blocks perform three times as good as blocks without interlocking capabilities, considering the same laying pattern. Even for the stacked bond laying pattern, where no structural load distribution occurs, paving blocks with interlocking effect can lead to reasonable horizontal deformation resistances. Furthermore, as the horizontal deformation in those superstructures is highly affected by the stiffness of their sand-filled joints, it should be ensured that these joints are completely filled, well compacted, and their width and quantity minimized.

In summary, this work has the intention to demonstrate the very different horizontal resistance of paving block pavements, to propose a method to identify this resistance, and to possibly contribute to future design concepts which will hopefully cover this type of damage scenario.

Chapter 4

The performance of paving block structures with mortar filled joints under temperature loading, accessed by means of numerical simulations (Hengl et al., 2017b)

Authored by   Herwig Hengl, Wolfgang Kluger-Eigl, Ronald Blab & Josef Füssl
Published in   *Road Materials & Pavement Design*, pages 1-20, 2017

Paving block structures with mortar filled vertical joints can exhibit a significantly higher load capacity as comparable structures with sand filled joints. For this reason, this pavement construction method is increasingly being used or would be used, respectively, if its performance could be estimated reliably. Specifically, the exact cause of cracks due to cooling in winter has not been fully understood yet and appropriate prediction tools do not exist. This motivated the development of a numerical simulation tool for such paving block structures under temperature loading, which is able to take the brittle failure mechanisms in-between paving blocks and paving blocks and the underlying mortar bed into account. By means of the proposed simulation tool in this paper, basic structural failure mechanisms of such paving block structures, due to different temperature events, could be identified and relationships between crack widths and different bonding strengths as well as installation temperatures were obtained. Finally, estimates for necessary bonding strengths between paving blocks and mortar bed to prevent large (visible) cracks due to temperature loads are given.

4.1   Introduction

Figure 4.1:   Crack in a paving block structure
resulting from thermally induced stress.

In recent decades, paving block structures have become a frequently used road construction method, especially in urban areas. Unfortunately, when it comes to rigidly laid paving block structures (structures with mortar filled vertical joints), cracks, usually induced by thermal stresses, are a common damage pattern (as exemplarily shown in Figure 4.1). Apart from the mechanical issues caused by such cracks, they also impair the visual appearance of these, not damaged very attractive, pavements. This greatly reduces the confidence in and acceptance of this type of construction and prevents a more frequent use.

A major reason for this performance problem can be attributed to the lack of appropriate design codes for the construction of rigidly laid paving block structures. In the German speaking region, they have been considered as a special construction method until now. Nevertheless, in 2007 a guideline 'Forschungsgesellschaft für Straßen- und Verkehrswesen (2007)' with recommendations was published and in 2009 the 'Wissenschaftlich-Technische Arbeitsgemeinschaft für Bauwerkserhaltung und Denkmalpflege (2009)' disclosed a leaflet. These documents contain execution suggestions as well as material definitions for paving block structures. To avoid temperature induced damage, both guidelines recommend the use of expansion joints,   whereby the second also mentions a positive influence of a strong adhesive bonding between the paving blocks and the mortar bed. Most of these recommendations are based on empirical observations and simple design rules, but deeper mechanical explanations are missing. This was the main motivation for the present work, which aims at describing the response of paving block structures due to temperature loading as realistically as possible. Before discussing the objectives of the present work in detail (4.1.2), a few fundamental considerations are made in the following.

4.1.1 Fundamental considerations

When a common building material is subject to a temperature load its volume changes. As the temperature increases the body expands (positive strain) and when it decreases the body contracts (negative strain). As long as the deformations of the body are not blocked the body remains free of stress. In case that the temperature is not evenly distributed over the whole body, even if the deformations are not blocked, temperature-induced stresses may occur. When two adjacent elements of a monolithic body are experiencing different thermal loads, their desired deformation is, in general, geometrically not compatible. Therefore, as long as this compatibility is maintained, temperature-induced stresses arise. This is demonstrated by means of a simple numerical model (shown in Figure 4.2), where two connected layers of a plate (frictionless supported on the bottom) are loaded by different temperatures. While the lower layer is maintained by the initial temperature of 0 °C, the upper layer is cooled down to -20 °C. The resulting normal stresses in longitudinal direction are given in Figure 4.2 (b), showing compression in the lower layer and tension in the upper layer. In a very simplified way,
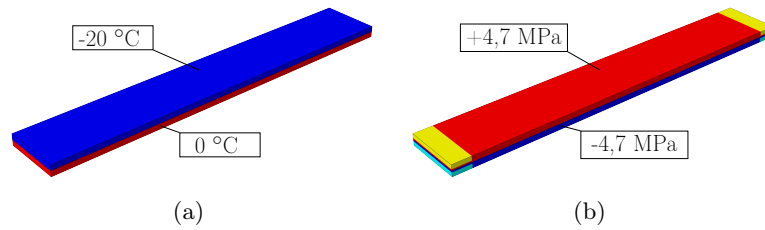

Figure 4.2:   Effect of non-constant temperature distribution in a two-layered plate which is freely deformable. (a) Forced temperature field, and (b) resulting normal stresses in longitudinal direction.

a paving block structure can be seen as such a two-layered plate. Then it is obvious that temperature drops, e.g. due to rainfalls or cooling in general, may lead to failure inducing stresses between paving blocks or between paving blocks and the mortar bed, respectively. In this respect, the initial temperature as well as the magnitude of the temperature drop is significant. Stresses evolve proportional to the difference between the initial temperature and the actual temperature, and cracks occur when the tensile stress exceeds the resisting tensile strength, concluding a low initial temperature is beneficial to prevent cracks. On the other hand, a low initial temperature, e.g. constructing during wintertime, may result in high compressive stresses in summer. A clear statement about the optimal initial temperature can not be made based on such simple considerations. A low initial temperature may prevent the occurrence of cracks, while a high initial temperature leads to less expansion and compressive stresses during summertimes. Furthermore, no statement about shear failure between paving blocks and the mortar bed is possible.

Moreover, if a homogeneous plate under constant temperature load can deform freely, the strain within the plate will be constant as well. Therefore, the stress will be constant when only the in-plane deformations are prevented and no bending occurs. Subsequently, we can easily show that the dimensions of such a structure don't affect

the thermally induced stresses. This statement can be confirmed by applying the simple force method $\sum_{v=1}^{n} \delta_{uv} \cdot X_v = -\delta_{u0}$ on a simply-supported beam, whereby δ_{uv} represents the compliance, δ_{u0} the displacement and X_v the unknown reaction force. The corresponding delta values $\delta_{11} = N_1^2 \cdot l_s/EA$ and $\delta_{10} = N_1 \cdot \Delta T \cdot \alpha T \cdot l_s$, with l_s for the beam length, EA for the tensile stiffness, ΔT for the temperature difference and N_1 for the normal force, show that the resulting reaction force in the axis of the beam, $X_1 = -\delta_{10}/\delta_{11}$, is independent on the length of the beam.

A paving block structure is obviously an inhomogeneous structure with specific interactions and more complex boundary conditions. Nevertheless, this simple considerations lead to the assumption that the dimensions of a paving block structure are of no great influence on the stress leading to crack occurance (which is sometimes claimed by engineers), but, in case of predominant cracks, on their width.

Such and other thoughts are to be investigated by means of numerical models in the present paper. Starting with a brief literature overview, the basic motivation and the research questions pursued are given in the following.

4.1.2   Motivation and research questions

Usually, when it comes to thermally induced stresses in paving block structures, the literature refers to articles dealing with thermal stress in concrete slabs or concrete pavements. Many authors concerned themselves with this topic, wherein only few of them, like Plannerer (1998), Rostasy and Kraus (2001), Röhling (2005), and Schikora and Eierle (1999), investigated thermal effects due to hydration in the early stage of various concrete constructions. Bondy (1995) and Schweighofer (2011) engaged themselves with thermal stress in concrete slabs and Maliha (2005) investigated the appearance of cracks in concrete pavements. Other contributions , focusing on the interaction between concrete slabs and base layers, can be found in Kolb (1988), Schütte (1997), and Petersson (1998). But since this construction method has gained significant market shares only recently, not much scientific research work is available yet. To the knowledge of the authors, only one work regarding numerical simulations of rigidly laid paving block structures, namely the dissertation of Buchholz (2010) dealing with thermally induced stresses, has been published. On the other hand, there have been several investigations regarding numerical tools for the performance evaluation of paving block structures with sand filled vertical joints, which can be found in Nishizawa et al. (1984), Jacobs and Houben (1988), Huurman et al. (1992), Lerch (2005), Ascher et al. (2006), Oeser and Chandra (2010), Füssl et al. (2016b), and Hengl and Füssl (2016), to mention only a few of them.

For this reason, the motivation of this work has been to develop a numerical simulation tool which is able to predict the effects of thermally induced stresses in paving block structures with mortar filled joints and their influence on the occurrence of cracks. By focusing on the interactions between paving blocks, as well as between paving blocks and the mortar bed, this simulation tool should allow us to gain new knowledge about the mechanical mechanisms in the structure and to perform mechanically-sound simulations which may help us to answer the following, in connection with this building method often discussed, questions:

- What's the impact of the bonding strength between paving blocks and the mortar bed on the mechanical performance of the paving block structure, and can a certain bonding strength be defined and practically achieved at which the structural

performance under temperature loading is satisfactory?

- What's the influence of the ambient temperature at construction (installation) of a paving block structure on the occurrence of cracks and, if there is a critical temperature boosting cracking, can shading measures during the construction reduce this effect?

- Based on a better understanding of the mechanical behaviour of paving block structures under temperature loading, how can the benefit of expansion joints be evaluated and how should they be arranged?

In the following section, Section 2, identification experiments giving insight into mechanical properties of the superstructure (paving blocks, joints, mortar bed) are described. In Section 3, the developed numerical simulation tool is proposed. The identification of different response mechanisms, based on the numerical results, represents the main content of Section 4. The findings of various parameter studies are presented within several subsection, like the positive effects of shading measures. A brief summary, concluding remarks and a future outlook are given in Section 5.

4.2 Identification experiments for the shear strength between paving blocks and mortar bed

4.2.1 Samples and test setup

To determine the maximum shear strength between paving blocks and mortar bed a new identification experiment has been developed. The main goal of this experiment was to compare different surfaces of paving blocks (split granite and formwork concrete) and the influence of transverse joints and primer. For the experiments five different samples were produced (Figure 4.3 (a-e)). These were made of three paving blocks (20/10/8 cm) paved on a 5 cm thick porous mortar bed (grain size 8 mm) with a joint width of 10 mm and finally filled with joint mortar (grain size 2 mm).
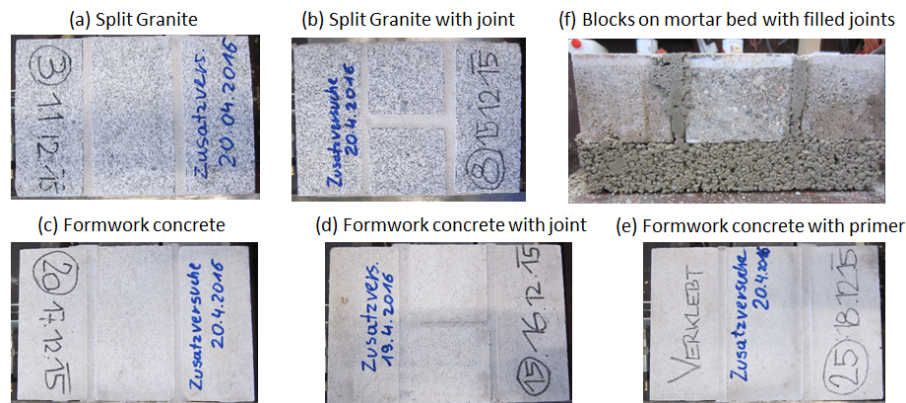

Figure 4.3: Samples for experiments (a-e) top view of different blocks and joints and (f) side view of blocks on mortar bed with filled joints.
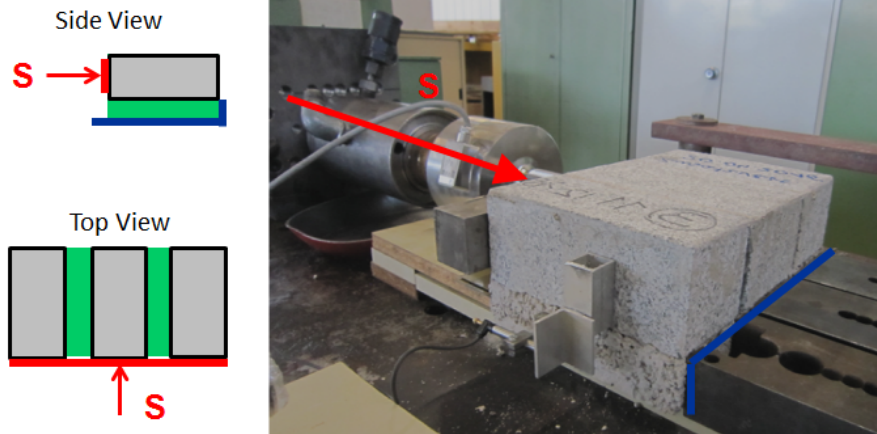
Figure 4.4: Test setup for shear experiments.

paving block [cm]	joint width [mm]	contact area [mm²]	dead load [kN]	contact pressure [MPa]	shear force [kN]	shear stress [MPa]	appearance of fracture	priming slurry	transverse joint
split granite 20/10/8	10	64000	0.14	0.002	32.8	0.51	roughly	no	no
split granite 20/10/8	10	64000	0.14	0.002	44.9	0.70	roughly	no	yes
concrete block 20/10/8	10	64000	0.14	0.002	16.5	0.26	smooth	no	yes
concrete block 20/10/8	10	64000	0.14	0.002	17.9	0.28	smooth	no	no
concrete block 20/10/8	10	64000	0.14	0.002	66.8	1.04	mortarbed crushed	yes	no

Table 4.1: Accomplished shear experiments at at TVFA Vienna.

The developed experimental setup is illustrated in Figure 4.4. All samples were fixed in position only through the mortar bed. Then, a shear force S with a rate of 200 N/s was applied to the paving blocks on one side of the sample, parallel to the continuous joints. The experiment was stopped when the maximum force S was reached and a clear failure mechanism was formed, respectively.

4.2.2 Test results

For the evaluation of the maximum shear stress between the paving blocks and the mortar bed, the maximum shear force S was divided by the contact surface A of 64 000 mm² for each test sample. The results for the different variations are given in Table 5.1.

The results clearly show the better performance of the split granite paving block compared to the formwork concrete paving block. The rough surface of the granite blocks can withstand nearly twice the shear force as the smooth surface of the concrete blocks. Also a difference between the arrangements with and without transversal joints was obtained for the granite block samples. No influence of the transversal joints was observed for the concrete block samples, which showed nearly the same shear strength for both tested samples. The positive influence of a primer could be demonstrated for concrete blocks. The achieved shear stress was four times higher than for concrete

blocks without primer, and two times higher than for granite blocks without transversal joints. In Figure 4.5 the different breaking patterns are displayed. The failure surfaces for the samples (a) and (b) are rough, while for the samples (c) and (d) rather smooth failure surfaces developed. Due to a very good bond between the paving blocks (e) and the mortar bed, partial failure of the mortar bed was obtained. Because only one
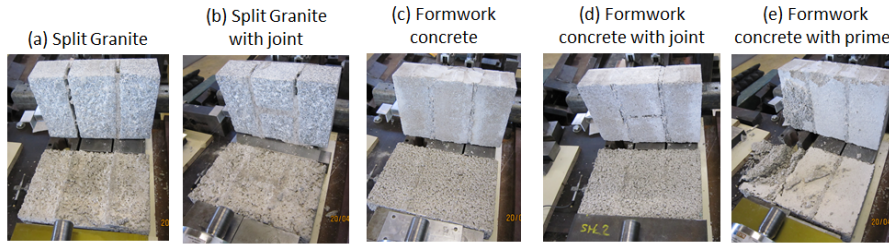

Figure 4.5: Breaking pattern for five different configurations.

sample was tested for each configuration, the obtained results allow only for a first estimate of the bonding strength. Nevertheless, the positive influence of split surfaces and the use of primer are obvious. Further investigations with different mortars and paving blocks are recommended to define appropriate values for load capacity analyses. However, the obtained results provide us with approximate shear strength values between different paving blocks and mortar bed, which will be sufficient for the interpretation of the subsequent numerical results. For this reason, these first experimental results have already been included within this paper.

4.3 Numerical model

The numerically modelled region of the considered paving block structure is shown in red in Figure 4.6, with a width B of 40 cm and half the road widths $L/2$ of 2, 4, and 8 m. Symmetry boundary conditions have been applied to all three vertical sectional areas. The exact geometry, the finite element mesh as well as loading, boundary and interaction conditions are given in Figure 4.7. The whole numerical model consists of a paving block superstructure with 5 rows of 20 paving blocks (20/10/10 cm) each, laid in a cross laying pattern. A mean elastic modulus of the paving blocks of 35 000 MPa was obtained by ultrasonic measurements according to Füssl et al. (2015b). The poisson ratio was set to 0.15, the thermal expansion coefficient to $1\,\mathrm{e}^{-5}\,1/K$, and the density to $2.4\,\mathrm{e}^{-9}\,\mathrm{t/mm^3}$. A table summarising all assigned material parameters to the numerical model and giving the associated sources can be found in Appendix A.

The interaction between paving blocks (for the 175 vertical joints) are realised by surface-based cohesive behaviour and a generalised traction separation law. As illustrated in Figure 4.8, a linear elastic traction separation relationship is assumed prior to damage and a linear post damage softening response. The area under the red curve in Figure 4.8 (b) corresponds to the fracture energy, which was set to 0.34 mJ according to Trunk and Wittmann (2001). Damage occurs when the maximum of the following ratios, $\max\{(\langle t_n\rangle/t_n^o), (t_s/t_s^o), (t_t/t_t^o)\}$, reaches a value of 1, as defined in Corp. (2016). Thereby, t_n, t_s, and t_t denote the traction forces in normal and two tangential directions of the respective contact surface, whereas the symbol $\langle\rangle$ is used to take into account
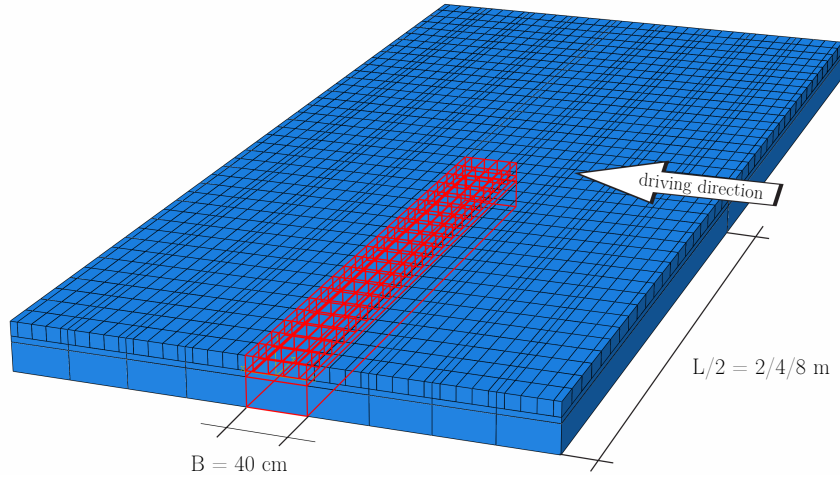
Figure 4.6: Considered paving block superstructure and numerically modelled region displayed in red.

that a purely compressive stress state will not initiate damage. The related strength values are designated as t_n^o, t_s^o, and t_t^o, respectively. At each contact point an overall damage variable D is introduced, capturing the combined effect of all active damage mechanisms by the introduction of an effective separation variable $\delta_m = \sqrt{\delta_n^2 + \delta_s^2 + \delta_t^2}$, as illustrated in Figure 4.8(a), according to Camanho and Davila (2002). δ_n, δ_s, and δ_t denote the separations between two contact surfaces (which belong together) in normal and the two tangential directions, respectively. The damage variable D is then computed as $D = \frac{\delta_m^f*(\delta_m^{max}-\delta_m^0)}{\delta_m^{max}*(\delta_m^f-\delta_m^0)}$, where $\delta_m^f = 2G/t_m^0$ represents the effective separation at complete failure of the interface, with t_m^0 as the effective traction at damage initiation and G as the fracture energy. δ_m^0 denotes the effective separation at damage initiation and δ_m^{max} represents the maximum value of effective separation obtained during the analysis history. This overall damage variable is a scalar which monotonically evolves from 0 to 1 as damage increases and affects the contact stress components as follows: $t_n = (1-D)\overline{t_n}, t_s = (1-D)\overline{t_s}, t_t = (1-D)\overline{t_t}$, where $\overline{t_n}, \overline{t_s}$, and $\overline{t_t}$ refer to the contact stress components predicted by the elastic traction-separation behaviour for the current separations without damage.

Unfortunately, such cohesive interaction models (describing strong softening behaviour) often lead to severe convergence difficulties. To stabilise the numerical solution viscous regularisation of the constitutive equations (an artificial damping procedure) has been applied. Thereby, the traction-separation laws are regularised by the usage of a viscous stiffness degradation variable D_v, as defined in $\frac{d(D_v)}{dt} = \frac{1}{\mu}*(D-D_v)$, where μ is a viscous coefficient, D denotes the overall damage variable and dt represents the current time step. D_v is substituting the overall damage variable in the damaged response of the stabilised cohesive surface interaction given as $t = (1-D_v)\overline{t}$. Thereby, the stabilised cohesive interaction permits stresses to be outside the limits of the traction-separation law. Further, D_v is used to update the material tangent stiffness matrix of the softening contact interaction. By using a value of 0.002 for the viscous coefficient μ

the convergence of the simulation has been improved without compromising the results. To exclude a significant influence of this procedure on the numerical solution, the viscous energy dissipation has been compared to the corresponding strain energy to verify that almost no artificial stiffness has been added to the system.

A bedding stiffness of 1 400 MPa/mm in normal and 609 MPa/mm in tangential direction was assigned to the vertical joint interactions, to consider the thickness and mechanical behaviour of the mortar within the joints.
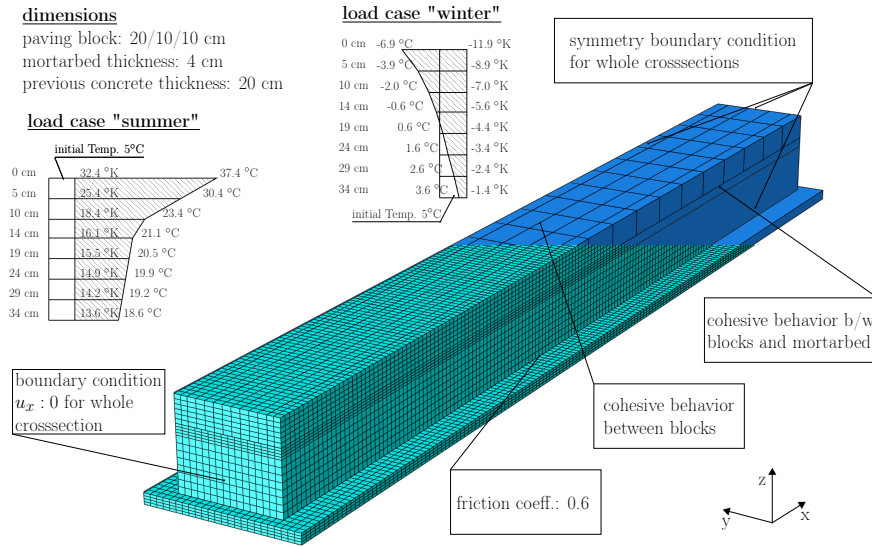
Figure 4.7: Geometry, interactions and boundary conditions of the numerical model, as well as the two main temperature load cases applied.

(a) Effective separation.

(b) Linear softening after damage initiation.
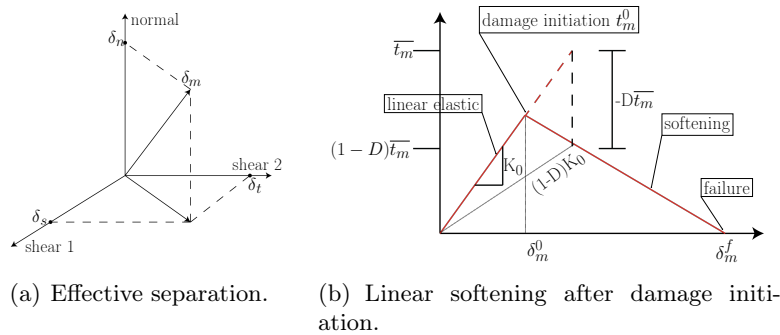
Figure 4.8: Surface-based cohesive behavior.

Below the superstructure a layer of mortar spans over the whole area with a thickness of 40 mm. Again, the material properties were obtained from experiments performed by TVFA Vienna, giving an elastic modulus of 14 000 MPa, a density of $1.9\,\mathrm{e}^{-9}$ t/mm^3,

a poisson ratio of 0.15 and a thermal expansion coefficient of 1 e^{-5}. The interaction between paving blocks and the mortar bed were again realised with a cohesive surface to surface contact.

The pervious concrete layer underneath the mortar bed has the same areal dimensions but a thickness of 200 mm. The material behaviour is defined by an elastic modulus of 14 000 MPa, a density of 1.9 e^{-9} t/mm^3, a poisson ratio of 0.15, and a thermal expansion coefficient of 1 e^{-5}. The interaction law between this layer and the layer of mortar is defined in the same way as the interaction between the layer of mortar and the paving blocks. The whole model, as visualised in Figure 4.7, is supported in vertical direction by a rigid sub-base layer. This sub-base layer interacts with the pervious concrete layer in tangential direction by a penalty frictional model with a frictional coefficient of 0.6.

The simulations were divided into two steps, first, the dead load of the paving block structure and, second, a static temperature gradient, defined by analytic fields, were applied. To define the temperature gradient the minimum temperature for the region of Vienna according to Wistuba (2003) was used. Although these temperature profiles are intended for asphalt pavements, due to the fact that the specific heat capacities of asphalt and concrete lie close together (at around 0.92 and 0.88 m^2/s), they could be also used for the investigated paving block structures. Differences in the thermal conductivity could be neglected too, considering the long periods of night and day temperatures of several hours. In layers below the mortar bed, the used temperature gradient could differ in a greater extent, due to the lower density of the material. To find out about these deviations, temperature measurements are ongoing on full-scale paving block structures at TU Vienna.

All FE simulations were run with the commercial Finite Element Software Abaqus, taking into account geometric non-linearity. More than 200 simulations were carried out on a HPC-cluster system at TU Vienna with an average total cpu time of 7.7 h for a 8 m model with 315 822 DOFs. In the course of the simulations, the maximum cohesive strength between paving blocks and the mortar bed, the maximum cohesive strength in-between paving blocks, the applied temperature, the model widths and the laying pattern have been varied.

4.4 Numerical results

4.4.1 Identification of response mechanisms under cooling

The cohesive strength between paving blocks and the underlying mortar bed is certainly one of the most important factors in determining the performance of such a structure under temperature loading (cooling). It can be assumed that the experimentally-obtained strength values in Section 2 are not always reached in practice, especially not continuously over large areas. Laying paving blocks on already hardened mortar bed, for example, might result in a greatly reduced bonding strength.

This motivated the following simulation program, where the performance of a paving block structure with 15 different cohesive strength values varied from 0.00001 MPa up to 10 MPa has been investigated. The whole possible range of bonding, between paving blocks and mortar bed, in practice should therefore be covered and all possible response mechanisms should be obtained. The in Figure 4.7 defined load case "winter" has been applied to all 15 configurations and as performance parameter the maximum

occurring crack width w_{cr}^{max}, defined as the maximum separation between two adjacent paving blocks, was chosen. The obtained maximum crack widths as a function of the cohesive shear strength between paving blocks and mortar bed, τ_{crit}, are plotted in Figure 4.9. It can be seen clearly that there is no smooth decrease in crack width with increasing cohesive strength. For very low as well as very high cohesive strength values the maximum crack width is almost constant, whereas a much larger crack width is obtained for a low bonding strength between paving blocks and mortar bed. The transition from one crack width plateau to the other takes place very quickly, which makes it possible to define a so-called transition zone, denoted as Region ③ in Figure 4.9. The cohesive strength areas divided by this zone are designated as Region ① and Region ②, respectively. By comparing this relationship with the corresponding deformation fields of the paving block structures, also three different basic failure mechanisms, which can be related to the three different regions defined in Figure 4.9, can be distinguished:

Region ①: In case of a very low cohesive strength between paving blocks and mortar bed only a single distinct crack occurs and, consequently, a large maximum crack width is established . Such a mechanism is shown in Figure 4.10 (a), for a cohesive strength of 0.00001 MPa, leading to a single crack of 0.29 mm. All the vertical joints between other paving blocks remain closed or have at most a small opening which can be attributed to numerical regularisation. Due to a perfectly homogeneous cohesive strength distribution between the paving blocks and the mortar bed, the single crack occurs close to the boundary of the model, triggered by the slightly higher local structural stiffness induced by the boundary conditions. This result is in good agreement with observations in the field, where indeed very often large cracks develop in the boundary regions of roads. However, this single crack could occur at any point in the structure where the structural stiffness is locally increased. This could be caused by stiffness differences in the mortar bed, a locally better toothing of joint mortar and mortar bed, or various structural installations preventing a thermal contraction of the superstructure.

Region ③: The opposite case is represented by a structure with a very high bonding strength between paving blocks and mortar bed, which is exemplarily illustrated in Figure 4.10 (c) (cohesive strength of 1 MPa). For these cases, a diffuse network of cracks has been developed , with a maximum crack width of 0.027 mm, being only one-tenth of the crack width obtained for models of Region ①. The paving blocks are more or less rigidly embedded into the mortar bed and, thus, transmit shear forces directly into the underlying layer. Each paving block deforms independently of the others and, thus, the resulting crack width seems to be only a function of the single paving block characteristics and the applied temperature loading. Paving blocks with larger dimensions would in this case lead to wider cracks, which would not be the case in Region ①.

Region ②: Finally, the transition zone between Region ① and Region ③ is designated as Region ②, consisting of paving block structures which show both, distinct cracks and additionally fine cracks between other paving blocks. An example is shown in Figure 4.10 (b), having a cohesive strength of 0.005 MPa. This failure pattern represents a logical intermediate state between the two others, and it is important to show that the numerical simulation tool is able to capture such 'mixed' failure mechanisms accurately. A reliable identification of the (practically relevant) transition zone, Region ③, should therefore be possible for different types of paving block structures.

The found relationship in Figure 4.9 and the qualitative division into three regions based on failure mechanisms could be an important insight for the further development

of such paving block structures. It could be aimed at a bonding strength which ensures that no single distinct cracks occur.

Nevertheless, more loading cases and model configurations need to be investigated to reliably identify cohesive strength values at which the critical Region ② starts. This has been done in the following.
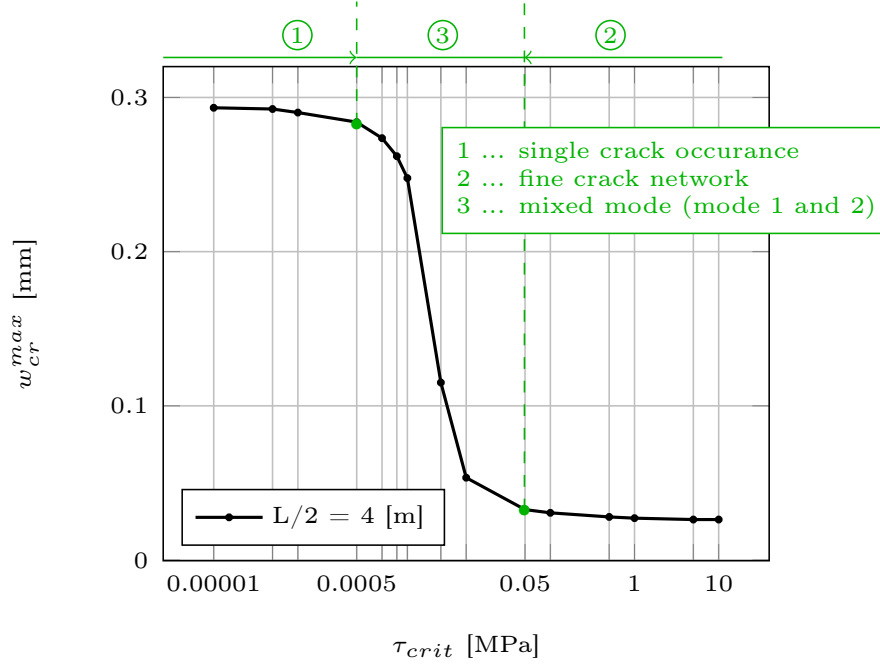

Figure 4.9: Maximum occurring crack widths w_{cr}^{max} as a function of the cohesive shear strength τ_{crit} between paving blocks and mortar bed, and the three identified regions showing different structural failure mechanisms.

4.4.2 Parameter studies

To figure out in which way the most important structural parameters influence the response of the model structure, e.g. the location of the three identified regions above, the following characteristics have been varied: (a) The road width, (b) the construction temperature, which was set to 5 °C for all previous simulations, and (c) the bonding strength of the mortar in the vertical joints.

(a) Road width

As mentioned within the fundamental considerations in Section 2, the dimensions of a homogeneous body do not influence its thermally induced stresses under specific assumptions. Nonetheless, for the paving block structure considered, showing in-homogeneous failure mechanisms, the width L of the road strongly influences the maximum crack width w_{cr}^{max}, as shown in Figure 4.11. The two additionally investigated road widths of $L/2 = 2$ and $L/2 = 8$, result in lower and higher, respectively, maximum crack widths.
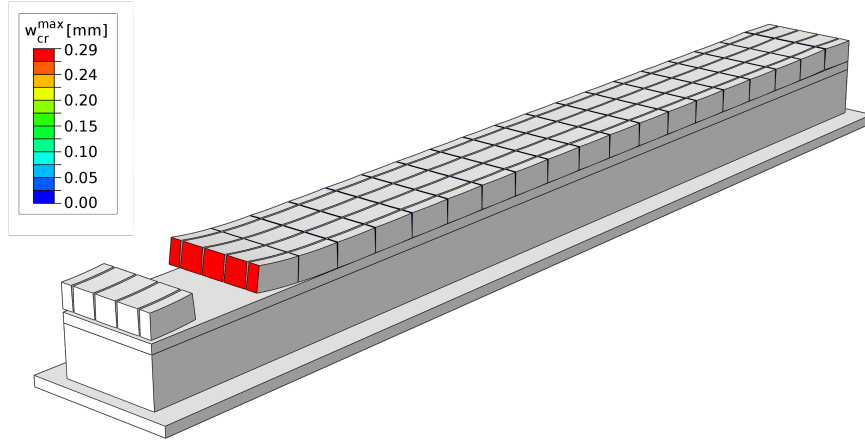
(a) $\tau_{crit} = 0.00001$ MPa (Region ①)
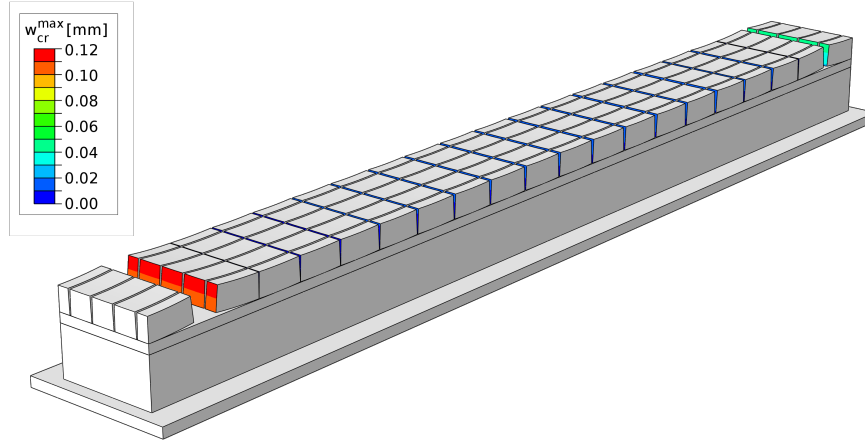
(b) $\tau_{crit} = 0.005$ MPa (Region ②)
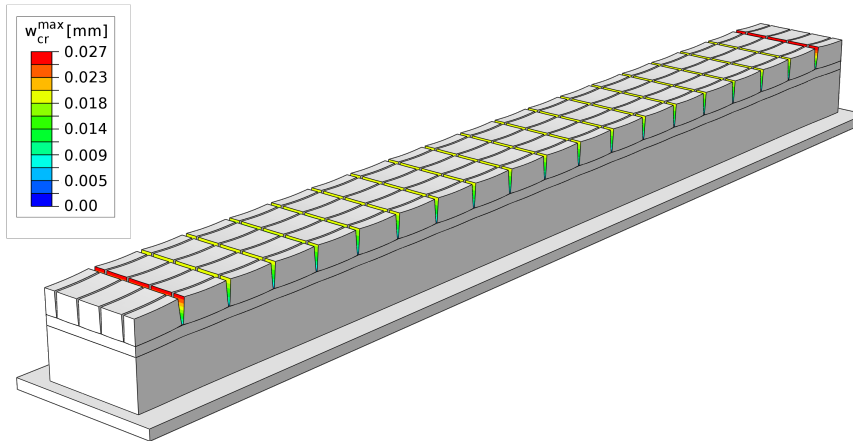
(c) $\tau_{crit} = 1$ MPa (Region ③)

Figure 4.10: Illustrative failure mechanisms for the three identi-
fied regions: (a) single distinct crack, (b) mixed mode, and
(c) fine crack network.

Understandably, this is only the case for Region ①, where single distinct cracks occur. In this region large parts of the structure behave as monolithic block and, thus, the length of the structure strongly influences the crack width. Interestingly, it seems that the maximum crack width increases overlinear with respect to the road width. In Region ② the road width doesn't affect the maximum crack width, which is in good agreement with the above-made observation that in this case the crack widths are only a function of the single paving block characteristics. Despite the large differences in Region ①, the location of the transition zone (Region ③) is hardly affected. This gives reason to believe that a certain bonding strength, ensuring a paving block structure to behave according to Region ②, may possible be defined.

Figure 4.11: Maximum occurring crack widths w_{cr}^{max} as a function of the cohesive shear strength τ_{crit} between paving blocks and mortar bed, for three different road widths L.

(b) Construction temperature

Since in reality the construction temperature can be higher than the assumed 5 °C in previous simulations, the relationship presented in Figure 4.9 has also been determined for 15, 30, 45, and 60 °C installation temperature (see Figure 4.12). The final temperature, however, was kept constant as defined by the "winter" loading case given in Figure 4.7. As expected, the maximum crack width increases with increasing installation temperature. But, also the critical cohesive strength value, defining the begin of the transition zone, increases one order of magnitude from about 0.01 MPa (for 5 °C) to about 0.1 MPa (for 60 °C). Comparing the latter value to the experimentally-obtained strength value of 0.28 MPa for conventional concrete paving blocks (also given in Figure 4.12), we can note that the boundary of the transition zone comes very close to

the measured values. Assuming that the bonding strength under laboratory conditions represents an upper bound to the strengths reached in the field, it is not unlikely that in practice paving block structures fall into the transition zone, Region ③. According to these simulation results, there is a risk that a combination of poor execution standards and high installation temperatures lead to large distinct cracks due to cooling events in winter. This could explain practical observations of elusive damage of certain paving block constructions.
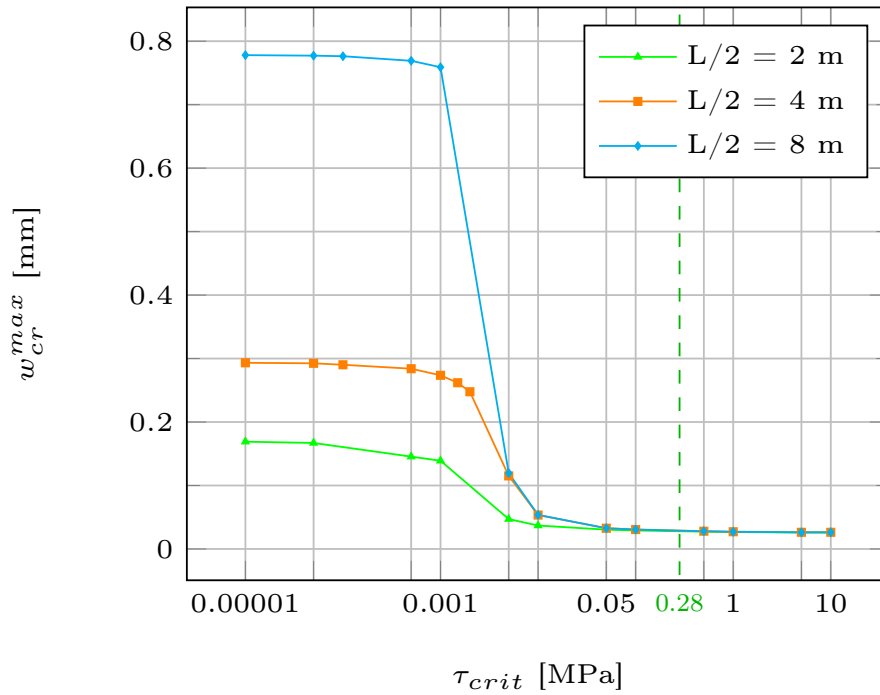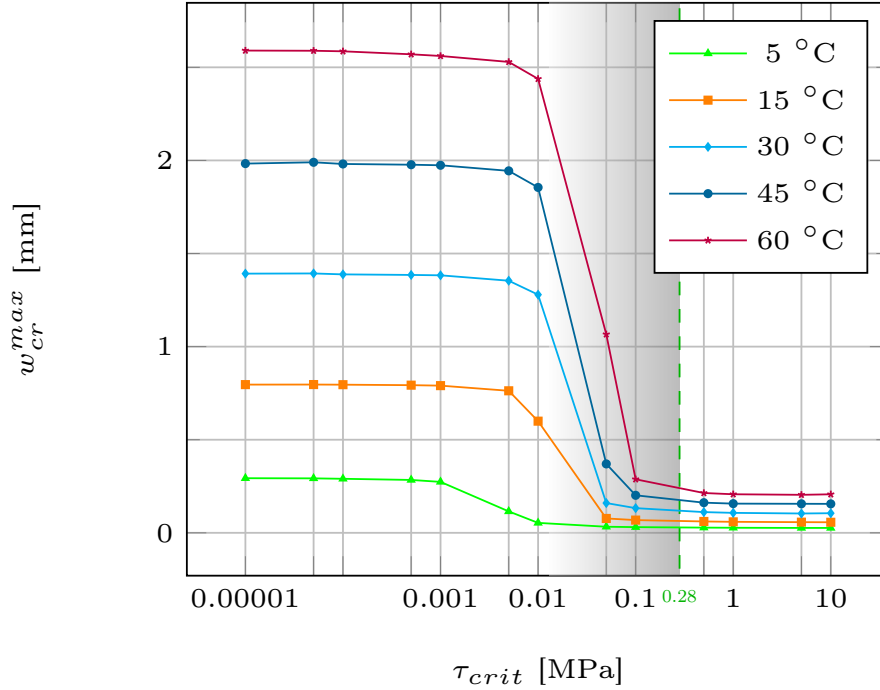

Figure 4.12: Maximum occurring crack widths w_{cr}^{max} as a function of the cohesive shear strength τ_{crit} between paving blocks and mortar bed, for 5 different construction (installation) temperatures.

(c) Bonding strength of vertical joints

Finally, the effect of the cohesive tensile strength between paving blocks (mainly determined by the mortar of the vertical joints) on the previous findings was of interest. Thus, the relationship proposed in Figure 4.9 has been extended to this strength, denoted $\sigma_{n,crit}$, in the third dimension (see Figure 4.13). The influence of $\sigma_{n,crit}$ on the identified three regions is negligible. Interestingly, the crack width of a single distinct crack according to Region ① increases with increasing bonding strength $\sigma_{n,crit}$ up to 2 MPa. A significant increase of the maximum crack width from about 0.25 mm to 0.35 mm was obtained, which can be traced back to an even higher stress and, subsequently, structural deformation concentration at the location of the critical crack. Accordingly, with respect to cracking, a higher cohesive tensile strength in vertical joints between paving blocks is not necessarily an advantage. Although, an additional data series with a cohesive strength between paving blocks of 4 MPa, which has been excluded from the

graph for illustrative reasons, showed no cracking anymore. However, this strength will not be achievable with conventional construction methods.
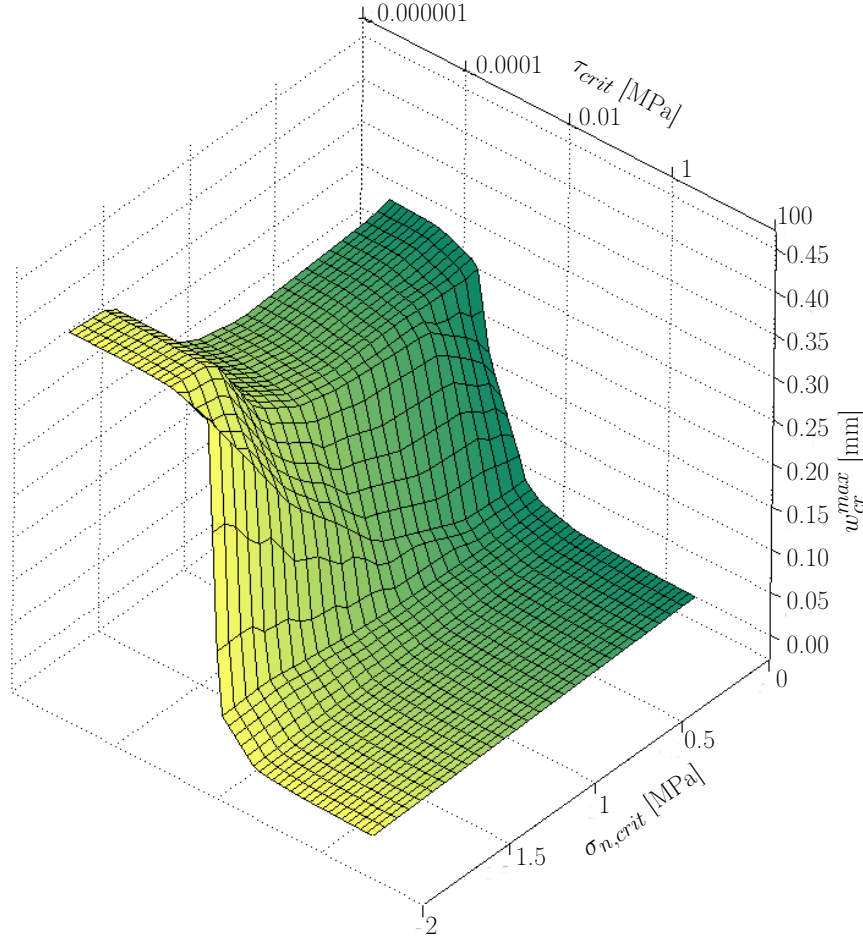
Figure 4.13: Influence of the cohesive shear strength between paving blocks and mortar bed τ_{crit} and the cohesive tensile strength of the vertical joints between paving blocks $\sigma_{n,crit}$ on the maximum occurring crack widths w_{cr}^{max}.

4.4.3 Influence of non-constant construction temperature

In all former simulation the construction temperature (initial temperature) was constant throughout the paving block structure, because no reliable information about temperature gradients during the construction process were available. However, they were not necessary to obtain the desired statements. Nevertheless, hydration of the mortar bed as well as solar radiation during the installation phase might lead to in-homogeneous initial temperature distributions, which subsequently influence the occurrence of cracks in a positive or negative way. A fictional but realistic in-homogeneous temperature profile is given in Figure 4.14 (a), where the surface is heated by solar radiation from 5 to 15 °C and the temperature of the mortar bed is slightly increased (10 °C) due to hydration. On the other hand, Figure 4.14 (c) shows a temperature profile only characterised

by the heated mortar bed, in case that the solar radiation is avoided by using shading measures on the construction site. Again, both models were loaded with a temperature field finally leading to the temperature distribution defined in Figure 4.7 for the load case "winter". The corresponding deformation fields can be found in Figures 4.14 (b) and (d), respectively. In case of no shading measures (surface temperature of 15 °C), a maximum crack width of 0.52 mm was obtained, while in the second case, where the surface temperature was assumed to be 10 °C lower, the crack width reduces to 0.39 mm. Thus, a 33 % higher crack width w_{cr}^{max} is established only due to a higher surface temperature. Based on this numerical result, it can be assumed that shading or cooling measures during construction are useful to reduce the risk of large cracks during wintertime. This has been an ongoing controversial topic in engineering practice.
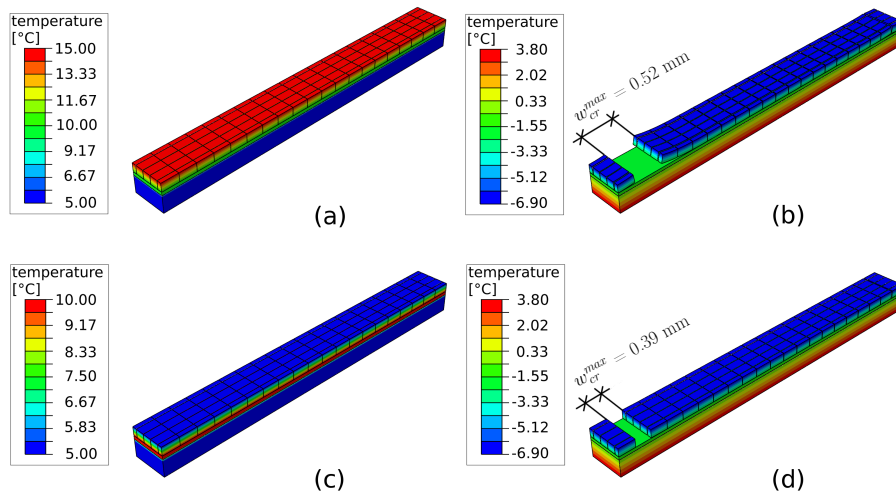
Figure 4.14: Influence of shading measures during construction at high temperatures on the occurring crack widths after cooling in wintertimes.

4.4.4 Expansion behaviour due to temperature increase during summer

According to Figure 4.12, a low construction temperature is preferable to avoid cracks during wintertime. Unfortunately, such low construction temperatures lead to a larger expansion of the superstructure in summertime, which may result in critical compressive stresses or lift off of the paving block superstructure. Such a lift off of paving blocks from the mortar bed can be observed regularly during summertime. To investigate this effect, simulations have been performed with a constant construction temperature of 5 °C and a summer temperature distribution according to Wistuba (2003), as defined in Figure 4.7. The cohesive tensile strength, σ_n^{crit}, has been varied from 0.00001 MPa to 1 MPa and the corresponding maximum lift off w_{lo}^{max} has been evaluated. The obtained relationship is shown in Figure 4.15 and two related deformation fields, showing the lift off of the paving block superstructure, are illustrated in Figure 4.16. Similarly to the parameter studies presented before, a highly non-linear relationship between the bonding strength and the considered performance parameter, in this case the amount

of lift off w_{lo}^{max}, has been obtained. The transition zone, however, between 'good' and 'bad' performance is slightly larger. Allowing a rotation of the curbstone, a lift off, as can be seen in Figure 4.16, was obtained for low values of the cohesive tensile strengths between paving blocks and the mortar bed. But, according to Figure 4.15, a cohesive tensile strength of about 0.1 MPa seems to be sufficient to avoid this phenomenon. Interestingly, the limit value of cohesive tensile strength (around 0.1 MPa), ensuring no lift off of the paving block structure, is of the same order of magnitude as the necessary cohesive shear strength to avoid distinct cracking.
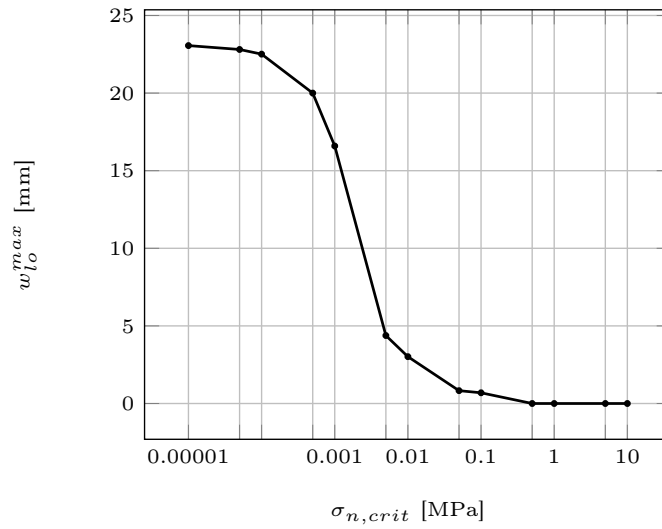
Figure 4.15: Maximum lift off w_{lo}^{max} of the paving block superstructure under load case "summer" as a function of the cohesive tensile strength $\sigma_{n,crit}$ between paving blocks and the mortar bed.

(a) $\sigma_{n,crit} = 0.01$ MPa   (b) $\sigma_{n,crit} = 0.00001$ MPa
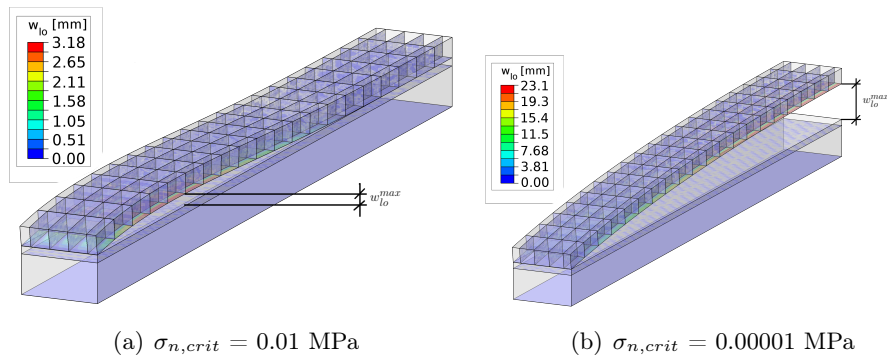
Figure 4.16: Illustration of lift off of the paving block superstructure due to load case "summer", for two different cohesive tensile strengths between paving blocks and mortar bed.
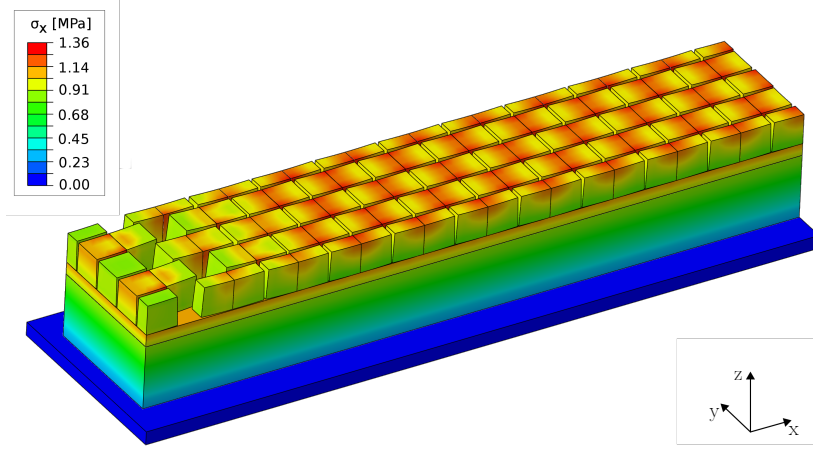
4.5   Conclusions and outlook

Figure 4.17: Outlook: Structural failure mechanism of a paving
block structure, laid in a running bond pattern.

In this paper, a numerical simulation tool has been proposed allowing for a realistic reproduction of failure mechanisms of paving block structures with mortar filled vertical joints under temperature loading. Temperature loads, representing cooling periods in winter as well as heated paving block structures in summer, have been applied using analytical fields. Cohesive interaction behaviour between paving blocks and between paving blocks and the mortar bed gave access to crack widths, which were assumed to be an important performance evaluation characteristic. The structural behaviour of numerical models with up to 556 cohesive interactions could be investigated stable. Therefore, it was necessary to employ viscous damage damping, but special attention was payed that viscous forces are ramped down sufficiently and comprehensive parameter studies were conducted to ensure the smallest possible effect of these regularisation measures.

Several hundred simulations with different bonding strength between paving blocks and paving blocks and mortar bed, temperature loading situations, and road widths have been performed to obtain a comprehensive picture of the mechanical behaviour of such pavement superstructures. Based on this extensive simulation program, two different failure mechanisms due to cooling in winter time could be distinguished and a rather small transition zone between them was identified. If there is a low bonding strength between paving blocks and mortar bed it is very likely that distinct single cracks will occur, while a rather fine crack network can be assumed in case of a high bonding strength. Since this fine cracks, distributed over the whole superstructure, are probably not be seen with the naked eye or even do not occur due to the not considered relaxation of mortar in the vertical joints, respectively, this case should be aimed at in practice. Thus, it is of outmost interest to identify the transition zone between those two failure mechanisms, which has been done in this work for several configurations.

Based on these investigations, answers to the three questions raised in the introduction can now be formulated:

- The bonding strength between paving blocks and mortar bed indeed seems to

have a very large impact on the performance of a paving block superstructure under temperature loading. A characteristic shear strength larger than 0.1 MPa avoids the occurrence of distinct large cracks according to the performed numerical investigation, even under the worst case scenario of very high installation temperatures (up to 60 °C). Shear strength values between 0.26 and 0.28 MPa were obtained experimentally for concrete paving blocks, and would therefore be sufficient. However, these values were obtained under laboratory conditions and, therefore, provide rather upper limits for the bonding strengths in the field. Thus, it is quite probable that a combination of poor execution and high construction temperatures cause paving structures to behave as it was numerically obtained for the transition zone, Region ③. This could be an explanation for elusive damage to paving block structures, frequently observed in engineering practice.

- A low installation (construction) temperature is basically beneficial to prevent cracking due to cooling during winter time, but it can lead to high compressive stresses and lift off of the paving blocks in summer. However, according to the performed simulations, a bonding strength of 0.1 MPa, in shear as well as normal direction to the interface between the paving blocks and the mortar bed, should be sufficient to avoid both distinct cracking in winter as well as lift off of the paving block superstructure in summer. Additionally, the numerical results give reason to believe that shading measures, in case of high solar radiation, are of benefit with respect to cracking in winter time.

- Based on the findings of this paper, expansion joints through the paving block superstructure only seem to be useful if the mentioned critical bonding strength cannot be reached and single large cracks are likely to occur. If only failure mechanisms according to Region ② (fine crack network) arise, expansion joints lose its purpose and may be omitted as long as the structure and connected installations can resist the compressive stresses in summer and an adequate bond between mortar bed and the pervious concrete layer is provided. Following this approach, also the challenge to predict the right location of expansion joints, which was seen often failed in retrospect, could be avoided.

In summary, the proposed numerical simulation tool allowed us to shed light on some unanswered questions regarding the performance of paving block structures with mortar filled joints, even if they cannot be answered fully yet. Further investigations will focus on different laying patterns, as exemplarily shown in Figure 4.17, combined temperature and traffic loading and the description of more complex failure mechanisms (including cracking through paving blocks). Furthermore, similar to the work in Füssl et al. (2015a) and Füssl et al. (2016a), the mechanical response under vertical loading will be investigated numerically. Also additional identification experiments on the mortar bed's cohesive strength to the pervious concrete layer are contemplated.

Paving Block Structures with mortar filled joints under vertical and temperature loading: full scale experiments and numerical simulations

Authored by Herwig Hengl, Wolfgang Kluger-Eigl, Ronald Blab & Josef Füssl
in preparation for submission to an international journal

In recent years paving block structures with mortar filled vertical joint have become a favorite alternative to asphalt pavements, mainly in intra-urban regions. Whereas paving block structures with sand filled joint are used for areas with light or low trafficked roads, paving block structures with mortar filled joint may be used in all areas, even when heavy traffic loads are expected. Unfortunately, immature design concepts of such structures often lead to unexpected cracks resulting from thermal loadings. This motivated the construction of three large paving block test fields in Waldegg, Austria. A numerical simulation tool was developed and compared to data obtained from the test fields. By means of the simulation tool proposed in this chapter basic structural failure mechanisms for rigid paving blocks structures on splitbed could be obtained. Finally, estimates for necessary friction coefficients between paving blocks and splitbed to prevent large cracks are given.

5.1   Introduction and motivation

Figure 5.1:   Cracks resulting from thermally induced stress

Paving block structures (pbs) have become a frequently used road construction method in urban areas. Thereby, increasingly applied is the construction of rigidly laid pbs, where the joints between paving blocks are filled with mortar. This rigidly laid pbs can be particularly beneficial when heavy traffic loadings are expected. Unfortunately, these structures often develop cracks on the surface, resulting from thermally induced stresses. These cracks affect the visual appearance but also the mechanical behaviour of these structures. As a consequence, the confidence and acceptance of this type of construction is reduced, which prevents it from a more frequent use.

As it comes to design codes for the construction of rigidly laid paving block structures, little information can be gained. In the German speaking region, rigid pbs are considered as a special construction method and only two guidelines offer recommendations for their planning and construction, namely: Forschungsgesellschaft für Straßen- und Verkehrswesen (2007) and Wissenschaftlich-Technische Arbeitsgemeinschaft für Bauwerkserhaltung und Denkmalpflege (2009). Both documents recommend the use of expansion joints and the latter mentions the positive influence of a strong adhesive bonding between the paving blocks and the mortar bed.

Nevertheless, extensive literature can be found regarding an equivalent problem: thermally induced stresses in concrete slabs and concrete pavements. Plannerer (1998), Rostasy and Kraus (2001), Röhling (2005), and Schikora and Eierle (1999) investigated thermal effects due to early stage hydration in concrete constructions. Bondy (1995), Schweighofer (2011), and Maliha (2005) engaged themself with thermal stresses and crack appearance in concrete pavements and slabs. Further contributions, Kolb (1988), Schütte (1997), and Petersson (1998) focuse on the interaction between concrete slabs and base layers.

To the authors knowledge, only two works regarding numerical simulations of rigidly

laid paving block structures, namely: Buchholz (2010) and Hengl et al. (2017b) can be found at the current moment. When it comes to numerical tools for paving block structures, several studies were published, which can be found in: Nishizawa et al. (1984), Jacobs and Houben (1988), Huurman et al. (1992), Lerch (2005), Ascher et al. (2006), Oeser and Chandra (2010), Füssl et al. (2016b), and Hengl and Füssl (2016), to mention only a short selection of them.

The lack of reliable design concepts concerning rigidly laid pbs was the main motivation for this work. To gain better understanding of the mechanisms and causes in rigidly laid pbs that lead to crack occurance were the focus of this work. More specifically, the following questions arose and should be answered in this work:

1. Can the main results gained from full scale temperature loading tests be reproduced with numerical simulations?

2. When, where, and why are cracks occuring in such paving block structures?

3. What is the impact of the friction coefficient or bonding between paving blocks and the beneath layers on the mechanical performance of the paving block structure and how do these parameters affect the distance between cracks?

4. How does the fracture energy of interfaces between materials influence the occurrence of cracks in paving block structures?

5. To which extend are sublayers influencing the vertical load bearing capacity?

6. Based on a better understanding of rigid paving block structures, can any recommendations be given regarding the construction method?

To answer that questions, a full scale field experiment with three different pbs was carried out with industry partners in Waldegg, Austria. The details of the field experiments can be found in Section 2. In Section 3 the numerical model and the results of various numerical simulations are given. A final conclusion is given in Section 4.

5.2   Full scale field experiments

To evaluate the horizontal displacements of rigid paving block structures under real climatic conditions, three full scale test fields were constructed in November 2015.

5.2.1   Testfield layout

Usually guidelines recommend a maximum field length of 6 to 10 m for rigid pbs and the installation of expansion joints between the fields to compensate thermal expansion and contraction. To encourage the occurrence of cracks these guidelines were consciously ignored and the test fields were constructed without expansion joints and field lengths of 15 m.

Test fields

Three test fields were constructed at Waldegg, Austria in Winter 2015. These test fields were constructed over a length of 15 meters and with a width of 1 m each, separated by gravel-filled gaps of 20 cm. Horizontal movement was prevented by a rigid concrete

bearing at the one end of the test fields. The opposite side of the pbs is not hindered in any way, allowing horizontal deformations to develop freely. The basic layout of the test field is shown in Figure 5.2.
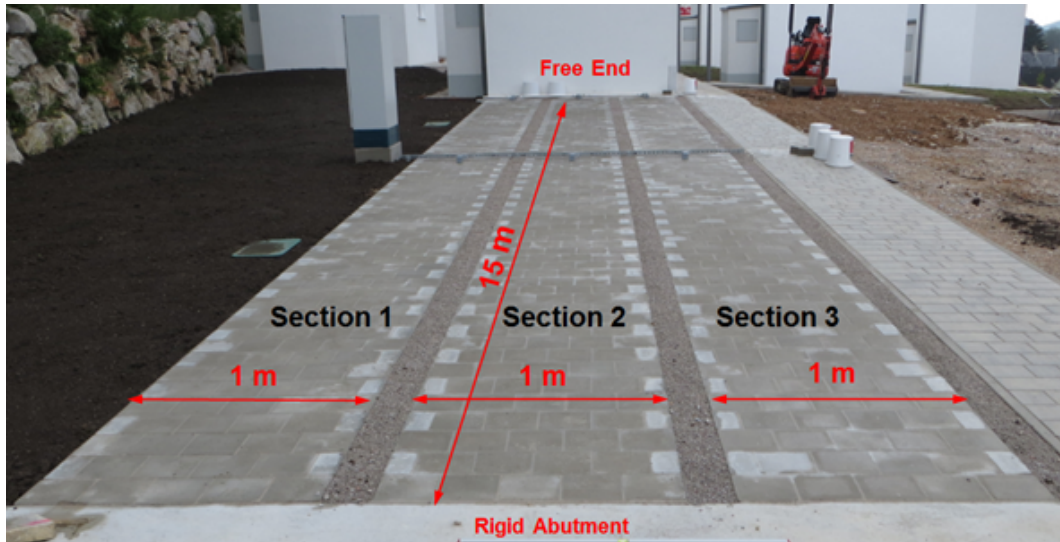
Figure 5.2:   Basic layout of the three different paving block structures installed for full scale temperature experiments

Pavement Structures

The composition of the three different paving block pavements investigated is schematically illustrated in Figure 5.3. The test fields can be refereed to as:

- Test field 1: concrete blocks with mortar-filled joints laid in a mortarbed on a pervious concrete base course

- Test field 2: concrete blocks with mortar-filled joints laid in mortarbed on an unbound base course

- Test field 3: concrete blocks with mortar-filled joints laid in splitbed on an unbound base course

Block Types and Laying Pattern

For all three test fields, concrete blocks with the dimensions 205/170/80 mm were used. The blocks were laid in a stretcher bond separated by joints of 10 mm width. The joints were then filled with cement mortar containing 2 mm aggregates. For the bedding a cement mortar with 8 mm aggregates was used.

Instrumentation

Six PT100 temperature sensors were built into test fields 1 and 2. They were placed on the surface, underneath the bedding (13 cm) and underneath the base course (-28 cm)
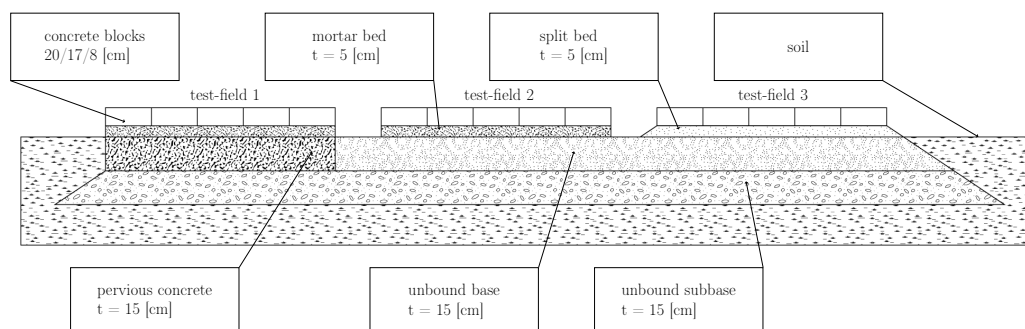
Figure 5.3:   Three different paving block structures investigated in full scale
            field experiments

to record the temperature in different depths of the pavement structure. Furthermore, six Wenglor CP35MHT80 laser distance sensors were applied to the pavement surfaces to record horizontal deformations. They were placed in the middle and at the free end of each test field, as can be seen in Figure 5.4. In addition, a weather station was set up nearby to collect air temperature, rain, wind, and solar radiation.
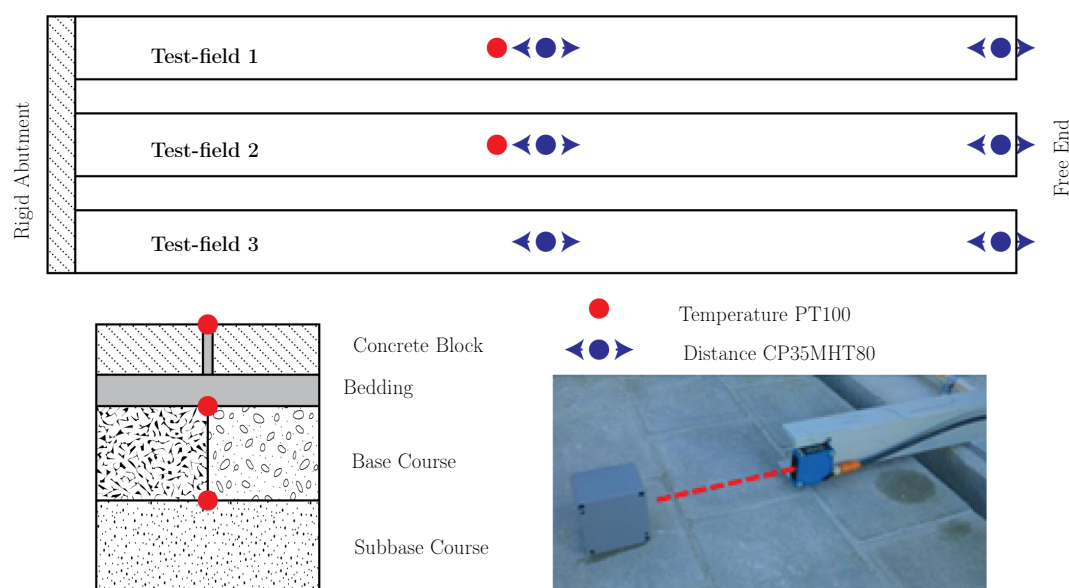
Figure 5.4:   Instrumentation on Test Field

Construction

The test field was built in November and December 2015. After finishing the rigid concrete bearing, the anti-frost layer was constructed for all three test sections at once. On November 25th, 2015 at air temperatures of about 0°C, the base course for Section 2 and 3, and the pervious concrete base for Section 1 were constructed. On November 26th, 2015 the mortarbed for test field 1 was applied and the concrete paving blocks were laid into the bedding. The block pavement and the mortarbed of Section 2 were

built on November 27th, 2015 and November 30th, 2015 at air temperatures between 3°C and 11°C. The concrete blocks of test field 3 were paved on splitbed afterwards. On Dezember 2nd, 2015 the joints of the three test fields were filled with cement mortar at air temperatures of about 10°C. Though the climatic conditions were not ideal for the construction of rigid pbs, the low construction temperatures were beneficial to obtain large deformations in summer.

5.2.2   Execution of full scale experiments

The experiments should deliver accurate temperatures in different layers of the pavement structures and correlated displacements due to the structures thermal expansion and contraction. The measurements were intended to be carried out for at least one year. Further, due to the design of the test fields, crack occurrence was expected and therefore visual inspections of the pavement surfaces were planned. The measurements can be listed as following:

- The temperature measurements, based on the temperature sensors built into test field 1 and 2, started on Dezember 25th, 2015 at an air temperature of 0°C. The measuring interval was set to 15 minutes.

- Horizontal deformation, which were measured in the middle and on the free end of the pavements surfaces, were obtained by laser distance sensors. This measurements also started on November 25th, 2015 and the measuring interval were set to 15 minutes.

- The aim of the visual inspection was to register surface damages, especially cracks. Therefore, inspections were planned after the first winter (May 2016), the first summer (October 2016), and in the second winter (December 2016). All damages were documented with videos and photos.

5.2.3   Results of full scale experiments

In a period of 13 months (till January 29th, 2017) over 260.000 temperature data points were recorded from sensors in the test fields and additional sensors which captured the air temperature. Temperature distributions of the air, on the pavements surface, beneath the bedding, and under the base course is shown in Figure 5.6 a. The minimum air temperature was -16,1°C and the maximum +33,4°C, leading to an air temperature range of approximately 50°K. The maximum temperature difference on the pavements surfaces was 54°K for the pavement surface, 39°K underneath the bedding, and 30°K underneath the base course.

The results further reveal, that there were no major discrepancy of temperatures beneath the pervious concrete layer and beneath the unbound base layer. The temperatures beneath the bedding and the base courses followed the air temperature with a time delay of 1.5 to 6 hours, depending on the layers depth. The daily surface temperature courses of hot summer days reveal extreme temperature increases of 26°K during 10 hours followed by a 14 hours decrease during the night. On cold winter days the pavements surface temperatures are generally higher than the air temperature and there are much less fluctuations (4°K) during a 24 hour period than in summer. For longer cold periods of one week or more the temperatures in the bedding and the base course fell below 0°C.

(a) Temperature data points   (b) Distance data points
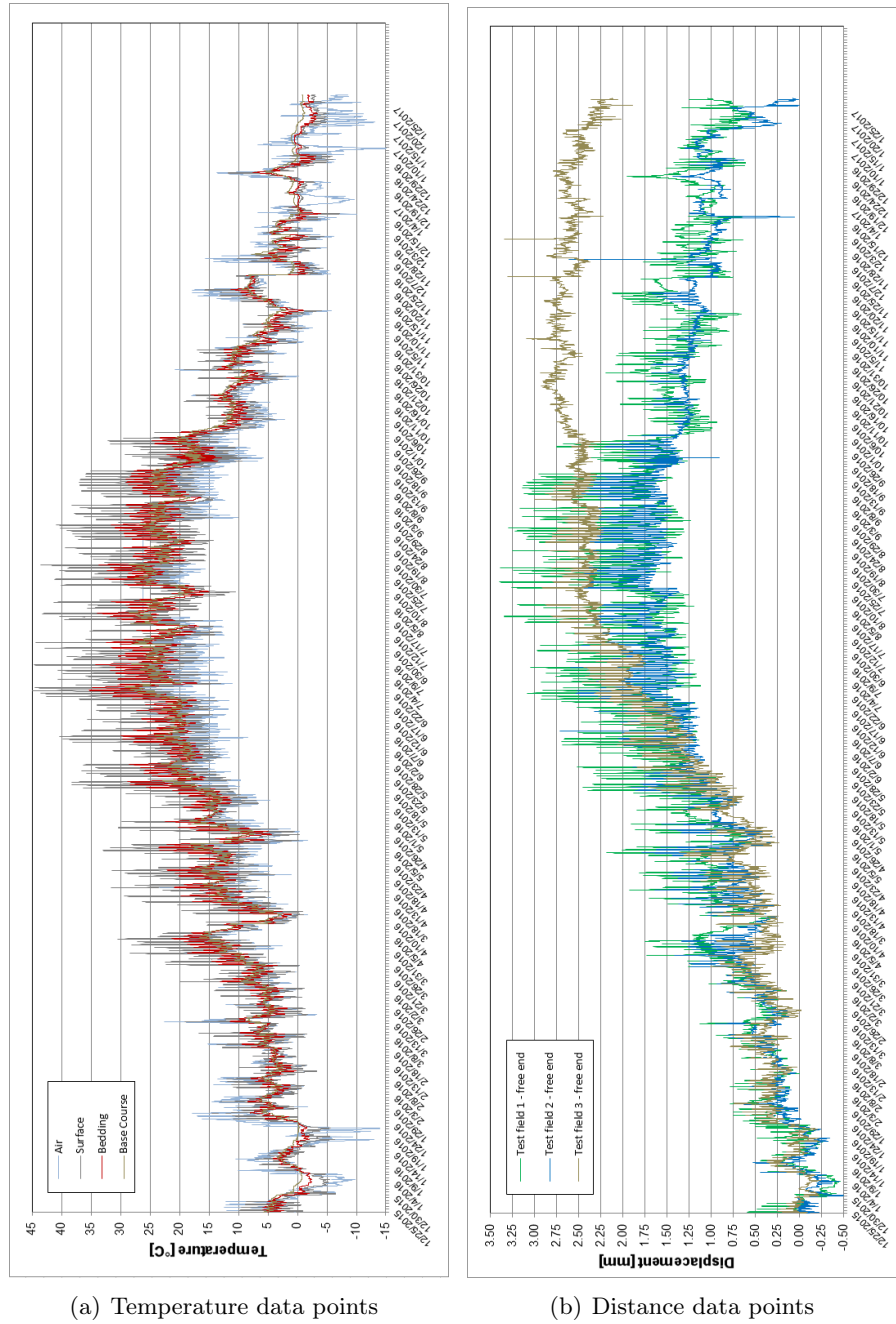
Figure 5.5: Results of temperature experiments

Deformation Analysis

In a period of 13 month (till January 29th, 2017) more then 220.000 distance data points were recorded from the distance sensors applied to the test fields surfaces. In Figure 5.6 b, the course of the horizontal deformation for the free end of the three test fields are presented. For each of the six sensors the minimum, the maximum, the mean, the range, and the standard deviation were calculated and are given summarised in Figure 5.1. The maximum compression of -0.6 mm was measured during the cold

Period 25.12.2015-29.01.2017	Test-field 1		Test-field 2		Test-field 3	
Displacement [mm]	Middle	Free End	Middle	Free End	Middle	Free End
Minimum	-0.5	-0.5	-0.6	-0.5	-0.6	-0.2
Maximum	+0.5	+3.4	+0.9	+2.7	+0.8	+3.4
Range	1.0	3.9	1.4	3.2	1.4	3.6
Mean Value	0.0	1.2	0.0	1.0	0.1	1.6
Deviation	0.1	0.7	0.2	0.6	0.2	1.0

Table 5.1: Statistical analysis of Displacements for test sections 1, 2, and 3

weeks in January 2016, where the temperatures were clearly below 0°C. The maximum expansion of 3.4 mm was measured in the beginning of August 2016.

The measurements show that the free end of the pbs can deform easily. In longitudinal direction the shear force increases, resulting from the interaction of the bound layer/layers to the unbound ones. As a consequence, the distance sensors in the middle of the structures only record measurements up to 0.9 mm, whereby at the free end of the structure almost 3.4 mm were recorded.

Based on the experimental observations, the following statements can be made:

- The temperature gradient over the cross section of the construction causes incompatible deformations and is, thereby, holding back the deformation of structural elements with the highest temperature loads. This leads to temperature-induced internal stresses.

- The constant temperature part in the cross section drives the bound layers of the structure to contract/expand. As far as the bonding between these layers is intact, the deformation happens uniform to a great extend. Nevertheless, differences of thermal expansion coefficients may result in internal stresses and distortion of cross-sections.

- The deformations of the structure, resulting from the temperature gradient as well as from the constant part of the thermal loading, are restrained by the friction to the unbound layers. Usually the center of displacement lies in the center of mass. When the contraction is blocked, this center shifts. In case of the test fields, the center of displacements can be found at the rigid concrete bearing prior to any crack occurrence. The structure contracts until the (constant) thermally induced stress in the cross-section is equal to the summed up shear stresses occurring due to friction to the unbound bases. This effect can be examined by means of the numerical simulation results as shown in Figure 5.11 a. As can be seen, the deformations in the structures' half with the rigid bearing are almost completely blocked. This explains the low displacement measurements obtained by the sensors in mid field compared with the sensors at the free end, as illustrated in Figure 5.1.

Figure 5.6 shows the interdependence of horizontal deformation and surface temperature for test field 1 and 3, respectively. The figure reveals the fact that the deformation of test field 1 (mortarbed on pervious concrete) are mainly reversible, while at test field 3 the cracks pervade the whole bound superstructure, leading to several independent parts of the structures with their own center of mass.

(a)

(b)
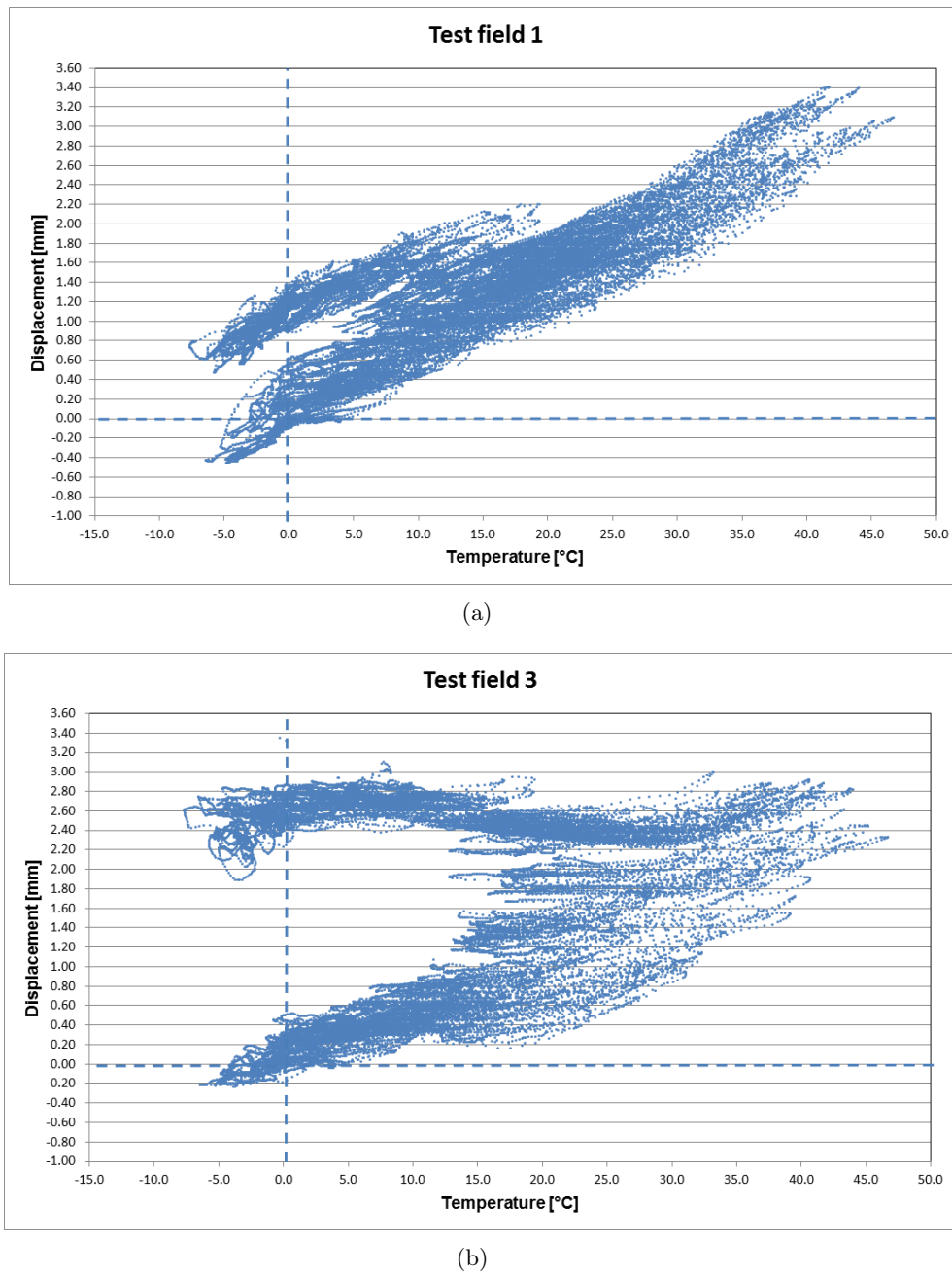
Figure 5.6: Interdependence of horizontal deformation and surface temperature for test field 1 and 3

Crack Distribution

The first visual inspection of the test fields were carried out in May 2016. No damage or cracks appeared in test sections 1 and 2. Nevertheless, on test field 3 three very fine cracks were found. Those cracks were about 5 m apart, so the spacing was approximately a third of the length of the test section. After summer the visual inspection in October 2016 showed also some fine cracks in test sections 1 and 2, approximately in the middle and a quarter of the section length. In test section 3 the cracks increased and the

spacing was approximately an eight of the length. Two cracks in the last third (row 58 and 73) were nearly 1 mm wide (Figure 5.7 b). During inspections in December 2016, three additional fine cracks were found in the last third of test field 1. On test field 2 two additional fine cracks were identified and the largest crack opened up to 1mm. Test field 3 was nearly unchanged compared to the last inspection. An overview of the cracks on test fields surfaces in May, October, and December 2016 is given in Figure 5.6.

(a) May 2016   (b) October 2016   (c) December 2016
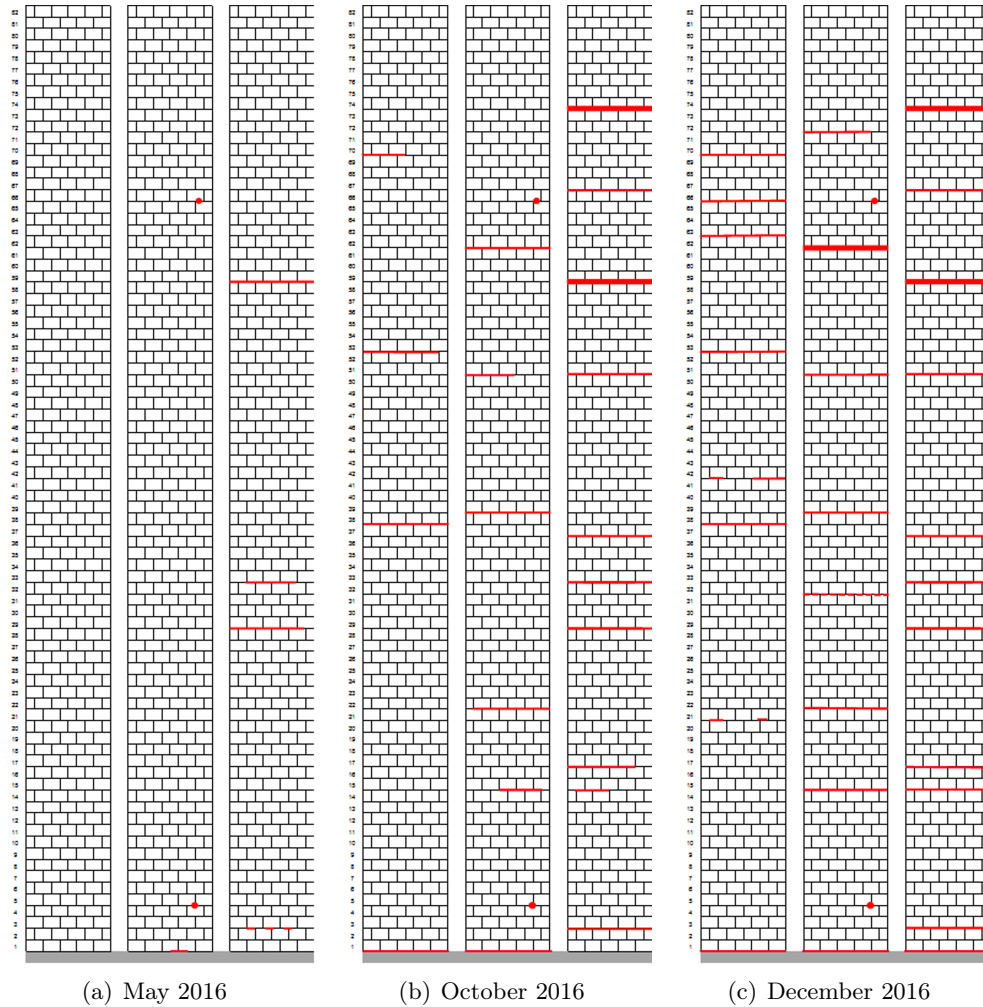
Figure 5.7: Overview of crack patterns on the three test fields, recorded at three different times.

5.2.4 Falling-weight-deflector experiments

To evaluate the load bearing capacity of the three different pavement structures, measurements with a Falling-Weight-Deflectometer (FWD) were carried out in June 2016. For each test field three measurement points were chosen, as illustrated in Figure 5.8, and loads of 50 kN, 75 kN, and 100 kN were applied with two repeat tests.

(a) Position

(b) FWD-Instrumentation
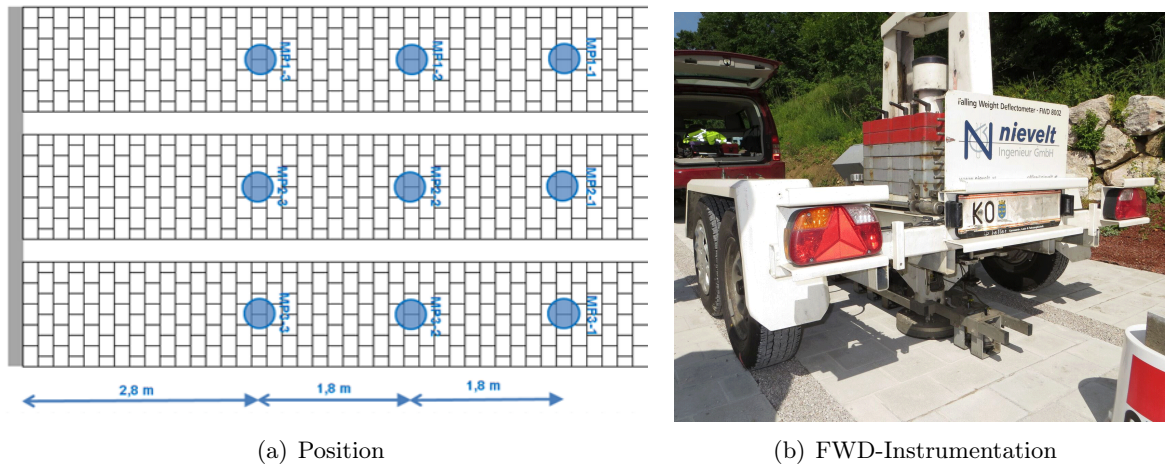
Figure 5.8: Falling-Weigth-Deflectometer (FWD) (b) and test positions on the three test fields (a).

5.2.5   Results falling-weight-deflector experiments

For each test section the deflections for all three measurement points are illustrated in Figure 5.9, for a load of 50 kN. The lowest deformations were measured for concrete blocks with bonded construction method on drainage concrete layer (test field 1). For concrete blocks with bound construction method on unbound base course (test field 2), the deformations in the center of the load are nearly twice as high as for test field 1. Nevertheless, test field 3 showed the largest deformations, approximately four times higher than for test field 2 and two times higher than for test field 1, as illustrated in Figure 5.9.

Figure 5.9: Measured deflection curve with the FWD for the three different paving block structures and for three different testing positions on each structure.

5.3   Numerical simulations

5.3.1   Numerical model

In a next step, the three test fields described in Section 2 were investigated by numerical models. The numerically modelled regions of test field 3 are shown exemplary in Figure 5.10. The mortar joints between the paving blocks were modelled as surface-to-surface intera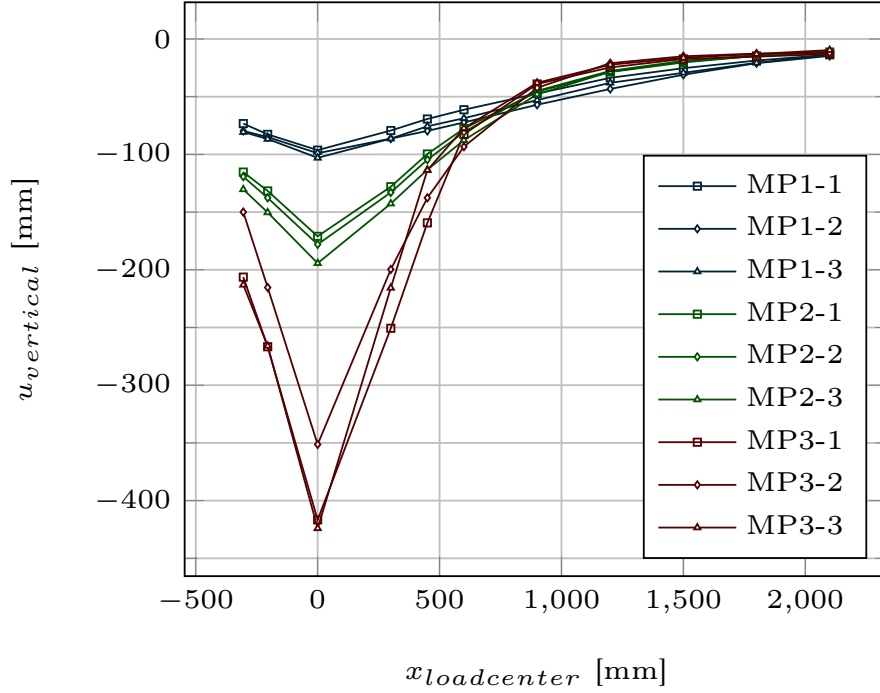ctions, therefore, the total length of the numerical model is only 1394 cm. These interactions were modelled as surface-based cohesive behaviour with a generalised traction-separation law. Damage occurs when the maximum of the ratios, $\max\{(\langle t_n \rangle / t_n^o), (t_s/t_s^o), (t_t/t_t^o)\}$, reaches the value of 1, whereby t_n, t_s, and t_t denote the traction forces in normal and tangential direction. The related strength values t_n^o, t_s^o, and t_t^o were set to 0.12 MPa and 0.11 MPa. The shear strength value was obtained from TVFA Vienna and the normal strength value from Buchholz (2010). The fracture energy for mortar of 0.03 $\frac{mJ}{mm^2}$ as in Trunk and Wittmann (2001) was reduced to 0.001 $\frac{mJ}{mm^2}$, to consider the brittle behaviour of the interface between paving block and joint mortar. Stabilization of the cohesive interaction was necessary to improve the convergence of the simulations. Further, to exclude a significant influence of viscous energy dissipation, a convergence study was carried out to ensure the quality of the solutions. A stabilization factor of 0.001 was found to deliver physically meaningful results at a justifiable computational cost. The material and interaction properties were mainly gained from previous identification experiments at TU Wien, as can be found in Füssl et al. (2015b), Füssl et al. (2015a), Füssl et al. (2016b), Füssl et al. (2016a), and Hengl

et al. (2017b).

Two kind of numerical simulations were performed: thermal loading simulations to capture the occurrence of cracks and vertical loading simulations to virtually reconstruct the falling-weight-deflector experiments.

For the thermal loading simulations, the symmetry of the model was utilized and symmetric boundary conditions were applied to the longitudinal axis, as illustrated in Figure 5.10. On one side of the pbs the horizontal displacement was prevented, as in the full scale field experiments.

Two simulation steps were then carried out, in the first step the dead load was applied and in a second step the temperature loading. The applied temperature gradient, as illustrated in Figure 5.10, was retrieved from the temperature experiments as described in Section 2. More precisely, experimentally obtained data from the particular summer day with the biggest difference between highest and lowest temperature was used.

For vertical loading simulations the geometry of the numerical model was changed to a width of 4.3 m and a length of 4.25 m. Thereby, the reaction of the underneath layers and the soil could be capture accurately. The deadload was applied in a first computational step and the vertical load in a second step. The load was applied by a fully modelled steel plate to ensure the right distribution of pressure in the loaded area.

The numerical simulations were carried out with the commercial Finite Element Software Abaqus. Geometric non-linearity and inelastic material behaviour of unbound layers were taken into account. More than 100 simulations were run at a HPC-Cluster at TU Wien. The average computation time for the thermal simulations with 627.516 DOF was around 21 hours. The average computation time of a vertical loading simulation took around 4 hours. In the course of the temperature simulations, the friction coefficient and the fracture energy were varied.
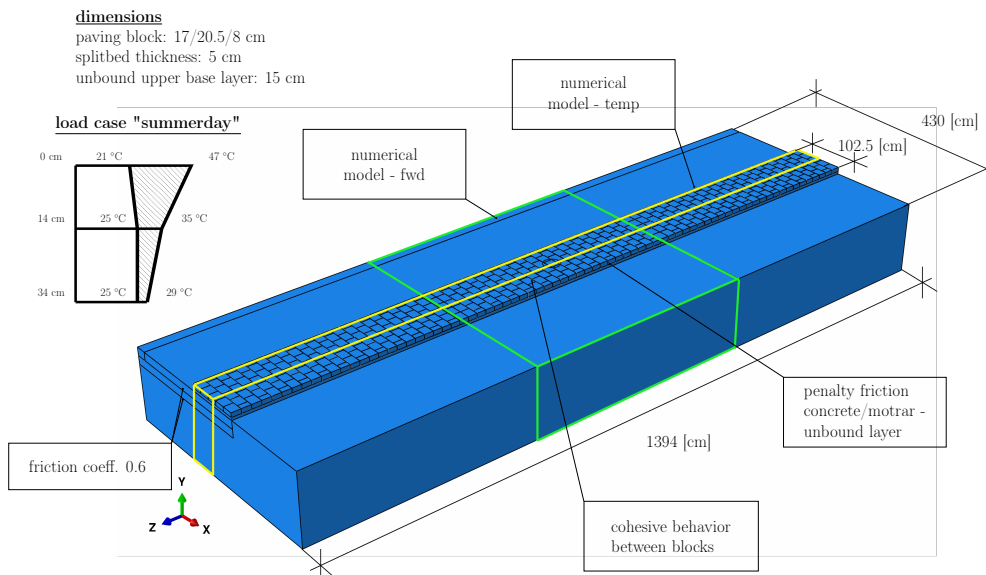

Figure 5.10:   Geometry, boundary, and interaction conditions of numerical models for temperature and FWD simulations.

5.3.2   Results of temperature simulations

A comparison of horizontal displacements due to abrupt cooling, as illustrated in Figure 5.10, obtained by full scale experiments and numerical simulations is given in Table 5.2. Although the results from the test field experiments could not be reproduced exactly by the numerical simulation tool, the horizontal deformations are in the same order of magnitude and qualitative differences of the structures' response are correlated. The interaction between paving blocks and the underlying layer is considered to be one of the most important factors in determining the performance of such a paving block structure under temperature loading (cooling). In Hengl et al. (2017b) the influence of the bonding strength between paving blocks and bonded layers beneath, as present in test field 2 and 3, was investigated. Therefore, the following simulation program aims mainly to isolate the parameters that influence the occurrence of cracks in rigid pbs laid on splitbed.

	Diff Exp. [mm]	Diff Sim. G_{F1} [mm]	Diff Sim. G_{F2} [mm]
u_h test field 1	1.62	3.55	3.55
u_h test field 2	1.02	1.67	1.75
u_h test field 3	0.52	0.30	0.51

Table 5.2: Comparison of horizontal displacements due to abrupt cooling obtain by test field experiments and numerical simulations, $G_{F1} = 0.001 \ [\frac{mJ}{mm^2}]$, $G_{F2} = 0.0025 \ [\frac{mJ}{mm^2}]$
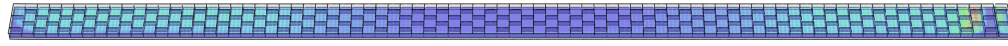
The friction coefficient between the paving blocks and the splitbed is a significant factor for crack occurrence of such structures and prevents or hampers its desired thermal contraction/expansion. It can be assumed that the experimentally obtained friction values between paving blocks and splitbed are exceeded in reality, resulting from intrusion of joint mortar into the splitbed, from unevenness of the splitbed or other blockings of paving block displacements. The influence of the friction coefficient on the number of occurring cracks and the width of these cracks can be found in the parameter study illustrated in Figure 5.13. The first major crack appears at a friction coefficient of around 0.1. The number of cracks is increasing as the friction increases, until it reaches a value of around 0.75. Then, the number of cracks stays to some extent constant, with 11 to 14 cracks and an average crack distance of about 1020 to 1190 mm. The cracks widths decrease as the contraction of the superstructure is distributed over several cracks. Due to the lift-off of the short rigid parts, only a small area stays in contact with the splitbed. Therefore, very high friction values would be necessary for a further crack occurrence.

Even at very low values of the friction coefficient fine cracks occur on the surface of the pbs, resulting mainly from the gradient of the thermal loading. Yet, these cracks do not open up significantly and are probably not be seen with the naked eye or even do not occur due to the not considered relaxation of mortar in the vertical joints, and respectively are neglected in the following discussion.

With an increasing friction coefficient, the normal stress resulting from blocked thermal contraction increases. This normal stress in the cross-section rises from the free end of the pbs until it reaches an equilibrium with the accumulated shear forces resulting from friction. As the contraction is blocked from that point on, no movement occurs and therefore no more friction is activated for the rest of the splitbed, as illustrated in
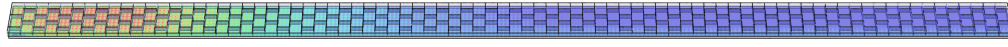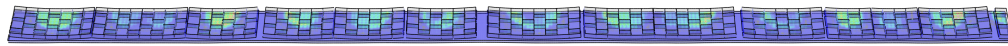
(a) 2.5% of thermal load applied

(b) 10% of thermal load applied
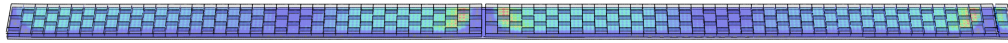
(c) 20% of thermal load applied

(d) 40% of thermal load applied

Figure 5.11: Shear forces between paving blocks and splitbed at different
time steps of the simulation, with a friction coefficient of 2.5 between
paving blocks and the underlying splitbed.

Figure 5.11 a.

The normal stress is respectively constant for that part of the superstructure. The occurrence of the first crack can happen at any joint in this region, but usually occurs close to the rigid bearing due to the increased local stiffness.

After this first cracks appears, the stress is decreasing with increasing crack width, as defined by the linear cohesive damage evolution law, which is determined by 0.001 $\frac{mJ}{mm^2}$. The center of the contraction shifts towards the middle as the contact interaction gets weaker with the increasing thermal load.

In the illustrated displacement field in Figure 5.6 a, the remaining temperature is not sufficient to open up the crack further then 0.22 mm. When the friction coefficient increases the crack opens up at a lower thermal loading, leaving more thermal contraction for the increase of the crack widths. Due to the opening of the crack, friction occurs, and the normal stresses in the superstructure increase until the next crack opens, as illustrated in Figure 5.11 a to d.

Another significant parameter is the fracture energy. Figure 5.14 shows the variation of the fraction energy from 0.00001 to 10 $[\frac{mJ}{mm^2}]$ with a steady friction coefficient between paving blocks and splitbed. The number of cracks is highly dependent on the fraction energy. For high values of fracture energy the cracks cannot open and stress is still transmitted between blocks. For reduces values of fracture energy of about 0.25 $[\frac{mJ}{mm^2}]$, the first crack can open up and the crack opening is quite high. When the fracture energy

(a) Friction coefficient between paving blocks and splitbed: 0,05

(b) Friction coefficient between paving blocks and splitbed: 0,1

(c) Friction coefficient between paving blocks and splitbed: 0,5

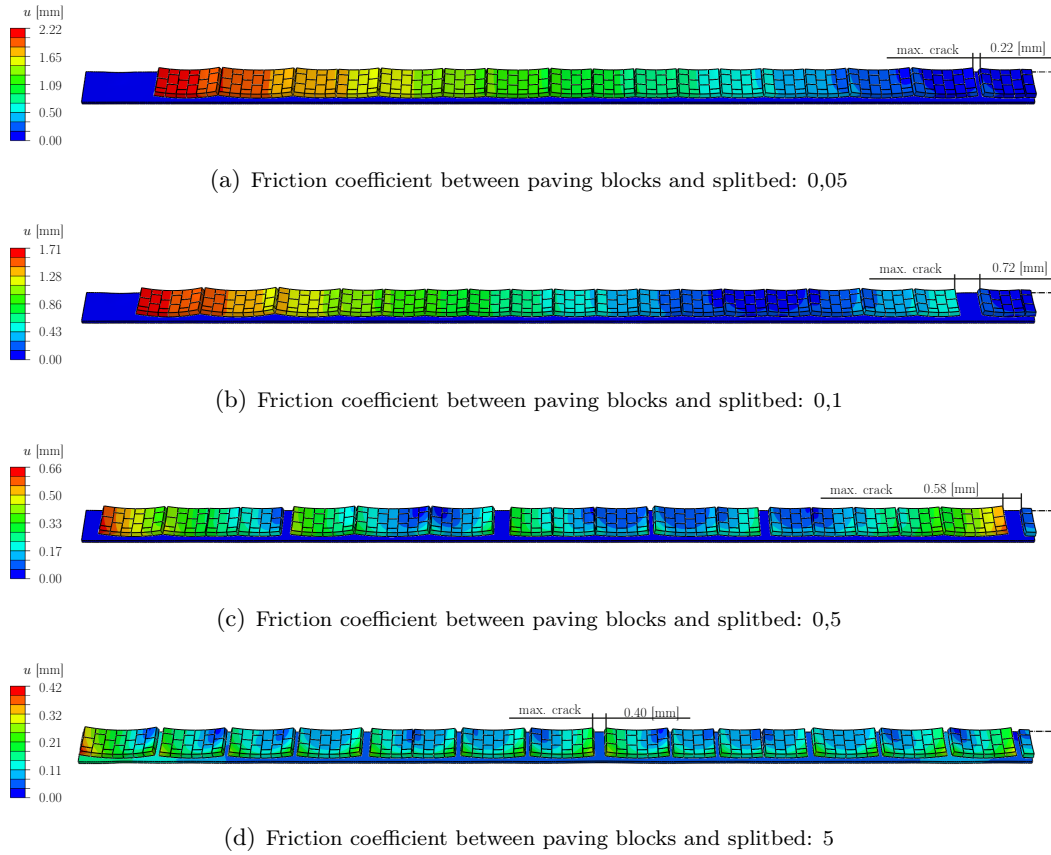(d) Friction coefficient between paving blocks and splitbed: 5

Figure 5.12: Resulting displacement fields obtained from simulations of
test field 3

is further reduced more and more cracks open up. But the crack opening diminishes as
the contraction is divided into several cracks.

5.3.3 Results of FWD simulations

To get to a good correlation with the field experiments the E-modulus of the soil had
to be increased to 490 MPa. It is assumed that this high stiffness results from a strong
compression and/or from consolidation due to neighboring buildings. The numerical
results show a good correlation with the mean values obtained by the FWD experi-
ments for each test field. Figure 5.16 illustrates the results from the FWD simulations
of the test fields compared with the average values from the FWD measurements. It
can be seen that the maximum deformation agrees very well, whereby the course of the
vertical deformation in distance with the load center varies significantly. It is assumed
that a to high stiffness for the loaded steelplate is the reason for that effect. Neverthe-
less, the deformation field of test field 3 can be found in Figure 5.15. The distribution
of vertical deformation along the bound superstructure can be seen. Whereas in the
perpendicular direction a strong deformation over the cross-section is found. A modi-
fication of the model under usage of symmetry boundary conditions will be used for a
further comprehensive parameter study.
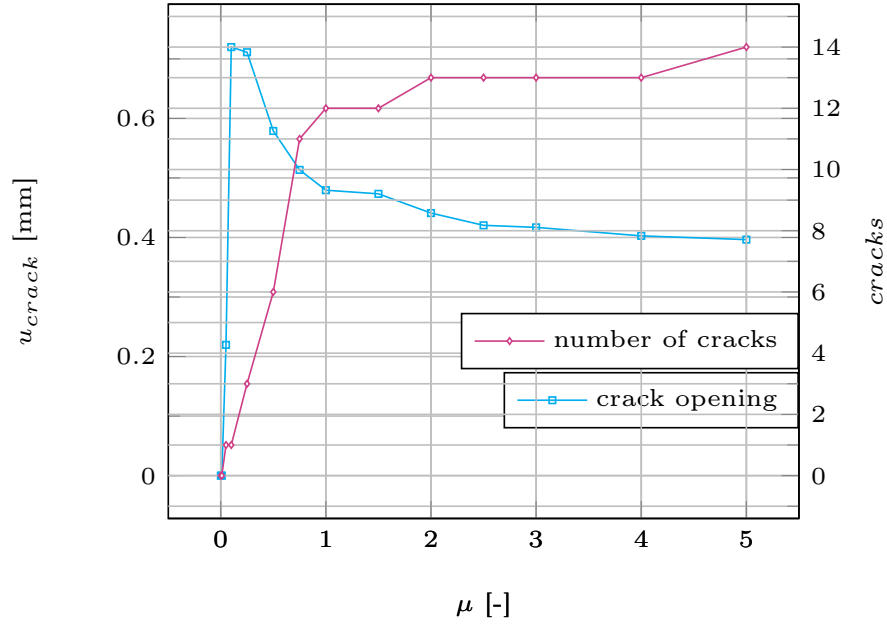
Figure 5.13: Maximum crack opening and number of appearing cracks for different friction coefficients between paving blocks and splitbed (test field 3).
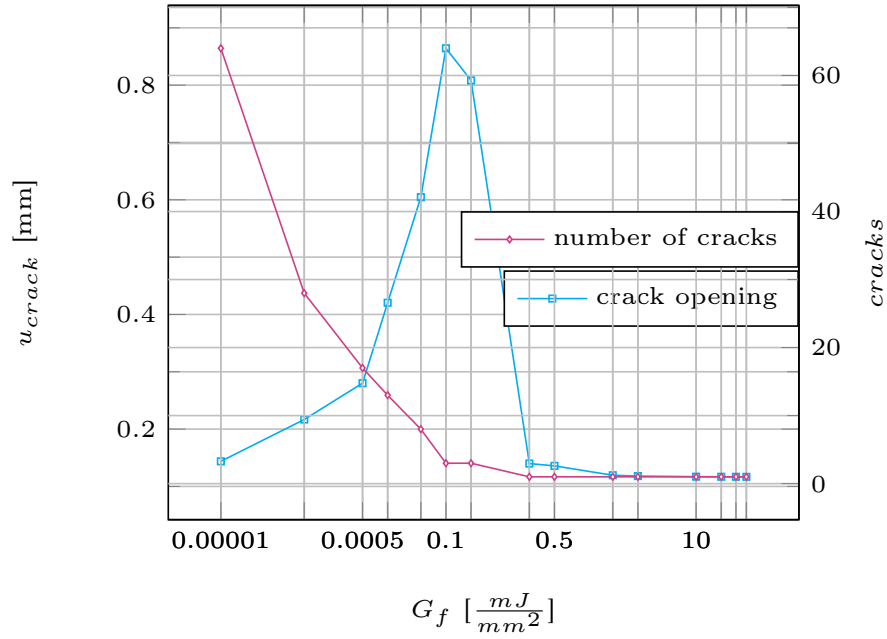
Figure 5.14: Maximum crack opening and number of cracks for different fracture energies of vertical joints (test field 3).
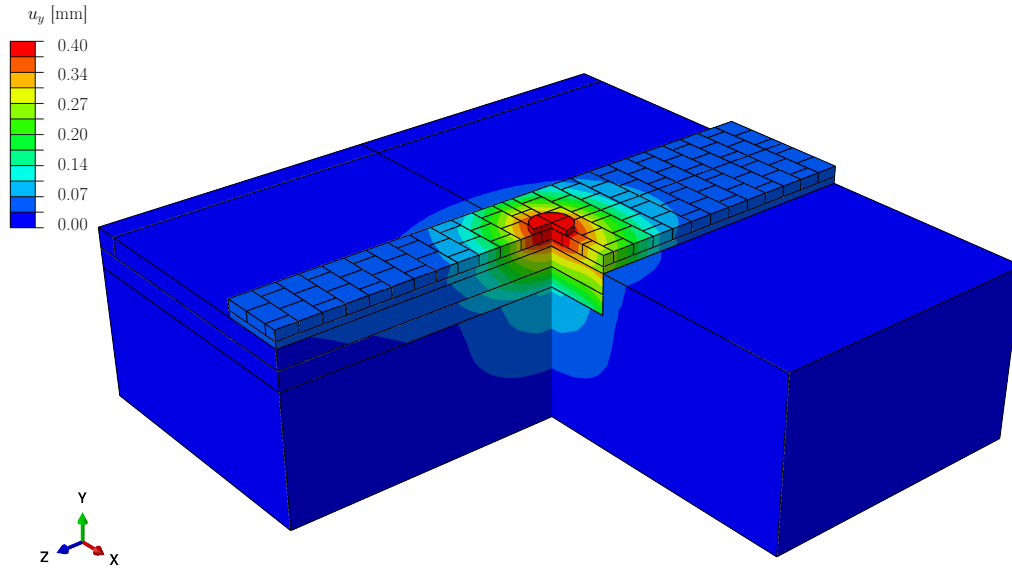
Figure 5.15:   Vertical displacement field obtained from vertical loading simulations on test field 3.
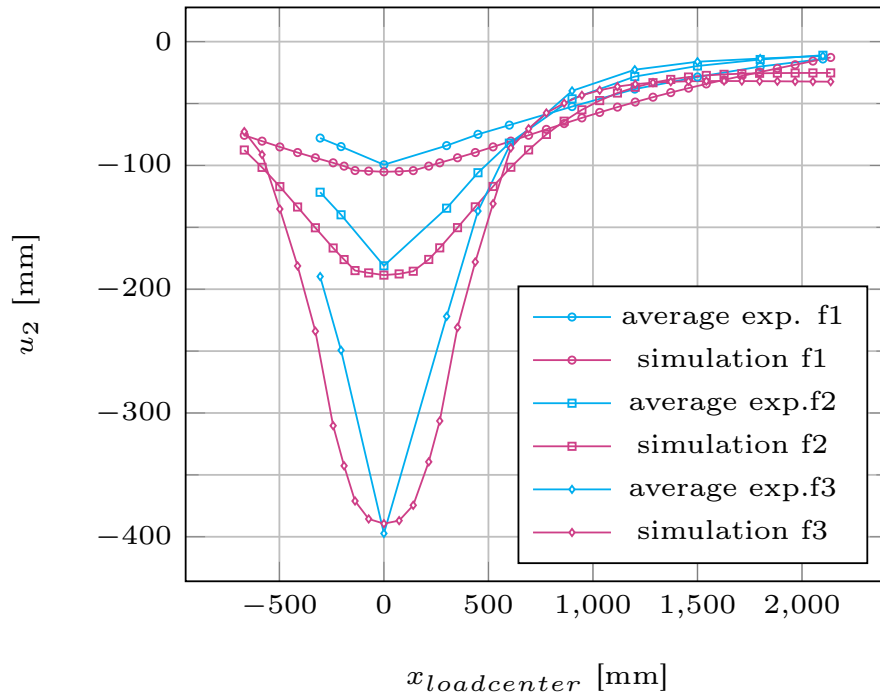
Figure 5.16: Results of falling-weight-deflector experiments compared to the corresponding numerical results.

5.4   Conclusion

The full scale field experiment made it possible to achieve important knowledge regarding temperature, displacement, and crack behaviour of paving block structures with

mortar-filled joints. Visual inspections revealed a significant difference regarding the number and width of cracks on the three test fields. On test field 1 (mortar bed on drainage concrete) far less cracks formed than on test field 2 (mortarbed on unbound base course). On test-field 3 (splitbed on unbound base course) two significant cracks with a width of 1 mm developed. These cracks occurred during the summer period 2016 and increased in width until winter 2016. Additional measurements with a falling weight deflectometer (FWD) revealed the differences of the load bearing capacities of the investigated testfields. Realistic temperature gradients were obtained and could be implemented into numerical models.

The results obtained from the test fields could be reconstructed by means of numerical simulation after adjusting the friction coefficient between paving blocks and splitbed, the fracture energy, and damage initiation values for the cohesive surface-to-surface interaction of the vertical joints between paving blocks. To reproduce the FWD results, the stiffness of the soil layer had to be increased. For the half of the test fields with the rigid concrete bearing, displacements of approximately 1 mm were measured. The distance sensors on the free end of the test fields measured displacements of 3 mm to 4 mm. These results correlate with insights obtained by numerical simulations.

The conclusions of this work can be summarized as follows:

- Normal stresses, leading to cracks on the surface of paving block structures with mortar-filled joints, result due to thermal loading either from the thermal gradient, from varying thermal expansion ratios within the bounded layers, or due to hampered or restricted contraction of the structure occurring from friction to the unbound sublayer. The stresses resulting from friction to the unbound sublayer are accumulated, beginning from the free end of the test field, until either: (1) the cohesive strength of the mortar bed is reached and cracks opening up, which decreases the internal stress, or (2) an equilibrium between the internal stresses in a cross-section of the structure and accumulated shear forces is found, subsequently, the structure stops contracting and no more frictional shear stresses occur, or (3) the whole contact area between paving blocks and splitbed exceeds the sticking friction and thereby contracts.

- The fiction coefficient between paving blocks and splitbed indeed seems to have a very large impact on the performance of a paving block superstructure under temperature loading. A characteristic friction coefficient lower than 0.8 MPa avoids the occurrence of distinct large cracks according to the performed numerical investigation, for the specific length of the test field. In case of longer paving block structures with mortar-filled joints, this value will decrease. Friction coefficient values around 0.6 MPa are usually found in literature for friction coefficients between concrete and unbound layers. It can be assumed that the experimentally-obtained friction coefficient values are exceeded in reality, resulting from intrusion of joint mortar into the splitbed, from unevenness of the splitbed, or other blockings of paving block displacements.

To obtain further insights, the extraction of drilling cores is planned. The pass through of cracks on test field 2 could explain the divergence of the crack occurrence between test field 2 and 3. For a further usage of the test fields, different methods for crack repair and their influence on load distribution and durability will be examined.

Conclusions and outlook

Concluding remarks

Based on the results obtained from the publications in the first part of this thesis, the main findings can be summarized as follows:

- In *Publication A* it is presented that the operation of the Mobile Load Simulator worked properly for the traffic simulation on the three different test sections conducted in cooperation by VUT and EMPA. Thus, this testing method can be recommended for superstructures with paving blocks. The installed soil pressure cells on the top of the upper base course and the subgrade were able to capture compressive stress peaks due to a tire rollover.

- On the basis of three different lab experiments, an appropriate characterization of the tangential as well as normal mechanical behaviour of the sand-filled joints was possible. The obtained mechanical behaviour could be implemented accurately into the finite element model, using Mohr–Coulomb friction in tangential direction and a non-linear elastic material law in normal direction.

- For the first time, the complex bedding and interaction behaviour of paving blocks could be considered within a numerical simulation tool realistically. A comparison between the experimentally- and numerically-obtained pressure stress states in the base courses showed a reasonable agreement. Nevertheless, the punctual conducted pressure measurements cannot be considered as fully sufficient for a profound validation of the proposed numerical simulation tool.

- In *Publication B*, the developed simulation tool could further realistically reproduce the load-bearing behaviour of superelevated paving block structures. The use of an arc length method to control the application of load increments allowed for a reliable determination of limit loads for different paving block structures, and, thus, allowed for a mechanically-sound analysis of such structures. The additional load carrying capacity of superelevated paving block structures is activated by compressive stresses at the contact surfaces between paving blocks, depending on the shape of the superelevated profile. These compressive stresses allow tangential forces to be transmitted between paving blocks by frictional resistance and occurring bending moments are suppressed until it reaches structural failure.

- Through an accurate description of the non-linear interaction behaviour between paving blocks, taking into account the frictional behaviour in tangential direction and the separation in normal direction, the structural behaviour of superelevated paving block structures could be simulated realistically. Two main failure

mechanisms could be identified, snap through buckling and a mechanism characterized by the development of a kinematic chain. The maximum applicable wheel load as well as the occurring failure mechanism depends on the magnitude of the superelevation.

- Considering three different loading situations and a large number of different superelevations, a range of optimal superelevations could be identified. Interestingly, the effect of different structural properties, such as horizontal support stiffness, paving block dimensions, number of paving blocks, etc., on this range is smaller than expected. For all investigated structures, the optimum superelevation lies between 0.028 and 0.042 times the road width.

- In *Publication C* numerous tangential shear experiments have been carried out at TVFA Vienna to identify the non-linear load transmission capability of different joint formations. The obtained data allowed to develop a user subroutine written in Fortran and thereby enhance the numerical simulation tool to enable horizontal resistance simulations.

- Mainly for this reason, very plausible 3D deformation mechanisms could be obtained for several laying patterns with different types of paving blocks. Interesting insights into load transfer mechanisms could be gained, showing a huge variety depending on the combination of laying pattern and type of paving block. The fully automation of the model creation, enabled by a comprehensive Python script, facilitated to run a huge amount of simulations. Finally, this allowed for a comprehensive performance evaluation of several paving block pavements with respect to their horizontal shifting resistance.

Finally it can be stated that numerical simulations are a suitable tool to assess vertical as well as horizontal loadings on paving block pavements. Sophisticated and automated model generation allows the study of such complex model geometries with a large number of interactions. For this reason, future work is devoted to the extension of the modelling capabilities together with an easy to use interface, to make this numerical simulation tool accessible for engineers.

The publications in the second part of this thesis mainly dealt with mechanical mechanisms of paving block structures with mortar-filled joints and the occurrence of cracks under thermal loading. Test field experiments allowed to achieve important knowledge of the mechanical mechanisms, especially with respect to temperature loading, displacement fields and structural brittle behaviour. Based on the obtained results, the following conclusions can be drawn:

- In *Publication D*, identification experiments for the bonding strength between paving block and mortar bed, carried out at TVFA Vienna, provided shear strength values for different paving blocks, which have been considered within this work.

- This bonding strength between paving blocks and mortar bed seems to have a very high impact on the performance of a paving block superstructure under temperature loading. A characteristic shear strength larger than 0.1 MPa avoids the occurrence of distinct large cracks according to the performed numerical investigation, even under the worst case scenario of very high installation temperatures (up to 60 °C). Shear strength values between 0.26 and 0.28 MPa were obtained

experimentally for concrete paving blocks, and would therefore be sufficient. However, these values were obtained by identification experiments under laboratory conditions and, therefore, provide rather upper limits for the realistic bonding strengths in the field. This could be an explanation for elusive damage to paving block structures, frequently observed in engineering practice.

- A low installation (construction) temperature is basically beneficial to prevent cracking due to cooling during winter time, but it can lead to high compressive stresses and lift off of the paving blocks in summer. However, according to the performed simulations, a bonding strength of 0.1 MPa, in shear as well as normal direction to the interface between the paving blocks and the mortar bed, should be sufficient to avoid both distinct cracking in winter as well as lift off of the paving block superstructure in summer. Additionally, the numerical results give reason to believe that shading measures, in case of high solar radiation, are of benefit with respect to cracking in winter time.

- Based on the findings, expansion joints through the paving block superstructure only seem to be useful if the mentioned critical bonding strength cannot be reached and single large cracks are likely to occur. For higher bonding strengths, a fine crack network arise and expansion joints lose its purpose and may be omitted as long as the structure and connected installations can resist the compressive stresses in summer and an adequate bond between mortar bed and the pervious concrete layer is provided, respectively. Following this approach also the challenge to predict the right location of expansion joints, which was seen often failed in retrospect, can be avoided.

- In *Chapter E*, field experiment made it possible to achieve important knowledge regarding temperature, displacement, and crack behaviour for block pavement structures with mortar-filled joints. The results obtained from test-fields could be reconstructed by means of numerical simulation after adjusting the friction coefficient between paving blocks and splitbed, the fracture energy and damage initiation values for the cohesive surface-to-surface interaction of the vertical joints between paving blocks.

- The fiction coefficient between paving blocks and splitbed indeed seems to have a very large impact on the performance of a paving block superstructure under temperature loading. A characteristic friction coefficient lower than 0.8 MPa avoids the occurrence of distinct large cracks according to the performed numerical investigation, for the specific length of the test field. In case of longer paving block structures with mortar-filled joints, this value will decrease. Friction coefficient values around 0,6 MPa are usually found in literature for friction coefficients between concrete blocks and unbound layers. It can be assumed that the experimentally-obtained friction coefficient values are exceeded in reality, resulting from intrusion of joint mortar into the splitbed, from unevenness of the splitbed or other blockings of paving block displacements.

- Further, the number and width of occurring cracks is depending on the fracture energy. At high values of fracture energy the cracks can not open up and stress is still transmitted between blocks, which represents a non brittle fracture. When the fracture energy decreases, the first crack can open up significantly, as it is

only one crack. The fracture energy necessary to prevent major cracks is further depending on the structures length. When the energy is further reduced more and more cracks open up. Subsequently, the crack opening diminishes as the contractions is divided by the many cracks.

In summary it can be stated, that 3D numerical simulations represent an appropriate method for the performance prediction of paving block structures. Sophisticated identification experiments allow to identify mechanical models and the corresponding material parameters. Thereby, the necessary input data for such simulations tools is obtained and full scale experiments allow for partial validation. Sophisticated contact modelling even allows the description of complex mechanical processes in paving block structures. Thus, numerical simulations are a useful addition to experimental studies and can strongly contribute to new insights into the complex mechanical behaviour of paving block structures.

Bibliography

Ascher, D. (2003). Generierung von FALT-FEM Eingabedaten für Betonpflasterbefestigungen, Diplomarbeit, Technische Universität Dresden.

Ascher, D., Lerch, T., Oeser, M., and Wellner, F. (2006). 3D-FEM Simulation of concrete block pavement. The 8th international conference on concrete block paving sustainable paving for our future, Interlocking Concrete Pavement Institute (ICPI), San Francisco.

BISAR (1989). Shell Pavement Design Methodology, Shell Petroleum Company, Netherlands.

Bondy, K. (1995). Cracking in ground-supported post-tensioned slabs on expansive soil, pti technical notes, Canoga Park, California.

Boyce, J. (1980). A non linear model for the elastic behaviour of granular materials under repeated loading, In: International symposium on soils under cyclic and transient loading, p. 285–294, Swansea.

Buchholz, J. (2010). Gebundene Pflasterbauweisen. PhD thesis, Universität Kassel.

Burmister, D. (1943). The theory of stresses and displacements in layered systems and applications to the design of airport runways, highway research board proceedings, Washington, DC.

Burmister, D. (1958). Evaluation of pavement systems of the washo road test by layered systems methods, bulletin 177, highway research board, Washington, DC.

Camanho, P. and Davila, C. (2002). Mixed-mode decohesion finite elements for the simulation of delamination in composite materials. NASA/TM-2002-211737, Hampton, Virginia.

Chazallon, C., Koval, G., Hornych, P., Allou, F., and Mouhoubi, S. (2009). Modelling of rutting of two flexible pavements with the shakedown theory and the finite element method, computers and geotechnics, 36, p. 798–809, Strasbourg, France.

Chiroux, R., Jr., W. F., Johnson, C., Shoop, S., and Raper, R. (2005). Three-dimensional finite element analysis of soil interaction with a rigid wheel, applied mathematics and computation 162, p.707–722, Auburn University, Alabama.

Corp., D. S. S. (2016). Abaqus analysis user's manual. Providence.

COURAGE (1999). Construction with unbound road aggregates in europe, final report, european commission - dgvii, 4th framework programme, road transport research, University of Nottingham.

Everseries Pavement Analysis Programs (1999). Washington state department of transportation, Olympia, WA.

F. Hugo, A. M. (2004). Significant findings from full-scale accelerated pavement testing, nchrp synthesis 325, transportation research board, Washington, D.C.

Forschungsgesellschaft für Straßen- und Verkehrswesen (2007). Arbeitspapier: Flächenbefestigungnen mit Pflasterdecken und Plattenbelägen in gebundener Ausführung, Vienna.

Füssl, J., Hengl, H., Eberhardsteiner, L., Kluger-Eigl, W., and Blab, R. (2016a). Numerical simulation tool for paving block structures assessed by means of full-scale accelerated pavement tests. International Journal of Pavement Engineering, Pages 1-13, doi: 10.1080/14680629.2017.1330221, TU Wien.

Füssl, J., Kluger-Eigl, W., and Blab, R. (2015a). Mechanical performance of pavement structures with paving slabs part i: full-scale accelerated tests as validation for a numerical simulation tool. Engineering Structures 98, Pages 212-220, doi: 10.1016/j.engstruct.2014.10.055, TU Wien.

Füssl, J., Kluger-Eigl, W., and Blab, R. (2016b). Experimental identification and mechanical interpretation of the interaction behavior between concrete paving blocks. International journal of pavement engineering, Vol. 17, Pages 478-488, doi: 10.1080/10298436.2014.993205, TU Wien.

Füssl, J., Kluger-Eigl, W., Eberhardsteiner, J., and Blab, R. (2015b). Mechanical performance of pavement structures with paving slabs part ii: numerical simulation tool validated by means of full-scale accelerated tests. Engineering Structures 98, Pages 221-229, doi: 10.1016/j.engstruct.2014.10.055, TU Wien.

Gleitz, T. (1996). Beitrag zur rechnerischen Erfassung des nichtlinearen Spannungs-Verformungsverhaltens ungebundener Tragschichtmaterialien in flexiblen Straßenkonstruktionen, Dissertation am Lehrstuhl Straßenbau der TU Dresden.

Hassani, A. (2006). Modelling and structural design of a concrete bock pavement system. International conference on concrete block paving, Tehran, Iran.

Hengl, H. and Füssl, J. (2016). The influence of superelevated profiles of paving block structures on their load-bearing behavior. Engineering Structures, Vol 117, Pages 195-203, doi: 10.1016/j.engstruct.2016.03.003, TU Wien.

Hengl, H., Kluger-Eigl, W., Blab, R., and Füssl, J. (2017a). Horizontal deformation resistance of paving block superstructures - influence of laying pattern and joint behavior. submitted to International Journal of Pavement Research and Technology, TU Wien.

Hengl, H., Kluger-Eigl, W., Blab, R., and Füssl, J. (2017b). The performance of paving block structures with mortar filled joints under temperature loading, accessed by means of numerical simulations. Road Materials and Pavement Design, Pages 1-20 doi: 10.1080/14680629.2017.1330221, TU Wien.

Hicks, R. and Monismith, C. (1971). Factors influencing the resilient behavior of granular materials, transp. res. rec., 345, p.15–31.

Hornych, P., Kazai, A., and Piau, J. (1998). Study of the resilient behaviour of unbound granular materials. in: Proceedings of fifth conference on bearing capacity of roads and airfields, vol. 3, p. 1277–1287, Trondheim.

Huang, Y. (2004). Pavement analysis and design, 2nd ed. pearson-prentice hall, Upper Saddle River, New Jersey.

Huurman, M. (2006). Validation of the new dutch design method for concrete block road pavements, 8th international conference on concrete block paving, San Francisco.

Huurman, M., Houben, L., and Kok., A. (1992). Development of a three-dimensional finite element model for concrete block pavements. Proceedings Fourth International Conference on Concrete Block Paving, Delft University of Technology.

Jacobs, M. and Houben, L. (1988). Wheel testing and finite element analysis of concrete block pavement. Delft University of Technology.

Janda, G. (2004). Erarbeitung eines Bemessungsvorschlages für Pflaster- und Plattenbefestigungen. Master thesis, TU Vienna.

Kolb, H. (1988). Ermittlung der Sohlreibung von Gründungskörpern unter horizontalem klimatischen Zwang. PhD thesis, TH Stuttgart.

Lekarp, F., Isacsson, U., and Dawson, A. (2000). State of the art. i: Resilient response of unbound aggregates, Journal of Transportation Engineering, p.66–75, Solna, Sweden.

Lerch, T. (2005). Investigation of the deformation behaviour of concrete block pavements under simulated traffic loading. PhD thesis, TU Dresden.

Maliha, R. (2005). Untersuchungen zu wirklichkeitsnahen Beanspruchungen in Fahrbahndecken aus Beton. PhD thesis, Universität Fridericiana zu Karlsruhe.

Mampearachchi, W. K. and Gunarathna, W. P. H. (2010). Finite-element model approach to determine support conditions and effective layout for concrete block paving, doi: 10.1061/(asce)mt.1943-5533.0000118. Journal of Materials in Civil Engineering, University of Moratuwa, Sri Lanka.

Nejad, F. M. and Shadravan, M. R. (2006). A study on behavior of block pavement using 3d finite element method. International conference on concrete block paving, Tehran, Iran.

Nishizawa, T. (2003). A tool for structural analysis of block pavements based on 3dfem, proc. 7th int. conf. on concrete block paving, p 1-4, Sun City, South Africa.

Nishizawa, T., Matsuno, S., and Komura, M. (1984). Analysis of interlocking block pavements by finite element method. International Conference on Concrete Block Paving, Kanazawa University.

Oeser, M. and Chandra, H. (2010). Segmented concrete block pavements: Analysis with optimized numerical tool. Betonwerk und Fertigteil-Technik 76.1, The University of New South Wales.

Partl, M. (2008). Full-scale accelerated pavement testing apt at empa – the new mobile load simulator, empa duebendorf, Duebendorf, Switzerland.

Petersson, D. (1998). Stresses in concrete structures from ground restraint. PhD thesis, Lund Inst. of Technology.

Plannerer, M. (1998). Temperaturspannungen in Betonbauteilen während der Erhärtung. PhD thesis, Technische Universität München.

Powell, R. (2012). A decade of full-scale accelerated pavement testing, advances in pavement design through full-scale accelerated pavement testing – jones, harvey, mateos & al-qadi (eds.), taylor & francis group, London.

Rostasy, F. and Kraus, M. (2001). Frühe Risse in massigen Betonbauteilen - Ingenieurmodelle für die Planung von Gegenmaßnahmen. Deutscher Ausschuss für Stahlbeton, TU Braunschweig.

RVS 03.08.63 (2008). Straßenplanung – Bautechnische Details – Oberbaubemessung Österreichische Forschungsgesellschaft Straße-Schiene-Verkehr, Vienna.

RVS 08.15.01 (2008). Technische Vertragsbedingungen – Unterbauplanum und ungebundene Tragschichten – Ungebundene Tragschichten Österreichische Forschungsgesellschaft Straße-Schiene-Verkehr, Vienna.

RVS 08.18.01 (2009). Technische Vertragsbedingungen – Pflasterarbeiten Randbegrenzungen – Pflasterstein- und Pflasterplattendecken, Randeinfassungen Österreichische Forschungsgesellschaft Straße-Schiene-Verkehr, Vienna.

Röhling, S. (2005). Zwangsspannungen infolge Hydratationswärme. Verlag Bau+Technik.

Schikora, K. and Eierle, B. (1999). Berechnungsmodelle für Betonbauteile unter frühem Temperaturzwang. Tagungsband Baustatik-Baupraxis 7, Balkema-Verlag, TU München.

Schweighofer, A. (2011). Zwangsspannungen im jungen Beton in Bodenplatten und Wänden. PhD thesis, TU Vienna.

Schütte, J. (1997). Einfluss der Lagerbedingungen auf Zwang in Betonbodenplatten. PhD thesis, TU Braunschweig.

Shackel, B. (1980a). An experimental investigation of the roles of the bedding and jointing sands in the performance of interlocking of concrete block pavements, Concrete/Beton No. 19, Johannesburg, South Africa.

Shackel, B. (1980b). The performance of interlocking pavements under accelerated trafficking", proc first int conf on concrete block paving., conc. publishing co., London.

Shackel, B. (1982). An experimental investigation of factors influencing the design of interlocking concrete block pavement for roads, proceedings of the australian road research board, 11, part 2, pp. 6-15, Vermont South, Victoria, Australia.

Shackel, B. (1990). Design and construction of interlocking concrete block pavements, elsevier applied science, London.

Sharp, K., Johnson-Clarke, J., and Fossey, D. (1999). A review of the australian alf program. presented at international conference on accelerated pavement testing, Reno.

Steyn, W. (2012a). A history of modern accelerated performance testing of pavement structures, advances in pavement design through full-scale accelerated pavement testing – jones, harvey, mateos & al-qadi (eds.), taylor & francis group, London.

Steyn, W. (2012b). Significant findings from full-scale accelerated pavement testing, nchrp synthesis 433, transportation research board, Washington, D.C.

Taylor, D. (1963). Fundamentals of soil mechanics. John Wiley & Sons, Inc., New York.

Timoshenko, S. and Goodier, J. (1987). Theory of elasticity. 3rd ed., McGraw-Hill Inc., New York.

Trunk, B. and Wittmann, F. (2001). Influence of size on fracture energy of concrete. Materials and Structures 34.5, Pages 260-265, Zürich.

Uzan, J. (1985). Characterization of granular materials, transp. res. rec. 1022, 52–59.

Werkmeister, S., Dawson, A., and Wellner, F. (2001). Permanent deformation behavior of granular materials and the shakedown concept, transportation research record 1757, Journal of the Transportation Research Board, pp.75–81, TU Dresden.

Wissenschaftlich-Technische Arbeitsgemeinschaft für Bauwerkserhaltung und Denkmalpflege (2009). Merkblatt: Gebundene Bauweise – Historisches Pflaster.

Wistuba, M. (2003). Klimaeinflüsse auf Asphaltstraßen: maßgebende Temperatur für die analytische Oberbaubemessung in Österreich. PhD thesis, TU Vienna.

Publications and Conference Contributions

Publications

Josef Füssl, Herwig Hengl, Wolfgang Kluger Eigl & Ronald Blab:
Numerical simulation tool for paving block structures assessed by means of full-scale accelerated pavement tests
published in International Journal of Pavement Engineering, 2016.

Herwig Hengl & Josef Füssl:
The influence of superelevated profiles of paving block structures on their load-bearing behavior
published in Engineering Structures, 2016.

Herwig Hengl, Wolfgang Kluger-Eigl, Ronald Blab & Josef Füssl:
Horizontal deformation resistance of paving block superstructures - influence of laying pattern and joint behavior
submitted to International Journal of Pavement Research and Technology, 2016.

Herwig Hengl, Wolfgang Kluger Eigl, Ronald Blab & Josef Füssl:
The performance of paving block structures with mortar filled joints under temperature loading, accessed by means of numerical simulations
published in Road Materials & Pavement Design, 2017.

Conference Papers

Anton Schweighofer, Markus Vill, Herwig Hengl, Johann Kollegger:
Simulation of shear load behavior of fifty year old post-tensioned concrete bridge girders.
In: *EURO-C 2010 Conference on Computational Modelling of Concrete Structures, Rohrmoos/Schladming.*
Computational Modelling of Concrete Structures, (2010), ISBN: 978-0-415-58479-1; p. 699 - 702.

Herwig Hengl, Josef Füssl & Wolfgang Kluger-Eigl:
The influence of arch supporting effect on the load bearing capacity of paving block superstructures.
In: *ICCBP 11th International Conference on Concrete Block Pavement*, FGSV, (2015).

Conference Presentations and Posters

Herwig Hengl, Josef Füssl & Wolfgang Kluger-Eigl:
The influence of arch supporting effect on the load bearing capacity of paving block superstructures.
ICCBP 11th International Conference on Concrete Block Pavement, Dresden, Germany, 09/09/2015-11/09/2015 (oral presentation)

Reports

Wolfgang Kluger-Eigl, Ronald Blab, Torsten Hessmann, Barbara Gagliano, Josef Füssl, Herwig Hengl:
CR-Projekt Pflasterbauweisen - 2. Forschungsjahr,
Bericht für Forum Qualitätspflaster (FQP); 2015; 167 S.

Wolfgang Kluger-Eigl, Ronald Blab, Barbara Gagliano, Herwig Hengl, Josef Füssl:
CR-Projekt Pflasterbauweisen - 3. Forschungsjahr,
Bericht für Forum Qualitätspflaster (FQP); 2016; 205 S.

Curriculum Vitae

Personal Data

Name:	**Dipl.-Ing. Herwig HENGL**
Date of Birth:	06th July 1982
Place of Birth:	Vienna, Austria
Nationality:	Austrian
Current address:	Burggasse 128/35, 1070 Wien, Austria

Education

10/2009 – 07/2017	Doctoral studies in Civil Engineering at Vienna University of Technology, Vienna, Austria
08/2004 – 10/2009	Diploma Studies in Civil Engineering at Vienna University of Technology, Vienna, Austria
09/1998 – 06/2003	High School Student in Computational Science, Korneuburg, Austria

Work experience

08/2015 – 05/2017	University Assistant, Vienna University of Technology, Austria
02/2014 – 08/2015	Project Assistant, Vienna University of Technology, Austria
10/2011–09/2013	Managing Director, Broet Sociedad Anonima, Buenos Aires, Argentina
02/2011–06/2011	Structural Engineer, Waagener-Biro Stahlbau AG, Vienna, Austria
11/2007–10/2009	Structural Engineer, ZT Hengl, Stockerau, Austria
07/2007–07/2007	Construction Engineer, Leyrer & Graf, Vienna, Austria
07/2006–07/2006	Construction Engineer, Leyrer & Graf, Vienna, Austria
07/2005–07/2005	Construction Engineer, Leyrer & Graf, Vienna, Austria
07/2004–07/2004	Construction Worker, Leyrer & Graf, Vienna, Austria
01/2003–11/2004	Software Engineer, self-employed, Vienna, Austria
06/2003–04/2004	Paramedic, Red Cross, Vienna, Austria
06/2001–08/2001	IT Assistent, Raiffeisen Informatik Zentrum, Austria
06/1999–07/1999	IT Assistent, Raiffeisen Informatik Zentrum, Austria
06/1998–07/1998	IT Assistent, Raiffeisen Informatik Zentrum, Austria